Investigating the Role of Calcium in the Biomechanical Response of Neutrophils to Mechanical Deformation Experienced in the Pulmonary Capillaries

by

Jeffrey J. Hsu

S.B. Mechanical Engineering
S.B. Biology
Massachusetts Institute of Technology, 2005

SUBMITTED TO THE BIOLOGICAL ENGINEERING DIVISION IN PARTIAL FULFILLMENT OF THE REQUIREMENTS FOR THE DEGREE OF

MASTER OF ENGINEERING IN BIOMEDICAL ENGINEERING
AT THE
MASSACHUSETTS INSTITUTE OF TECHNOLOGY

SEPTEMBER 2006

Signature of Author .....
Biological Engineering Division
July 26, 2006

Certified by .....
Roger D. Kamm
Professor of Mechanical Engineering and Biological Engineering, MIT
Associate Head, Department of Mechanical Engineering, MIT
Thesis Supervisor

Accepted by .....
Bevin P. Engelward
Associate Professor of Biological Engineering, MIT
Chair, Master of Engineering in Biomedical Engineering Program

This page intentionally left blank.

Investigating the Role of Calcium in the Biomechanical Response of Neutrophils to Mechanical Deformation Experienced in the Pulmonary Capillaries

by

Jeffrey J. Hsu

Submitted to the MIT Biological Engineering Division on
July 26, 2006
in Partial Fulfillment of the Requirements for the Degree of
Master of Engineering in Biomedical Engineering

ABSTRACT

Neutrophils in the pulmonary microcirculation are subjected to mechanical deformation while traveling through capillaries of sizes much smaller than the mean neutrophil diameter. This deformation has been shown to result in significant reductions in both the shear storage and shear loss moduli of the cell, with subsequent recovery towards their initial values. Also, deformation above a threshold stimulus results in neutrophil activation, evidenced by pseudopod projection from the cell. These two events are thought to occur via independent pathways, yet little is known about the mechanosensing signaling involved. Other work has demonstrated that physiological deformation of neutrophils induces a marked increase in the levels of cytosolic calcium, suggesting that this occurrence may trigger the biomechanical response observed in the cell.

The aim of this thesis was to elucidate the role of calcium in the neutrophil response to the mechanical deformation experienced during transit through the pulmonary capillaries. Chelating intracellular calcium in neutrophils resulted in (i) decreased deformability of the cells into a microchannel, (ii) attenuation of the drop in shear storage modulus (G') observed in untreated cells upon deformation, and (iii) shorter activation times. These findings suggest that cytosolic calcium holds an important function in the neutrophil transit through the capillaries, and inhibition of normal calcium release within the cell can lead to leukostasis-like conditions.

Thesis Supervisor: Roger D. Kamm, Ph.D.
Title: Professor of Mechanical and Biological Engineering
Associate Head, Department of Mechanical Engineering

This page intentionally left blank.

TABLE OF CONTENTS

ACKNOWLEDGMENTS

The completion of this thesis would not have been possible without the help of the numerous people that have supported me along the way.

First, I would like to thank Prof. Roger Kamm. As my thesis supervisor, he has given me invaluable feedback on my work, helping me to more fully understand the fundamental principles behind the project. The door to his office is almost always open, as he is readily available to answer any questions that his students might have for him. This constant guidance, coupled with his kindness and patience, has made this past year of graduate school an immensely enriching experience.

Many others in Prof. Kamm's laboratory have assisted me greatly during the course of this work. TaeYoon Kim and Hyungsuk Lee assisted me with my calculations of the shear moduli. Alisha Siemienski was always ready to answer various questions I had about experimental procedures and theory. Sid Chung was incredibly helpful throughout the course of my research; he assisted me with the design of my silicon wafers, the patterning of my microchannels onto them, and the plasma treatment for bonding my PDMS chip. He also shared his vast knowledge of microfluidics and microfluidic fabrication. Vernella Vickerman offered useful advice and collaborated with me on a neutrophil transmigration experiment that is not presented in this thesis. Nur Aida Abdul Rahim, Peter Mack, Terry Gaige, and Nathan Hammond also offered helpful advice throughout the duration of my research. Furthermore, the rest of the Kamm Lab (a.k.a. the "Kammsters") provided a friendly and cooperative research environment that made my research experience enjoyable as well as education.

Also, members of collaborating laboratories were extremely helpful to this work. Dr. Richard Lee and Hayden Huang kindly assisted with the isolation of neutrophils, and

allowed me to use the equipment in Dr. Lee's laboratory. Jan Lammerding (Lee Lab) offered his help with the flow cytometry experiments. Dr. F. William Luscinskas, Richard Froio, and Gail Newton donated HL-60 cells and their excess neutrophils for use in my experiments. Jorge Ferrer (Lang Lab) taught me how to use the microscope and readily answered questions I had about imaging. Yu Yao (Dewey Lab) provided me with agents I needed for my experiments. Judith Su (So Lab) loaned the objective heater used to provide physiological temperatures in my experiments, and also donated the microbeads used to calibrate pressures in my setup.

Lastly, I would like to thank my parents, Paul and Nellie Hsu, my brother and sister, Kenneth and Melisa Hsu, and my friends for their compassionate support during this past year. Their encouragement and continuous prayers were invaluable to the completion of this work.

1.0 INTRODUCTION

1.1 Background

Neutrophils, also known as polymorphonuclear leukocytes (PMN), play a vital role in the primary human immune response to tissue injury and infection. Produced in the bone marrow, only a very small percentage (~3%) of the total number of neutrophils in the body is present in the circulation; the majority remains sequestered in the bone marrow, likely for storage purposes. Nevertheless, neutrophils make up most of the white blood cell population in the blood (approximately 50-70%). Once released from the bone marrow, PMNs travel through the circulation for 7-10 hours. At this point, neutrophils may become activated, initiating their migration into adjacent tissue, where the average neutrophil lifespan is no more than a few days. [1] In addition, neutrophils are terminally differentiated, enabling them to devote their resources to their immune responsibilities instead of cell division.

1.1.1 Neutrophil Morphology

Along with eosinophils and basophils, neutrophils belong to the granulocytic family of cells. As their name implies, granulocytic cells have a granulated cytoplasm, containing granules that aid in the digestion and elimination of bacteria during the immune response. Neutrophil granules typically range in size from 0.1-0.8 μm in diameter, [2, 3] and are classified as either azurophil or specific granules. Azurophilic granules are the larger and denser of the two, and contain enzymes (such as peroxidase and lysozyme) that assist in killing phagocytosed microorganisms. The smaller, rod-shaped specific granules contain the enzymes collagenase and lysozyme, as well as the bacteriocidal agent lactoferrin. [1]

Additionally, characteristic of neutrophils are their multilobed, segmented nuclei, as seen in Figure 1.1 below. The segments are connected by thin strands of chromatin, and the resulting morphology serves an important purpose in the cell's physiologic actions. To migrate to sites of infection, neutrophils must squeeze through endothelial cells that line the circulatory vessel wall. With their segmented nuclei, neutrophils are able to more easily accomplish this process of transmigration, contributing to their being among the first of the immune cells to arrive at sites of inflammation.

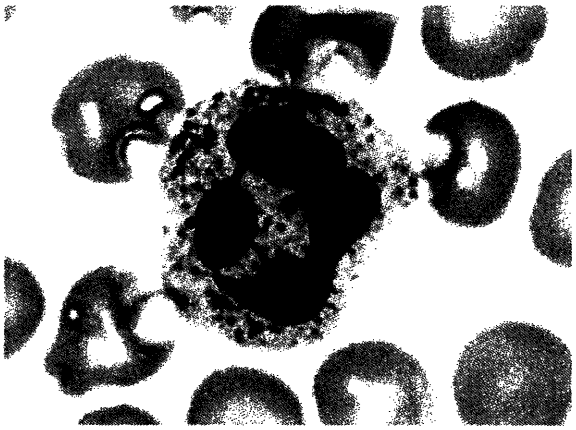

Figure 1.1: Neutrophil image.
This neutrophil was stained with a Wright Giemsa stain, giving the segmented, multilobed nucleus a purple tint. (Adapted from [4].)

Another morphological feature of neutrophils that renders them amenable to the deformations they experience is the folding of their membranes. The cell, its nucleus, and its numerous granules exhibit membranous folds; scanning electron microscopy reveals the numerous folds that exist on the cell membrane (Figure 1.2). As the neutrophil squeezes between or through endothelial cells or through a narrow capillary, these folds provide the additional surface area needed by the neutrophil and its constituents as they deform. Nonetheless, the membrane surface area remains constant, setting an upper bound for both deformation and swelling. [5] Furthermore, the outer membranous folds (microvilli) have

been suggested to enable the neutrophils to physically interact with endothelial cells through the ~0.5 μm glycocalyx layer that coats the apical surface of the endothelium. [6, 7]

Figure 1.2: Scanning electron microscopy (SEM) of neutrophil.
In this SEM image, the folded membrane of the neutrophil can be seen as the cell migrates through the bone marrow endothelium. [8]

1.1.2 Cytoskeletal Structure

Like most cells, the neutrophil cytoskeletal network primarily consists of actin (at an estimated concentration of 200 μM, [9] along with much lower concentrations of intermediate filaments and microtubules. [10] In the resting state, approximately 60-70% of the actin in neutrophils exist in the monomeric, globular form (G-actin), [11] and the cell takes on a roughly spherical shape, with an average diameter of 6.8 μm. [12] Upon neutrophil activation by chemoattractants like formyl-methionyl-leucyl-phenylalanine (FMLP), the actin cytoskeleton undergoes dramatic changes; in a dynamic process involving both actin depolymerization and polymerization, net G-actin content decreases by 26.5%, while the net amount of polymerized, filamentous actin (F-actin) experiences a two-fold increase. [13] Accompanying these changes are changes in cell shape and a redistribution of F-actin, particularly into the pseudopods at the leading edge of the neutrophil. [14]

1.1.3 Neutrophils in the Inflammatory Process

As one of the immune system's first responders to infection, neutrophils migrate to sites of inflammation within thirty minutes of injury onset. Much of this highly complex process remains to be elucidated, yet research in the past two decades has given tremendous insight into the mechanisms by which neutrophils reach the inflammation site.

Emigration of neutrophils into tissue is a multi-stage process (see Figure 1.3) that primarily occurs in the postcapillary venules. Upon entering this region of the vasculature, neutrophils are pushed towards the vessel wall by flowing red blood cells (RBC), which exist at a much higher concentration in the blood than that of neutrophils. Near the wall, neutrophils are able to engage in a process known as "neutrophil rolling," in which they weakly adhere to endothelial cells through interactions between selectin membrane proteins on both cells (L-selectin on neutrophils; P- and E-selectin on endothelial cells). Forces imposed on the neutrophil by the flowing blood push it forward along the endothelial wall as it "patrols" for a nearby infection. In inflamed tissues, bacterial byproducts cause the upregulation of P- and E-selectin on nearby endothelial cells, resulting in increased rolling. [15]

Yet increased neutrophil rolling alone is insufficient for transmigration; for neutrophils to migrate into the tissue space, integrins on the neutrophil surface must first be activated to allow for firm adhesion to the endothelial wall. Two β_2-integrins in particular – CD11a/CD18 (also referred to as LFA-1, or $\alpha_L\beta_2$) and CD11b/CD18 (Mac-1, or $\alpha_M\beta_2$) – have been implicated in this process. [16-18] In the normal state, these integrins exist in an inactive conformation, unable to strongly bind to constitutively expressed surface proteins on the endothelium, such as ICAM-1, and thus preventing non-specific binding. Near the site of infection, however, endothelial cells are stimulated to express chemokines (such as

PAF [19] and IL-8 [20]) on their apical surface, which, upon contact with a rolling neutrophil, will transduce a signal that subsequently results in a conformational change in certain integrins. For instance, work by Shamri et al. has shown that immobilized chemokines on the apical surface of endothelial cells can trigger a conformational change in LFA-1, from a bent (inactive) state to an extended (partially activated) one. [21] For activation of LFA-1 to be completed, it has to immediately bind to ICAM-1 after extension. This, along with association of the integrin to the focal adhesion protein talin, results in firm adhesion and cell arrest on the endothelium.

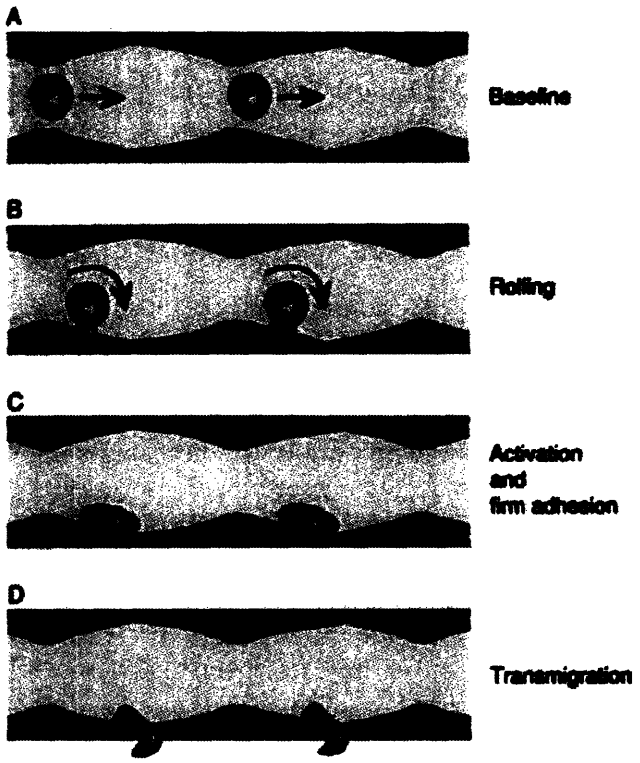

Figure 1.3: Endothelial cell – neutrophil interaction cascade in the inflammation process. (A) After release from the bone marrow, neutrophils travel through the arteriole circulation remaining relatively non-adherent to the vessel wall. (B) Once the neutrophils enter the post-capillary venules, they travel along the endothelial wall in a selectin-mediated process termed "neutrophil rolling." Approximately 100 μm from a site of infection, upregulation of E-selectin on endothelial cells is induced by cytokines from the infection site, resulting in increased rolling. (C) Once the neutrophil reaches the vessel region closest to the site of infection, chemokines on the endothelial surface induce conformational changes in integrins on the neutrophil, activating them to bind to ICAM-1 on endothelial cells and firmly adhere to the surface. (D) After the neutrophil arrests on the endothelium, a chemotactic gradient is required for transmigration to occur. If such a gradient is present, the neutrophil will migrate through the cell layer and up the gradient towards the inflammation site. [18]

Given the right conditions (flow-imposed shear stress [22], chemotactic gradient [23]), the arrested neutrophil will migrate through the endothelial layer, as well as through the layer of pericytes that surround the blood vessel, in a complex and coordinated process called diapedesis. [24] Remarkably but not surprisingly, the emigration process is quite selective; endothelial cells ensure that only the appropriate cells are getting through the vessel wall, thereby preventing a deluge of irrelevant substances from hampering the immune response at the inflammation site. This selectivity is a result of interactions between several proteins on the neutrophil and on endothelial cell membranes, which serve to form tight seals around the migrating neutrophil. Over the past few years, the signaling pathways and relevant proteins of transendothelial migration have been elucidated (see Figure 1.4 for a schematic of these pathways). CD99 and PECAM-1 (or CD31) have been shown to form homophilic interactions during the transmigration process. [25, 26] Ostermann et al discovered that junctional adhesion molecule 1 (JAM1) at endothelial cell junctions is a ligand for LFA-1 on leukocytes, [27] and Ma et al have used real-time imaging to suggest that JAM1 plays a key role in forming a seal around the migrating neutrophil. [28] Additionally, the same method of real-time imaging has allowed for the visualization of VE-cadherin dynamics during transmigration; situated at endothelial cell junctions, it acts as a gatekeeper and encircles neutrophils as they migrate through. [29]

Interestingly, neutrophils have been observed to migrate not only at cell-cell junctions (known as paracellular transmigration), but also through the body of an endothelial cell (transcellular transmigration). The latter had only been observed *in vivo* [30] until recently [31], and further suggests the active role that endothelial cells play in the migration process. One of the earlier studies of cellular events during transmigration found that the neutrophil adhesion and transmigration process coincide with increased levels of intracellular

calcium in the endothelial cells, [32] an increase that is a requirement for efficient transmigration. [33] More recent work has investigated endothelial signaling in neutrophil diapedesis, [34, 35] but the cellular processes involved in the complex act of transcellular transmigration still remain largely unknown.

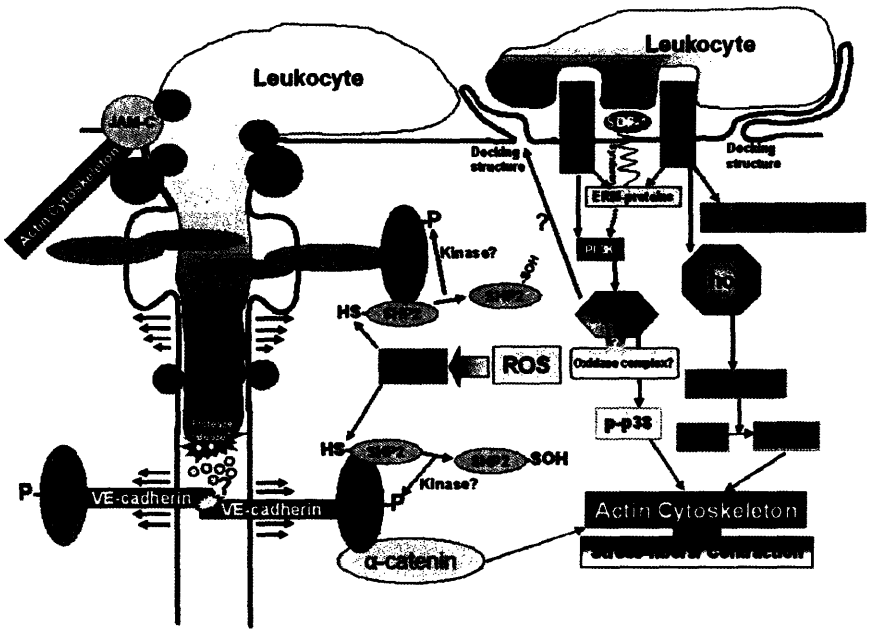

Figure 1.4: A schematic presentation of the signaling processes and proteins involved in leukocyte transendothelial migration. [33]

Lastly, once in the tissue, chemotactic gradients guide the neutrophils to the sites of inflammation, where they can carry out their defensive functions. Upon reaching a site, they can employ various mechanisms by which they can neutralize pathogens. Like macrophages, neutrophils are phagocytic cells; with the use of pseudopod extensions from their membranes, neutrophils engulf bacteria into structures known as phagosomes, which then fuse with granules in the cell that digest and eliminate the bacteria. Additionally, neutrophils can release reactive oxygen intermediates (ROI), cytokines, and proteolytic enzymes that help to kill foreign pathogens.

1.2 Studying the Mechanical Behavior of Neutrophils

The study of neutrophils offers the advantage of investigating the properties of cell that normally exists in isolation. Studies of adherent cells, such as fibroblasts and endothelial cells, are often complicated by the need to understand the numerous and dynamic interactions between the cell and the matrix to which it is adhered. Neutrophils, on the other hand, flow through the circulatory system unbound to a matrix, and while the migration process results in neutrophil interaction with cells and matrices in the tissue, studying the neutrophil in isolation still allows for relevant insight into the physiological properties of the cell, at least during the time leading up to endothelial adhesion. Several experimental methods have been used to uncover the mechanical properties of neutrophils.

1.2.1 Micropipette Aspiration

A classical experiment used to study the mechanical behavior of the passive neutrophil is micropipette aspiration, in which a micropipette is placed in close proximity to a resting neutrophil (see Figure 1.5). A negative pressure drop is imposed inside the micropipette, such that the neutrophil is trapped at the mouth; decreasing the pressure beyond this threshold pressure results in further deformation of the neutrophil into the micropipette. After removing the imposed negative pressure, the neutrophil is released from the pipette and eventually recovers its original spherical shape.

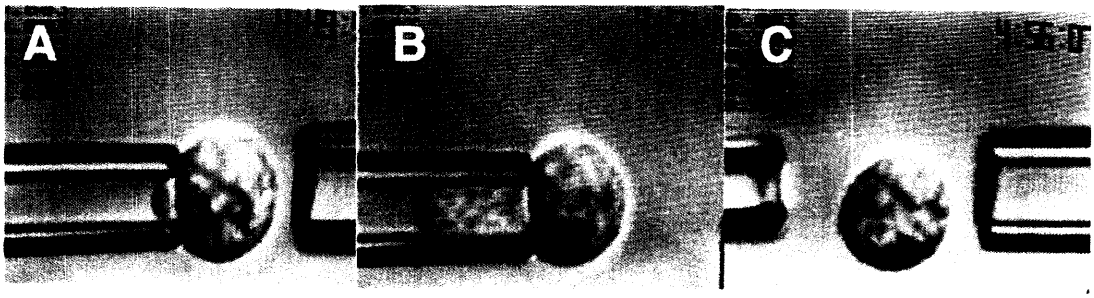

Figure 1.5: Micropipette aspiration of neutrophils.
(A) Imposing a negative pressure in the pipette equal to the threshold pressure traps the neutrophils at the pipette tip, with a hemispherical portion of the cell inside the pipette. (B) Decreasing the pressure beyond the threshold pressure results in further deformation into the pipette. (C) The neutrophils recovers to its original spherical shape after being released from the pipette.
(Pipette caliber: 3.4 um Figure modified from [36].)

Micropipette aspiration of neutrophils has helped to reveal elements of their complex rheology. Upon entering the micropipette, the neutrophil undergoes an instantaneous deformation, characteristic of an elastic material. After it is released from the pipette, however, it exhibits a viscoelastic, time-dependent recovery of its original shape. Early attempts to model this mechanical behavior considered the cell to be a homogeneous standard viscoelastic solid, [37, 38] and while these models were able to capture various characteristics, the neutrophil's non-homogeneous structure called for a more complex description.

More recently, a compound drop model description of the neutrophil has become prominent in the area of leukocyte modeling. [39] It consists of three layers: a thin cortical shell (with persistent isotropic surface tension), a viscoelastic or viscous interior (cytoplasm), and an inner core (nucleus). Unlike the models that had preceded it (such as the Maxwell liquid model with constant cortical tension [40], and the power-law fluid model [41]), the compound drop model is able to capture the rapid initial recoil phase of recovery without having to continuously change the material properties of the cell. This model has thus been shown to be more representative of leukocyte mechanical behavior

than the prior, simpler models. Yet it still has its shortcomings: for one, the shape of the neutrophil's segmented nucleus is not explicitly represented in the compound drop model's core. Experiments performed to validate the compound drop model for neutrophils made use of lymphocytes, which have a symmetrical, non-segmented nucleus. Thus, while many features of the neutrophil behavior in the micropipette aspiration experiment are explained in the compound drop model, there remains much room for improvement in the modeling of these complex cells.

1.2.2 Optical Trapping

The development of the laser optically trap has proven to be a valuable advance in our ability to make rheological measurements on cells. Optical trapping, often referred to as "optical tweezers," has been used to apply controlled picoNewton level forces onto cells via beads adhered to their surfaces. This method has been used, for example, to study the deformability of erythrocytes, [42] and subsequently, the increased erythrocyte stiffness that results from the onset of malaria. [43]

Using this technique, Yanai et al. measured the intracellular elasticity and viscosity of migrating neutrophils. [44, 45] Trapping intracellular granules within different regions of the cell (leading edge, body, and trailing edge), they applied both oscillatory and stepwise forces onto the granules, and measured their subsequent amplitudes or displacements. Results from the experiment showed significantly different stiffness values between the leading edge (pseudopodal region) and the body/trailing edge of the locomoting neutrophil, with respective stiffness values of ~5 Pa and ~1 Pa (using a timescale of 100 ms). Longer timescales of roughly 10 s produced lower stiffness values, in the range of 0.04 – 0.7 Pa according to their method.

1.2.3 Particle-Tracking Microrheology

A major disadvantage of many mechanical measurement methods is their active nature; experiments such as AFM and cell poking disturb the cell, making it difficult to determine the properties of the cell in its passive state. One method that has been used to make passive measurements of the mechanical properties of cells, particularly neutrophils, [46] is particle-tracking microrheology. This technique, developed by Mason et al. [47, 48] extrapolates the frequency-dependent complex shear modulus $G^*(\omega)$ from the time-dependent mean square displacement $\langle \Delta r^2 \rangle$ of particles within the cell. Assuming that the internal composition of the cell is a viscoelastic material, particle-tracking microrheology allows for a passive measurement of the storage ($G'(\omega)$) and loss ($G''(\omega)$) moduli of cells.

Neutrophils are particularly amenable to particle-tracking measurements of their mechanical properties because of the granules found in their cytoplasm. The motions of these granules, which are approximately spherical in shape and nearly constant in diameter, can be tracked, their time-dependent mean square displacement measured, and the cell's complex shear modulus extracted. In this study, multiple particle-tracking microrheology is used to determine the effects of mechanical deformation on the neutrophil's mechanical properties.

1.3 Neutrophil Response to Stimuli

1.3.1 Activation by Biochemical Agents

When exposed to biochemical agents involved in the inflammatory process, such as cytokines (tumor necrosis factor-α, or TNF-α), chemokines (interleukin-8, or IL-8), and FMLP, neutrophils are activated to migrate. Subsequently, the cells begin to form

pseudopods along their periphery and attain an irregular shape, losing the spherical shape characteristic of their passive state (see Figure 1.6)

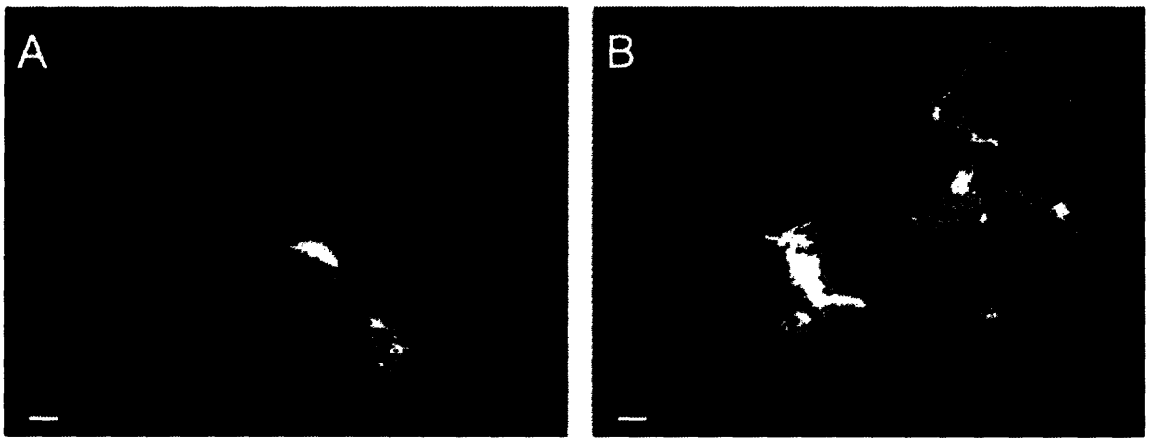

Figure 1.6: Increase in F-actin content upon stimulation with FMLP.
Rat neutrophils isolated from the circulation were stained with rhodamine-phalloidin to visualize F-actin using a confocal microscope. *A*: Non-stimulated cells were generally spherical, with some cells exhibiting pseudopod formation. F-actin content was found to be high in these newly formed pseudopods. *B*: After stimulation with FMLP, neutrophils attained a distorted, irregular shape. F-actin content in the center of the cell was seen to decrease, while high F-actin content was seen in the pseudopod regions.
Scale bar: 2 μm. (Adapted from [49])

Studying the characteristics of activated neutrophils is a difficult task: upon stimulation, neutrophils can behave in a variety of ways. Nevertheless, some general properties of activated cells have been uncovered. After stimulation with FMLP, neutrophils have been shown to be markedly stiffer and more likely to be retained in the pulmonary vasculature. [50] This stiffening can likely be explained by an increase in F-actin polymerization that is observed in human neutrophils within 10 s of being exposed to FMLP. [51] Similarly, rat neutrophils respond to FMLP challenging with an increase in F-actin formation, as well as increased sequestration within the pulmonary capillaries (neutropenia). [49]

1.3.2 Response to Mechanical Deformation

Neutrophils in the microcirculation must undergo some degree of mechanical deformation in order to traverse through systems such as the muscle, renal, pulmonary capillary microvasculature. While neutrophils have diameters which range from 6 – 8 μm, pulmonary capillaries have been shown to have diameters that range from 2 – 15 μm. [12] Thus, in traveling from the arteriole to venule sections of the circulation, neutrophils are subjected to mechanical deformation through the capillary bed.

Physiological levels of mechanical deformation have been shown to stimulate functional changes in neutrophils. [52] After being deformed through 3- and 5 μm pore filters, the cells exhibited a transient increase in their cytosolic free calcium concentration that peaked 30 seconds after deformation. Also, the neutrophils that underwent a larger degree of deformation (through the 3 μm filter) expressed higher levels of the CD11b/CD18 adhesion protein. Further research found that deformation also increases neutrophil adhesiveness to ICAM-1, an adhesion molecule found on endothelial cells, due to the upregulation of CD11b/CD18. [53] The combined results of these studies hints at a possible role for the mechanical deformation experienced by neutrophils in small capillaries; the increased adhesiveness to the vessel wall stimulated by deformation could explain why neutrophils tend to transmigrate primarily in the postcapillary venules.

Additionally, recent work has revealed that neutrophils exhibit interesting biomechanical and cellular responses to mechanical deformation. [46, 54] First, deformation causes a significant drop in both the shear and loss moduli of the cell; within approximately 10 sec after deformation, these properties are reduced by roughly half their initial values. Within one minute, however, both the shear and loss moduli recover to nearly their initial values. This change in the viscoelastic properties of the cell is possibly due to a

deformation-induced disruption of the cytoskeleton, but it remains unclear whether these cytoskeletal events involve the rupture of binding proteins between actin filaments or the depolymerization of the actin filaments. Secondly, above a threshold deformation rate, neutrophil activation was observed, with newly-formed, granule-free pseudopods seen projecting from the deformed neutrophil. This activation is dependent on the deformation rate, exhibiting an inverse relationship. These two responses are thought to be independent of each other, but the pathways involved have not yet been discovered.

Furthermore, the same work revealed the dynamic effects that mechanical deformation has on the neutrophil cytoskeleton, namely F-actin. After being deformed through a 3 μm pore filter, neutrophils exhibited an initial drop in F-actin content to approximately 80% of its initial value. Within 1 minute, however, this value recovers to nearly its initial level (95%). This drop-and-recovery response of F-actin content resembles that of the neutrophil moduli values described above, suggesting an important role for cytoskeletal rearrangement in the mechanical properties of the cell.

1.3.3 Analogous Responses in Other Cell Types

Interestingly, similar responses to deformation have been observed in another cell type: human fibroblasts. Work by Pender and McCulloch has shown that human gingival fibroblasts exhibit dynamic changes in F-actin content in response to substrate stretching. [55] Quantifying the F-actin content with FITC-phalloidin, they found that 10 s after stretching, F-actin content was reduced by 50%. Additionally, F-actin increased to approximately 150% of its initial value 50 s after stretching, and recovers its initial value at approximately 80 s. The addition of EGTA (chelator of extracellular Ca^{2+}) and pertussis toxin (inhibitor of GTP-binding proteins) in separate experiment altered the

normal actin response, suggesting roles for both calcium influx and GTP-binding proteins in fibroblast mechanotransduction.

Although the experiments with fibroblasts measured F-actin content rather than shear and loss modulus values, the initial drop and subsequent recovery resemble the trend seen in the neutrophil response to deformation. As actin is a significant component of the cytoskeleton, which in effect gives the cell its mechanical characteristics, a comparison between F-actin content and modulus values is conceivable and is commonly suggested in the literature. [56] Calcium and GTP-binding proteins have been implicated in the cytoskeletal response of fibroblasts, yet similar experiments have not been performed on neutrophils undergoing mechanical deformation.

1.3.4 Calcium Activity in Neutrophil Activation

Cytosolic calcium is an important second messenger in numerous signaling pathways within cells, [57] where the endoplasmic reticulum holds stores of Ca^{2+} ions for quick release into the cytoplasm upon receiving appropriate cues. Extracellular calcium can also enter the cell through ligand-gated or stretch-activated ion channels, such as those found in endothelial cells. [58] Although it is clearly an important part of proper cell function, the role of Ca^{2+} in the cytosol of unstimulated and stimulated neutrophils is not completely understood.

Previous work by others has examined the dynamics of neutrophil Ca^{2+} levels upon stimulation with chemoattractants, particularly FMLP. Exposure to FMLP has been shown to induce a dramatic but transient increase in $[Ca^{2+}]_i$, which recovers to resting values within minutes. [59, 60] This rise in cytosolic Ca^{2+} levels was previously thought to initiate the signal for the concomitant occurrences of increased actin polymerization and activation

upon FMLP stimulation. Yet other work, which buffered and/or depleted intracellular Ca^{2+}, found that actin polymerization and cell activation (as indicated by chemotaxis, exocytosis, or superoxide generation) were independent of a rise in $[Ca^{2+}]_i$. [59, 61, 62]

In addition to chemical stimulants, mechanical deformation of neutrophils has also produced transient rises in $[Ca^{2+}]_i$. As mentioned earlier, Kitagawa et al. showed that deformation through micrometer-sized pores produced an increase in $[Ca^{2+}]_i$ that peaked 30 seconds after deformation. [52] This increase was not as sharp as that seen after FMLP stimulation, but significant nonetheless. Also, Laffafian and Hallett "poked" neutrophils with a blunt micropipette, inducing a small-scale membrane deformation. [62] Within seconds after mechanically perturbing the cell membrane, they noticed a local increase in Ca^{2+} levels.

The response of intracellular Ca^{2+} to both chemical and mechanical stimuli suggests that it plays an important role in the neutrophil's response. Exactly what this role is, however, remains unclear.

1.4 Soft Lithography Microfabrication for Biological Studies

Over the past several years, the use of soft lithography microfabrication in the fields of biology and medicine has burgeoned. [63, 64] The process of microfabrication takes advantage of technology that has been used in the manufacturing of semiconductors for over 30 years to produce systems on the micrometer size scale. Among the many advantages of the microfabrication method is its ability to accurately reproduce small geometries, allowing researchers greater control over their experiments.

Soft lithography microfabrication couples this size control with a remarkable flexibility to design biological systems. From "lab-on-a-chip" biosensors to cell

manipulation devices, numerous possibilities for experiments have arisen due to the advent of this fabrication method. Unlike the photolithographic methods primarily used to produce microfabricated products, soft lithography microfabrication (after its initial step) does not require elaborate laboratory facilities or equipment and is thus relatively inexpensive and efficient. The process begins with the patterning of a positive relief of the design onto a silicon wafer using the methods of photolithography, which allows for geometric resolution of approximately 1 μm. Once the pattern is made, an elastomer is poured onto the wafer and cured, producing an elastomeric mold or a stamp that can be used to pattern chemicals onto various surfaces.

The elastomer most commonly used in biological experiments is polydimethylsiloxane (PDMS); as an optically transparent (wavelengths between 230-700 nm), nontoxic, and gas-permeable elastomer, it is highly compatible with imaging of biological samples without undesired surface interactions. Compared to the etching processes of microfabrication, the replica molding of PDMS is fast and simple. PDMS also bonds well and easily to surfaces such as glass and other PDMS layers, providing tight seals that prevent leakage of fluid.

One application of soft lithography microfabrication has been the study of the forces exerted by endothelial cells. Tan et al. produced a pattern of microneedle-like elastomeric posts, onto which they seeded endothelial cells. [65] Once the cells had adhered to the top surfaces of the posts and spread, the forces exerted by the cells at different regions of the cell body were extrapolated from the deflection of each post. With this assay, the subcellular distribution of forces throughout the cell could be determined.

Additionally, a common application for soft lithography microfabrication is in the production of microfluidic channels and networks. [66] The micrometer-sized patterns that soft lithography is capable of producing render the method amenable to the creation of microchannel systems, which offer many experimental advantages: small sample volumes, use of fewer cells, potential for high-throughput parallel designs, and shorter reaction times. Using this technology, groups have developed microfluidic flow cytometers, immunoassay systems, capillary electrophoresis devices, and combinatorial screening devices, among others.

In this study, a microfluidic channel produced by soft lithography microfabrication is used to study the rheological response of single neutrophils to mechanical deformation. Unlike the commonly used method of micropipette aspiration, which can have marked variability due to various micropipette dimensions, the accuracy of replica molding provides us with a repeatable test that can be performed on multiple single cells.

1.5 Physiological Significance of the Present Study

After their release from the bone marrow, circulating neutrophils first encounter the pulmonary microvasculature, a complex network of 50-100 capillary segments that circulating cells must deform through to travel from the arterial to the venous side of the pulmonary circulation. [67] While erythrocytes readily deform through these narrow vessels (with diameters as small as 2 μm), neutrophils have a relatively low deformability; as a result, the pulmonary microvasculature contains a high concentration of neutrophils, with 75% of all intravascular neutrophils residing in this system. [68]

This margination of cells in this region occurs in the normal physiological state, and as the lungs are constantly exposed to foreign pathogens inhaled during normal breathing, it makes sense to have a high concentration of immune cells readily available to combat such bacteria.

Yet the sequestration of neutrophils in the pulmonary system can pose a serious, life-threatening problem in the pathological state. For instance, patients with acute myeloid leukemia have been shown to have leukocytes with decreased deformability. [69] A condition known as leukostasis results, in which leukocytes aggregate in the vasculature at supraphysiological levels. Leukostasis can have tragic consequences: respiratory failure (such as in acute respiratory distress syndrome, or ARDS), intracranial hemorrhage, myocardial infarction, metabolic abnormalities, etc. The excessive margination and activation of these immune cells can cause them to carry out their defensive functions against the body's own tissues, which results in the recruitment of more white cells in a positive feedback loop manner. Overall, however, leukostasis remains poorly understood, and further research is needed to elucidate its mechanisms.

1.5.1 Objective

The results of previous studies have suggested that neutrophils do not merely passively deform through narrow capillaries; rather, active intracellular responses to deformation appear to occur, possibly facilitating neutrophil transit. For instance, Kitagawa et al. revealed that upregulation of adhesion receptors, as well as transient rises in $[Ca^{2+}]_i$, were part of the deformation response. [52] Yap and Kamm have shown that physiologic mechanical deformation can produce dynamic rheological changes in

neutrophils, consisting of initial drops in stiffness and viscosity that subsequently recover towards their pre-deformation values. Concurrently, the F-actin content of neutrophils decreased immediately following deformation, suggesting the occurrence of actin depolymerization events. Additionally, they found that the same mechanical stimulus can induce neutrophil activation. [46, 54, 70]

Considering these observations, neutrophils presumably respond to deformation in an active manner that assists them in repeatedly negotiating the small diameters of microvascular networks. Impairment of such processes may result in decreased cell deformability, leading to excessive sequestration of neutrophils in these microcirculatory systems. Among the many implications of this pathological margination of neutrophils are destructive inflammation, produced by the overabundance of activated cells, and tissue ischemia, resulting from the obstruction of capillary blood flow by rigid leukocytes. The key first step to preventing such conditions is understanding the cellular events that occur in response to deformation. Yet, the signaling interactions involved in this response are currently unclear.

This study aims to further the current understanding of the deformation response by determining whether a connection exists between the findings of Kitagawa et al. and Yap and Kamm. More specifically, it investigates the role of intracellular Ca^{2+} in the shear modulus and activation responses to deformation. With extensive evidence of calcium's ability to modulate the cytoskeleton, [71, 72] we hypothesize that the reported increase in $[Ca^{2+}]_i$ is a critical element of the observed biomechanical response of the neutrophil. Hopefully this work will provide insight that will help augment the treatments currently available for pathological inflammation and its related conditions.

2.0 MATERIALS AND METHODS

2.1 Neutrophil Isolation

In accordance with a protocol approved by the Brigham and Women's Hospital (BWH) Institutional Review Board (IRB) and the MIT Committee on the Use of Humans as Experimental Subjects (COUHES), approximately 30 mL of human venous blood was drawn from healthy volunteers at the BWH. The blood draw procedure involved venipuncture into syringes containing 3 mL of 0.1 M of sodium citrate, which served as an anticoagulant. After diluting the blood with 20 mL Hank's Balanced Salt Solution (HBSS), the diluted blood was split and carefully layered onto 10 mL of Ficoll-Paque PLUS (Amersham Biosciences, Uppsala, Sweden). Both tubes were placed in a centrifuge and spun at 1400-1500 rpm at room temperature for 30 min. This spin step separated the erythrocytes and neutrophils (pellet) from the monocytes and blood plasma, as shown in Figure 2.1 below.

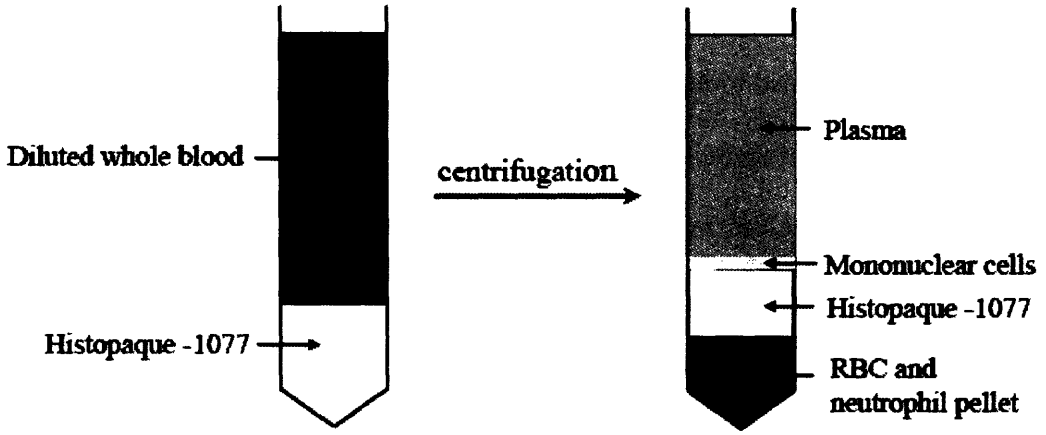

Figure 2.1: Schematic of separation layer contents after first step of neutrophil isolation. Figure taken from [54] with permission.

After spinning, approximately 10 mL of plasma was saved for later use, and the remaining supernatant (plasma, mononuclear cells, and Histopaque layer) were aspirated,

and the RBC/neutrophil pellet was resuspended in ~7 mL HBSS (without Ca^{2+} and Mg^{2+}) and ~15 mL 2% Dextran (Pharmacia Corp., Peapack, NJ) to create a 1:1 dextran solution . The tubes were left to sit at room temperature for 30 min, during which the RBCs sedimented at the bottom of the tubes. The neutrophil-rich supernatant was collected, diluted in HBSS, and spun down at 1400-1500 rpm for 5 min at room temperature. After aspirating the supernatant, the remaining pellet was exposed to 3 mL of cold water for 30 sec, to induce lysis of the remaining RBCs. Approximately 45 mL HBSS was quickly added after the 30 sec period to prevent the neutrophils from being lysed as well. The solution was then spun down again, resuspended in 10 mL of HBSS, and counted with a haemotocytometer. The cell suspensions contained > 95% neutrophils, and cells were used within 5 hours after the isolation was completed.

2.2 Calcium Chelation

To chelate intracellular calcium in neutrophils, the acetoxymethyl ester derivative of 1,2-bis(o-aminophenoxy)ethane-*N*,*N*,*N*',*N*'–tetraacetic acid, or BAPTA-AM, (Invitrogen, Inc., Carlsbad, CA) was added to neutrophils at a concentration of 3.5 μM In its original form, this calcium-chelating agent is non-active, uncharged, and can readily permeate the cell membrane. Once inside the cell, non-specific esterases within the cell cleave the lipophilic blocking groups, rendering the agent active and less likely to exit the cell.

Loading the chelating agent first required dissolving it in DMSO, followed by addition to the cell solution. The amount of DMSO present in the final loading solution was 0.035%. Neutrophils were incubated in the chelator loading solution for 20-30 minutes at 37°C, and then added to the macrofluidic setup for analysis. To differentiate the effects of

BAPTA-AM and its loading vehicle, DMSO, a control group of cells were exposed to a concentration of DMSO equivalent to that used to load BAPTA into the cells.

Extracellular calcium was also chelated for part of this experiment. The neutrophil isolation process involves the addition of citrate to freshly drawn blood. As an anticoagulant, citrate chelates calcium. To further ensure that extracellular calcium was not present in this portion of the study, ethylenediaminetetraacetic acid (Sigma-Aldrich, Co., St. Louis, MO), or EDTA, was added to the plasma saved from the isolation procedure, at a concentration of 2 mM. EDTA was added to the autologous plasma instead of directly to the cell solution because of its effect of lowering pH. Since the isolated neutrophils are washed several times in Ca^{2+}-free HBSS, it was assumed that the cell solution was already Ca^{2+}-free, and the only source of extracellular Ca^{2+} would be from the plasma. By adding EDTA solely to the plasma, the pH effects were minimized. Additionally, cells were suspended in a saline solution that lacked both calcium and magnesium.

2.2.1 Assessing the Effectiveness of Calcium Chelation Qualitatively

To determine if BAPTA-AM was in fact chelating intracellular Ca^{2+}, Fluo-3-AM (Invitrogen Corp., Carlsbad, CA) was loaded into both untreated and BAPTA-treated neutrophils (2mM, 30 min at 37°C). Inside cells, Fluo-3 does not fluoresce until it binds to Ca^{2+}, after which it fluoresces maximally at ~525nm. Untreated and BAPTA-treated cells, both loaded with Fluo-3, were visualized under a fluorescent microscope (Eclipse TE300, 40×, Melville, NY) to observe the effects of BAPTA treatment on Ca^{2+} levels inside cells.

2.2.2 Quantifying the Calcium Levels in BAPTA-treated Neutrophils

Fluo-3 does not enter all cells equally; consequently, there are fluctuations in the amount of fluorescence seen between cells, preventing quantification of Ca^{2-} levels. To circumvent this deficiency, another Ca^{2-} dye, Fura Red (Fura Red AM, Invitrogen Corp., Carlsbad, CA) was co-loaded with fluo-3 (30 min at 37°C), at a concentration of 4mM. Fura Red is typically used with Fluo-3 to quantify intracellular Ca^{2+} levels, [73, 74] and the ratio of Fluo-3/Fura Red is taken to be the measure of $[Ca^{2+}]_i$. Fura Red is spectrally different from Fluo-3: upon excitation at 488nm, Fura Red emits maximally at ~650nm when not bound to Ca^{2+}. Upon binding to Ca^{2+}, Fura Red's fluorescence is reduced dramatically. Since both dyes are assumed to be present at approximately equal levels inside each cell, the Fluo-3 / Fura Red ratio should remain relatively consistent from cell to cell, and provides a high sensitivity, low noise measure of $[Ca^{2-}]_i$. [75]

Two groups of cells were co-loaded with Fluo-3 and Fura Red: untreated and BAPTA-treated (3.5 μM). After incubating the cells in the appropriate loading solution, the cells were subjected to flow cytometry analysis (Cytomics FC500, Beckman Coulter, Inc., Fullerton, CA). Untreated cells were analyzed for autofluorescence, serving as a negative control. As a positive control, both sets of cells were stimulated with FMLP (200nM) immediately before flow cytometry analysis, as FMLP has been shown to elicit an increase in $[Ca^{2+}]_i$. [76] Fluorescence was measured within 30 seconds after FMLP addition. Additionally, the stimulated cells were again analyzed several minutes after FMLP addition, to inspect the transience of the stimulated response. All analyses were performed at 23°C, and 30,000 cells were examined during each experimental run.

2.3 Design and Microfabrication of Experimental System

2.3.1 Patterning the Channel Design onto a Silicon Wafer

The microfluidic system used in the experiment was designed to allow neutrophils to experience deformations similar to those experienced in the pulmonary microcirculation. To accomplish this, the basic design was comprised of two reservoirs connected by a microchannel, which had dimensions similar to those of pulmonary capillaries. This design, which was drawn in AutoCAD (Autodesk, Inc., San Rafael, CA), is shown below in Figure 2.2A.

Three different designs were created for the microchannel, and they can be seen in Figure 2.2B below. The first was a straight channel with constant dimensions throughout its length. The next two designs were meant to solve problems experienced with clustering of cells near the channel entrance. One consisted of a graduated entrance for the cell into the channel, with an initial entrance width that was approximately twice the size of the rest of the channel. The other design was similar, except for an asymmetric positioning of the graduated portion of the channel entrance.

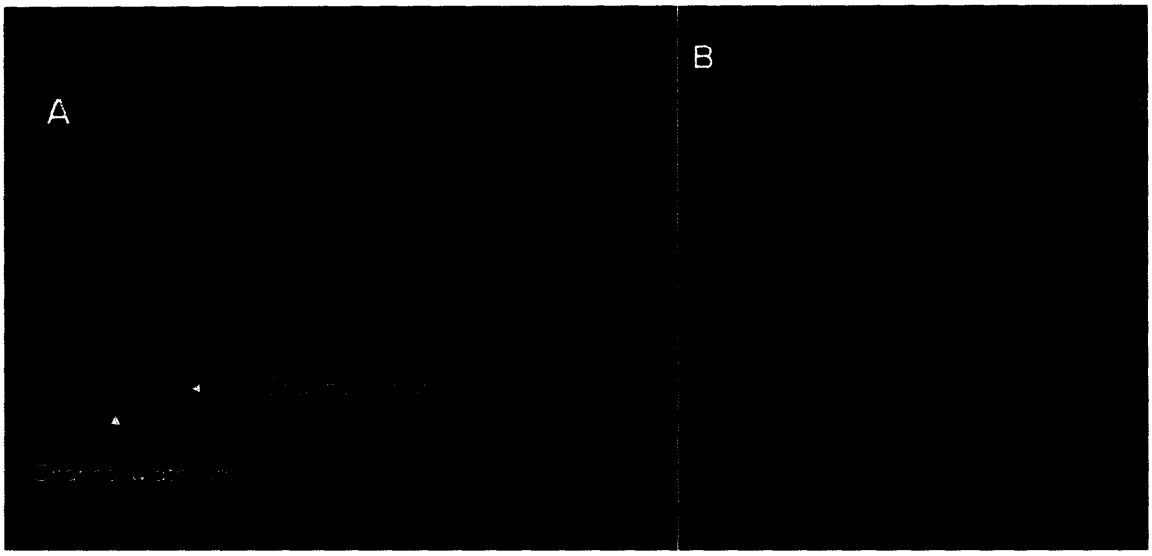

Figure 2.2: Design of microfluidic device.
(A) The design of one "chip" includes two elliptical reservoirs, which are 1mm x 3.5 mm in size, connected by a microchannel of varying widths (3 – 7 μm), heights (2 – 3 μm), and channel entrance designs. The chip has dimensions of 15 mm x 10 mm. (B) The three channel entrance designs include: (top) constant width, (middle) graduated entrance, and (bottom) asymmetric graduated entrance. (Images courtesy of S. Chung.)

To allow for flexibility in the experiment, many different combinations of channel width and channel type (straight, graduated, or asymmetric) were designed to be patterned onto the silicon wafer, from which the devices would be made. In this study, however, only the first channel design (straight) was used. Nevertheless, future experiments can make use of the other designs. The wafer design can be seen in Figure 2.3 below.

The design was fabricated onto chromium masks (Phototronics, Inc., Brookfield, CT) using a process known as two-level photolithography. [77, 78] The process begins with the spin-coating of a thin layer of SU-8 2002 photoresist (Microchem Corp., Newton, MA) onto a silicon wafer (Wafernet, Inc., San Jose, CA). The thickness of this first layer is desired to be approximately 2-3 μm, or the desired height of the microchannel. The coated wafer is then prebaked at 95 C for 2 minutes, and exposed to UV light for 11.5 seconds

through the first chromium mask (microchannel). To crosslink the SU-8 photoresist in the areas exposed to UV light, the wafer is postbaked at 95 C for 2 minutes.

Figure 2.3: Design of pattern on silicon wafer.
The design for a single wafer includes 36 chips, with 15 different designs of various combinations of channel width and entrance geometry. The boxes on the left and right sides of the design are for alignment purposes. (Image courtesy of S. Chung.)

To pattern the reservoirs onto the wafer, the wafer was spin-coated with SU-8 2015 to a thickness of approximately 15 μm, and pre-baked at 95 °C for 4 minutes. Using an alignment grid found on both chromium masks, the second chromium mask (reservoirs) was aligned over the patterned microchannels, and exposed to UV light for 20 seconds. The wafer was then post-baked for 3 minutes at 95 °C to cross-link the exposed regions. Afterwards, SU-8 developer (Microchem Corp., Newton, MA) was added on top of the

wafer for 5 minutes to develop the channel features. Lastly, the heights of the microchannels were measured with a Dektak 2 profilometer (Veeco Instruments, Woodbury, NY). A picture of a finished wafer can be seen in Figure 2.4.

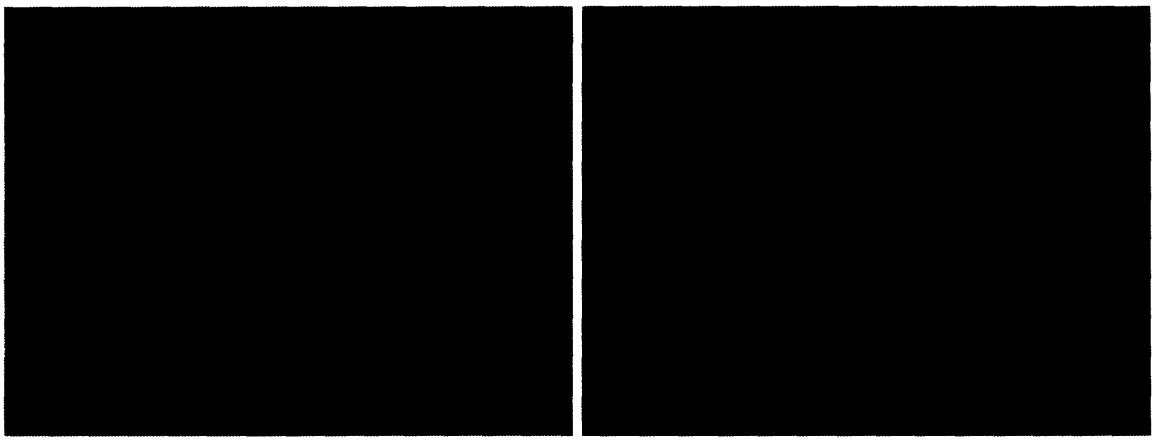

Figure 2.4: Microchannel-patterned silicon wafer.
Left: Full image of a silicon wafer with 36 microchannel systems patterned onto it.
Right: Close-up image of microchannels, as well as labeling system for individual channel characteristics (lower left hand corner of each rectangle). (Images courtesy of S. Chung.)

2.3.2 Production of PDMS Microchannel Chips

To prevent adhesion of PDMS to the wafers during the curing process, all master wafers were treated once with trimethylchlorosilane (Sigma-Aldrich, St. Louis, MO), which involves incubating the wafer in a Petri dish along with a few drops of trimethylchlorosilane.

PDMS was prepared by mixing a 1:10 (weight) solution of curing agent and PDMS prepolymer (SYLGARD 184 Silicone Elastomer Kit, Dow Corning, Midland, MI). After the solution was degassed for approximately 20-30 minutes to remove trapped air bubbles, the PDMS was poured on top of the master wafer and cured at 80°C for 2-3 hours. After the PDMS had cured, it was carefully peeled from the master wafer, and the desired chips were cut out. Images of the PDMS microfluidic channel and channel entrances can be found in

Figure 2.5. Two holes were bored in each reservoir with a 16-gauge adaptor needle to provide inlet and outlet ports for tubing.

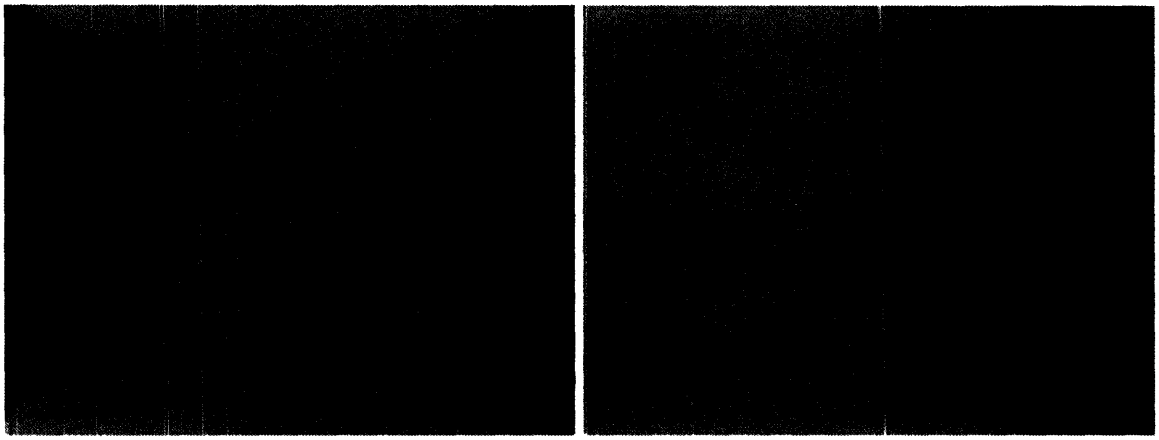

Figure 2.5: PDMS microfluidic system.
Left: An image of the microchannel connecting the upstream and downstream reservoirs, fabricated with PDMS. Right: A view of the channel entrance at higher magnification. (Images courtesy of S. Chung.)

2.3.3 Permanent Bonding of PDMS Chips to Coverslip

To complete the construction of the microfluidic system, the PDMS chips had to be permanently bonded to a glass coverslip. First, the coverslip was coated in PRIME Coat (Dow Corning, Midland, MI) to promote stronger adherence between the glass and PDMS. The coverslip was then spin-coated at 6000 rpm with a thin layer of PDMS, and cured at 80°C for 2-3 hours.

Using a plasma cleaner and sterilizer (Harrick Scientific Corporation, Ossining, NY), the PDMS chip and the coated coverslip were subjected to plasma oxidation for 1 minute. Immediately afterwards, the exposed surfaces were placed into contact, forming a permanent bond between the two pieces. A schematic of the entire chip production process, from photolithography to plasma treatment, can be seen in Figure 2.6 below.

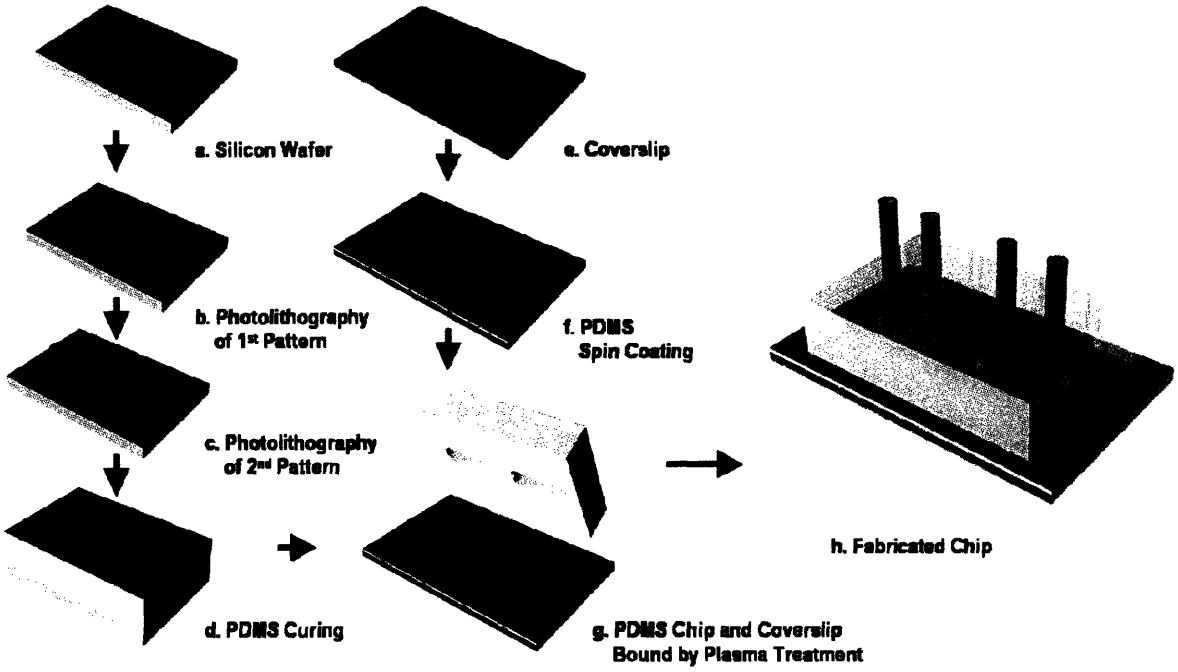

Figure 2.6: Schematic of chip production process.
The first step of the process involves spin-coating a (a) silicon wafer with SU-8 photoresist, to the desired height, *H*, of the first level. (b) The wafer is then exposed to UV light through the microchannel-patterned chromium mask and post-baked. (c) Next, a second layer of SU-8 is spin-coated onto the wafer, to a height of approximately 15 μm. The wafer is again exposed to UV light, this time through a different chromium mask with the reservoirs patterned on it, post-baked, and developed with SU-8 developer. (d) PDMS is poured onto the wafer and cured. (e) A glass coverslip is (f) coated with a thin layer of PDMS and cured. (g) Four holes are bored into the PDMS chip, and the chip is bound to the PDMS-coated coverslip by plasma treatment. Plastic tubing is inserted into each hole, producing (h) the final fabricated chip. (Figure courtesy of S. Chung.)

2.3.4 Setup of Macrofluidic System

Establishing a pressure differential across the microchannel to drive the flow of neutrophils through the channel required the use of a macrofluidic system (see Figure 2.7 for schematic). The upstream side of the channel consisted of three major components. A low-pressure upstream reservoir is mounted onto a linear slide (Rapid Advance Unislides, Velmex, Inc., Bloomfield, NY), capable of being moved vertically with millimeter-scale positioning. This low-pressure reservoir was used to establish a controlled pressure drop across the microchannel; the difference between its height and the downstream reservoir's height created the pressure differential across the channel. This low-pressure reservoir was

connected via a three-way valve to the PDMS chip, as well as a high-pressure upstream reservoir, mounted approximately 50 cm above the microfluidic system. Additionally, a syringe, used to purge air bubbles from the system as well as introduce neutrophils into the channel, was also connected to the PDMS chip. The downstream end of the channel consisted of two components: the downstream reservoir, which rested at a fixed height, and a syringe. The syringe on the downstream end was used to clear trapped air bubbles from this side of the microchannel. All components were connected to each other with plastic tubing (I.D. 0.5 mm) and 23-gauge adapter needles. Furthermore, the reservoirs had dimensions much larger than those of the microchannel (cm vs. μm), allowing for the assumption that the height of the fluid in each reservoir remained constant during the time-course of the experiment.

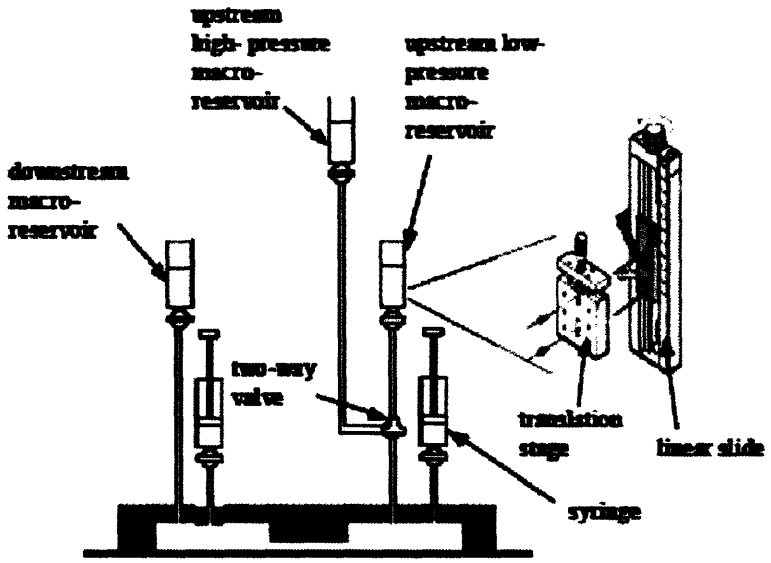

Figure 2.7: Macrofluidic system setup.
The schematic shows the reservoirs and syringes placed at the downstream (left side) and upstream (right) sides of the microchannel.
(Figure modified slightly from [54], with permission.)

2.3.5 Imaging Setup

To view the microchannel and entering neutrophils, the microfluidic system was mounted onto the stage of a differential interference contrast (DIC) microscope (Eclipse TE2000, Nikon, Inc., Melville, NY). The DIC microscope was equipped with an oil immersion condenser lens (N.A. 1.4) and a 100× / 1.4 N.A. Plan Apochromat objective lens. The objective was fitted with an objective heater (Bioptech, Inc., Butler, PA) that was set to 37°C. Using a video camera (CCD-100, Dage-MTI, Inc., Michigan City, IN), live video was recorded onto an SVHS cassette at 30 frames per second with a video cassette recorder (SVO-9500MD, Sony Corporation, New York, NY). The videos were transferred to a computer using a frame grabber card (Scion LG-3, Frederick, MD), and converted to digital format using Scion Image (Version 4.0.2, Scion Corporation, Frederick, MD) and ImageJ (Version 1.36b, National Institute of Health, Bethesda, MD). A schematic of the imaging setup can be seen below in Figure 2.8.

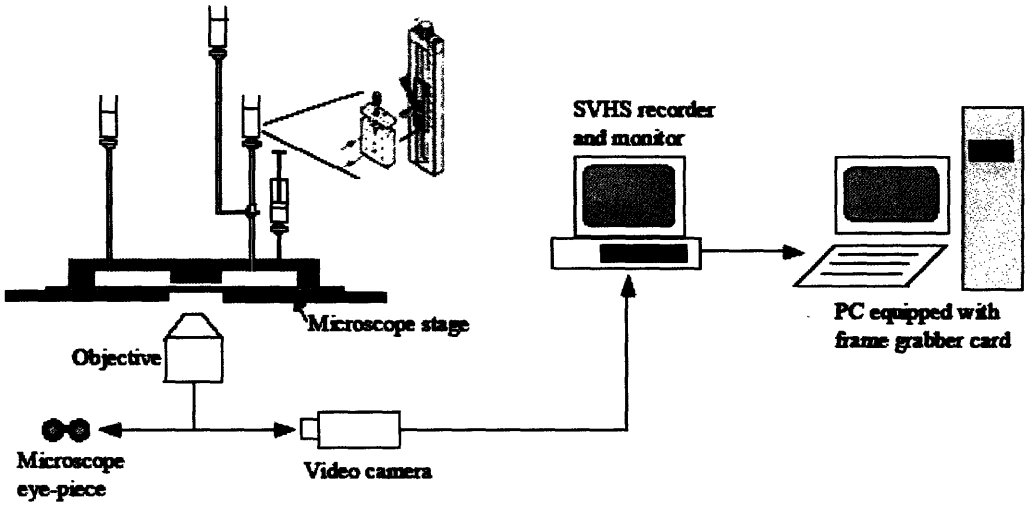

Figure 2.8: Imaging setup.
With the microfluidic system mounted on the microscope stage, the resulting image was split between the microscope eye-piece and the video camera. Live video was recorded onto an SVHS cassette, and subsequently transferred to a computer. (Figure from [54], with permission.)

2.3.6 Neutrophil Deformation Assay

Before each experiment, a 1% solution of Pluronic F108 ($PEO_{129}/PPO_{56}/PPO_{129}$ triblock copolymers, BASF Corp., Mount Olive, NJ) in Ca^{2+}/Mg^{2+}-free HBSS was injected into the microfluidic system, and incubated for 2 hours. Coating of the PDMS surfaces with this compound served to reduce adhesion between PDMS and the proteins on the neutrophil surface. After the incubation period, the microfluidic system was flushed with medium (Ca^{2+}/Mg^{2+}-free HBSS + 2% autologous plasma obtained from the neutrophil isolation process) for 15 minutes.

With medium in each of the three reservoirs, air bubbles were removed from the microfluidic and macrofluidic systems with the use of the syringe ports. Medium was drawn through the upstream and downstream sides of the microchannel with the syringes, using negative pressure to prevent high pressure from being applied to the microfluidic reservoirs.

To adjust the reservoirs for zero flow (and zero pressure drop) conditions through the microchannel, 0.5 μm yellow-green fluorescent beads (Molecular Probes, Eugene, OR) were added to the upstream microfluidic reservoir with the syringe. With the three-way valve open to the high-pressure reservoir, the beads flowed rapidly through the microchannel into the downstream reservoir. After a sufficient number of beads were near the channel, the valve was switched, such that the channel was exposed to the low-pressure upstream reservoir. The height of this reservoir was adjusted until a bead was approximately stationary inside the channel, and this height served as the zero pressure drop height. During the course of each experiment, this zero pressure drop height was re-measured, to account for any possible changes that may have occurred during the course of the experiment.

Setting the three-way valve to the high-pressure reservoir, the beads were mostly cleared from the microfluidic system, and neutrophils were added to the high-pressure reservoir. The cells were introduced into the microfluidic system with the syringe. When cells were seen near the microchannel, the three-way valve was set to the low-pressure reservoir, and this reservoir was set to the desired pressure drop height. Once a neutrophil entered the channel completely, the low-pressure reservoir was moved to its zero pressure height, trapping the neutrophil inside the microchannel.

2.3.7 Multiple Particle Tracking Microrheology Analysis of Neutrophils

After the video images were transferred to a computer, multiple particle tracking was performed on the granules found in the neutrophils. Using particle-tracking algorithms [79] (particle-tracking commands and code scripts can be found in Appendices A and B, respectively) written for RSI-IDL Software (Version 5.0, ITT Visual Information Solutions, Boulder, CO), the Brownian motion of granules within the neutrophil was tracked between the time the trapped neutrophil came into focus and the time that a pseudopod formed. When analyzing the images, the regions between the nucleus and the cell's leading and trailing edges were divided into two zones: Zone 1 (¼ of the length from the nucleus to the cell edge) and Zone 2 (the remaining ¾ of the distance). Granules chosen for tracking were found in this latter region, farther away from the nucleus (see Figure 2.9). Additionally, granules located near the wall and at the cell periphery were excluded from tracking, avoiding wall effects.

Within the RSI IDL software, other criteria for granule selection were established. Only granules in frame for at least 30 frames (1 second) were chosen. Granules had to be circular, with an eccentricity of 0.3 or less (corresponding to a <5% difference between

major and minor axes). Using a visualization feature in the software, each selected granule was visually examined, ensuring that only a single particle was being tracked by the algorithm, and preventing granules exhibiting directed motion from being tracked.

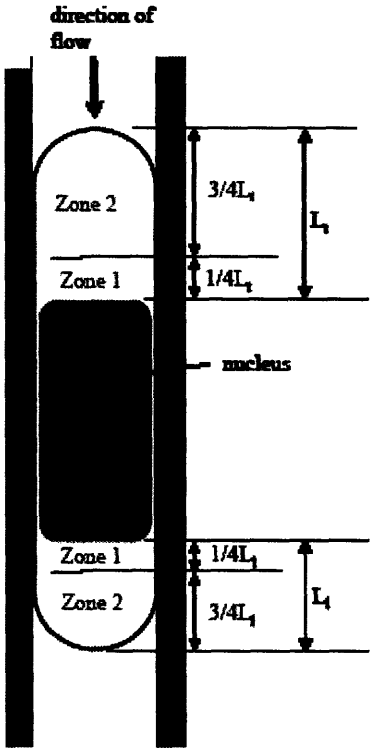

Figure 2.9: Location criterion for granule selection
The neutrophil's cytoplasm was divided into two regions: Zone 1 and Zone 2. Granules chosen for particle-tracking were found in Zone 2. Figure from [54], with permission.

From the RSI IDL algorithms, a mean square displacement (MSD) for each particle was computed. After averaging the MSD of all the selected particles, the two components of the complex shear modulus ($G'(\omega)$ and $G''(\omega)$) were calculated using the methods of Mason et al. [47, 48] This procedure was performed in Matlab (Version 7.0.4, The Mathworks, Inc., Natick, MA), and the m-files used for the modulus calculation can be found in Appendix A.3. For these analyses, the granule radius was taken to be 300 nm [44]

and the time lag was chosen to be 1/30 second (corresponding to a frequency measurement of 30 Hz). The analysis was performed on the deformed neutrophil every 5 seconds.

To obtain initial values of G'(ω) and G"(ω), neutrophils suspended in medium were introduced between a glass slide and a glass coverslip (attached by double-sided tape). Round, passive cells were imaged for several seconds, and the particle-tracking analysis was performed on them. Granules located at the periphery of the cell were excluded from the track to avoid the effects of the cell edge.

2.3.8 Statistical Analysis of Data

To compare results with one another, data were subjected to two-tailed student's t-tests; p-values of less than 0.05 were considered to be a statistically significant difference. Results below are expressed in average values ± standard error (SE).

3.0 RESULTS

3.1 Effectiveness of Calcium Chelation

The following section presents the results of the assays performed to test the effectiveness of the Ca^{2+} chelation procedure.

3.1.1 Fluorescent Imaging of Ca^{2+} Levels

To assess the effectiveness of the Ca^{2+}-chelator, BAPTA-AM, on the neutrophils, Fluo-3, AM (Invitrogen Corp., Carlsbad, CA) was loaded into both untreated and BAPTA-treated cells, at a concentration of 2mM. Fluo-3, AM is able to penetrate the cell membrane, and is activated to bind Ca^{2+} upon entering the intracellular environment. Upon binding, Fluo-3 fluoresces (Excitation: 488 nm, Emission: ~525 nm), and is thus a reporter of Ca^{2+} levels inside the cell. A qualitative analysis of the Ca^{2+}-chelating effects of BAPTA-AM reveals a marked decrease in Fluo-3 fluorescence in 5 μM BAPTA-treated cells (see Figure 3.1). Increasing the concentration of BAPTA (10 μM) further diminishes the fluorescence of Fluo-3.

Figure 3.1: Qualitative assessment of Ca^{2+}-chelation, using fluo-3. (A) Untreated neutrophils loaded with 2mM fluo-3. (B) Neutrophils loaded with 5 μM BAPTA-AM and 2mM fluo-3. (C) Neutrophils loaded with 10 μM BAPTA-AM and 2 mM fluo-3. Cells were plated at equal densities, and images were taken at the same microscope settings (40x) and at 23°C. Scale bar: 10 μm.

3.1.2 Quantitative Measurements of $[Ca^{2+}]_i$ with Flow Cytometry

To obtain a more quantitative measurement of the effects of BAPTA on Ca^{2+} levels inside the cells, neutrophils were subjected to flow cytometry analysis. Two sets of cells were tested: one loaded with 2 μM Fluo-3 and 5 μM Fura Red, and another loaded with 3.5 μM BAPTA, 2 μM Fluo-3, and 5 μM Fura Red. Both Fluo-3 and Fura Red are Ca^{2+} dyes, and the ratio of Fluo-3 to Fura Red is commonly used to quantify $[Ca^{2+}]_i$. [75] Absolute concentrations, however, require an instrument calibration that was unable to be performed for this work. Nevertheless, the relative values of the Fluo-3/Fura Red ratio between sets allow a quantification of changes in Ca^{2+} levels.

The mean ratio values for both sets of cells are presented in Table 1. All cells were excited at 488 nm at room temperature (23°C). Fluo-3 fluorescence measurements were taken at 525 nm, and Fura Red values were obtained at 610 nm. The addition of BAPTA effectively decreases the resting Fluo-3/Fura Red ratio by ~18%.

Table 3.1: Fluo-3 / Fura Red values for non-stimulated cells.

Cell Type	Fluo-3/Fura Red Mean Fluorescence
No BAPTA	2.75 ± 0.31
3.5 μM BAPTA	2.25 ± 0.16

Values expressed are average ± S.E. n = 4.

Of critical importance in this work is the effectiveness of BAPTA in chelating transient elevations in $[Ca^{2+}]_i$, since it has been shown that mechanical deformation induces such an increase. [52] To assess BAPTA's ability to buffer this rise, cells were stimulated with 200nM FMLP and immediately analyzed by flow cytometry at 23°C. The time course of this response for both sets of cells is shown below in Figure 3.2, and the fluorescence histograms can be found in Appendix A.7.

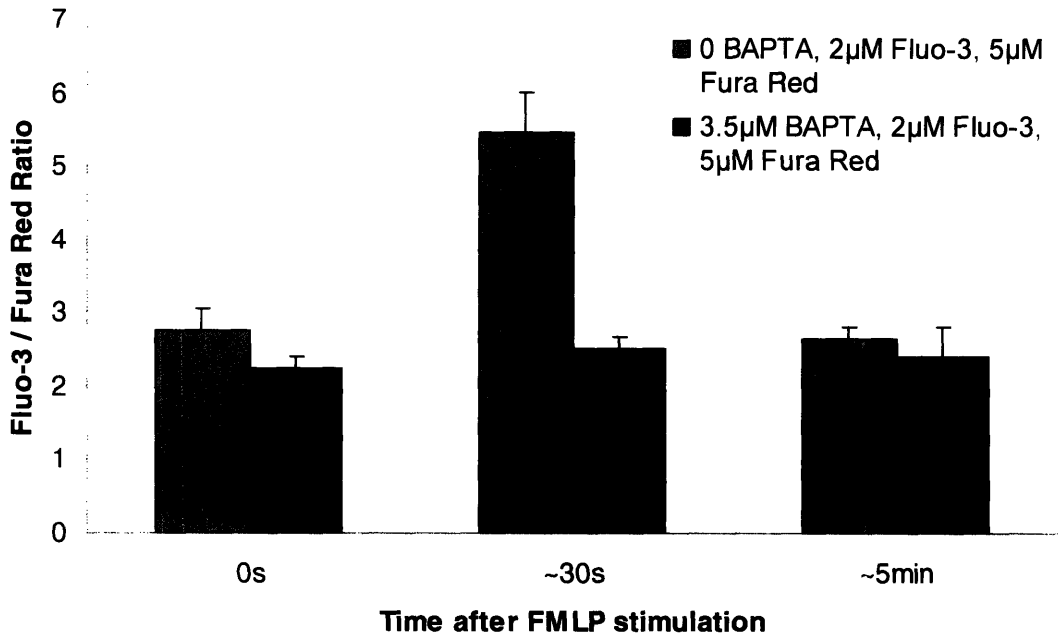

Figure 3.2: Ca^{2+} levels upon FMLP stimulation.
For measurements at 0s, n=4. For 30s and 5 min, n=2. Each test analyzed 30,000 cells at 23°C.

Stimulation with FMLP induces an ~100% increase in the Fluo-3/Fura Red ratio in untreated cells, while neutrophils treated with BAPTA abrogate approximately 90% of rise in the ratio. Both increases are transient, as analyses several minutes after stimulation reveal Ca^{2+} levels that are near the initial values for each cell type.

The Fluo-3/Fura Red ratio values and their changes are not necessarily directly proportional to the changes in $[Ca^{2+}]_i$. [75] Environmental conditions (particularly temperature and instrumental setup) largely determine the values of fluorescent measurements obtained, and thus, quantification of $[Ca^{2+}]_i$ requires calibration of the instrument used for the experiment. This calibration was not performed in this work, but the objective of this part of the project was to determine the effectiveness of BAPTA in curbing stimulated increases in $[Ca^{2+}]_i$. These results show that the chelating agent was indeed effective at buffering the FMLP-induced rise.

3.2 Shear Modulus Measurements with Particle Tracking

The shear modulus values of three sets of neutrophils (untreated, 0.035% DMSO treated, and 3.5 μM BAPTA-AM) were measured in their passive state and in their mechanically deformed state. The following results are from experiments conducted at 37°C.

3.2.1 Measurements of Round Passive Neutrophils

Multiple particle tracking analyses were performed on neutrophils in their passive state, as determined by their spherical morphology and lack of pseudopod or uropod formation (seen in Figure 3.3).

Figure 3.3: Round passive neutrophil.
An image of the round passive neutrophils subjected to multiple particle-tracking analysis. The arrows point to granules that are typically tracked during the analyses. Scale bar: 5 μm.

The particle tracking analysis was performed on: untreated cells, cells treated with 3.5 μM BAPTA-AM, and cells exposed to 0.035% DMSO (loading vehicle for BAPTA). Calculating the shear modulus required measurements of the MSD values of the particles selected for tracking. Typical MSD plots obtained in this work are shown in Figure 19 below. Particles that were selected for tracking stayed in focus for at least 30 frames (1 sec); while some particles were in focus for much longer, many of them were tracked for only

slightly more than 30 frames. Thus, the number of individual MSD curves (Figure 19A) is dramatically reduced at time lags greater than 1 sec, and consequently, the averaged MSD curve (Figure 19B) becomes much noisier at longer time lags. The plots in Figure 3.4, therefore, only show data obtained during the first 30 frames for each granule.

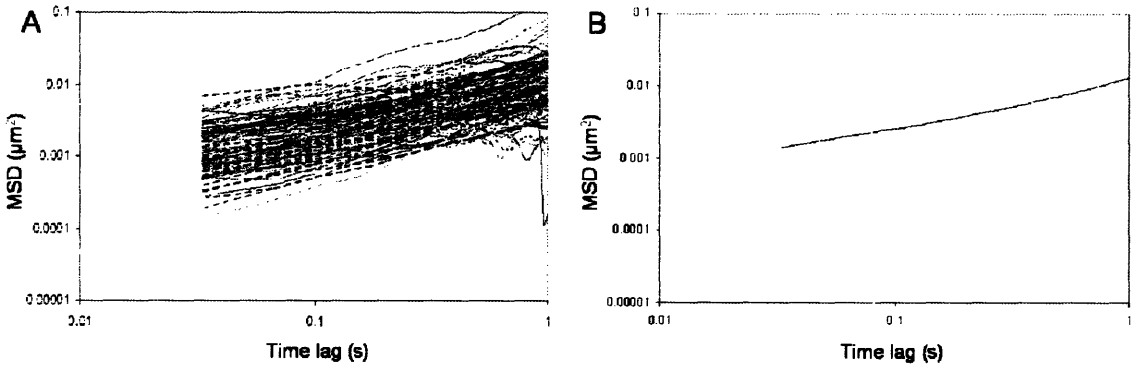

Figure 3.4: Typical MSD plots.
(A) Individual MSD plots for individual particles from several untreated, passive neutrophils at 37°C (n=8, N=125). (B) Averaged MSD plot of particles from untreated, passive neutrophils at 37°C (n=8, N=125).

Using these MSD data and the multiple particle-tracking microrheology equations from Mason [48], the two components of the complex shear modulus, G' and G", were both plotted against frequency, ω. Sample plots are shown in Figure 3.5. At low frequencies, the data exhibit considerable noise, which occurs because fewer particles are tracked for times longer than 1 second. As frequency increases, however, the values stabilize and monotonically rise. Because of the consistency of the data at these higher frequencies, all modulus measurements were taken at 30 Hz, corresponding to a time lag of 1/30 sec.

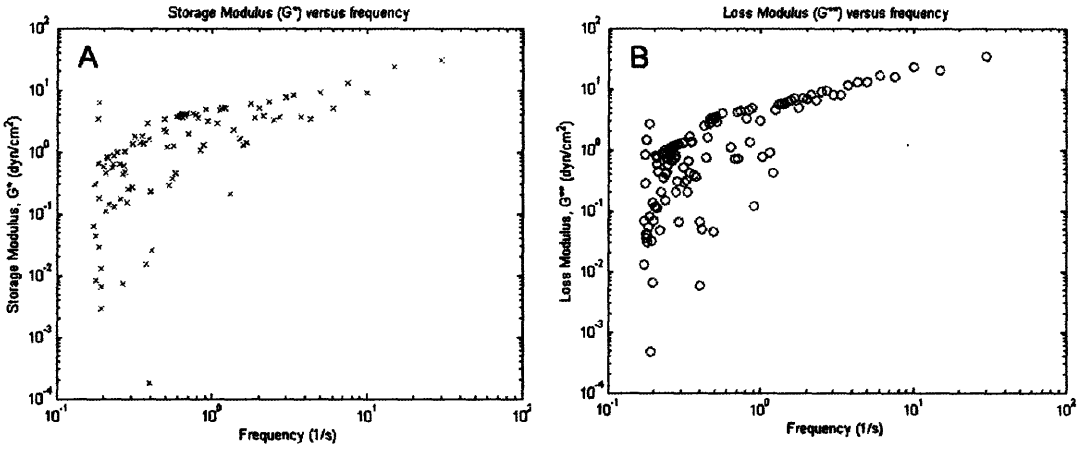

Figure 3.5: Typical complex shear modulus plots.
(A) Storage modulus (G') versus frequency (ω) plot obtained from multiple particle-tracking microrheology analysis of an untreated, passive neutrophil at 37°C. (B) Loss modulus (G") versus frequency (ω) plot for the same cell.

Table 3.2 shows the shear storage (G') and shear loss (G") modulus values for passive cells in the three populations.

Table 3.2: Modulus values for passive cells.

Cell Type	G' (dynes / cm^2)	G" (dynes / cm^2)	n	N
Untreated	31.6 ± 2.1	50.7 ± 9.5	6	38
0.035% DMSO	31.3 ± 1.3	55.8 ± 7.9	4	22
3.5 μM BAPTA-AM	25.9 ± 2.9	47.9 ± 2.8	4	20

Values expressed are average ± S.E. n = number of cells, N = total number of granules tracked.

These values were used as the control values against which the modulus values of deformed cells were compared. The shear storage modulus of Ca^{2+}-chelated cells appears to be ~15% lower than that of the control cells. However, the difference is only statistically significant ($p<0.05$) when compared to untreated neutrophils.

3.2.2 Measurements of Deformed Neutrophils

In order to evaluate the effect of Ca^{2+} chelation on the normal neutrophil response to mechanical deformation, untreated and treated cells were deformed into a 7 μm x 2 μm

(width × height) microchannel. Using the equation for effective diameter, $D_{eff} = \sqrt{\frac{4wh}{\pi}}$, the effective diameter for the channel was calculated to be 4.22 μm. This value was larger than the effective diameters of the channel used by Yap and Kamm (3.1 μm and 4.0 μm) [46], but was found to be necessary in order to deform Ca^{2+}-chelated cells into the microchannel at a reasonable driving pressure. A pressure drop of ΔP = 30mm H_2O was used to introduce the neutrophils into the channel, which is within the range used by Yap and Kamm [46], as well as the range of pressures experienced in the pulmonary capillaries. [80] Figure 3.6 shows a sample image sequence of the deformation process. Inside the channel, the neutrophils possessed a length-to-width ratio of approximately 2.7-2.8, which is consistent with what is expected for the dimensions of the channels used in these experiments.

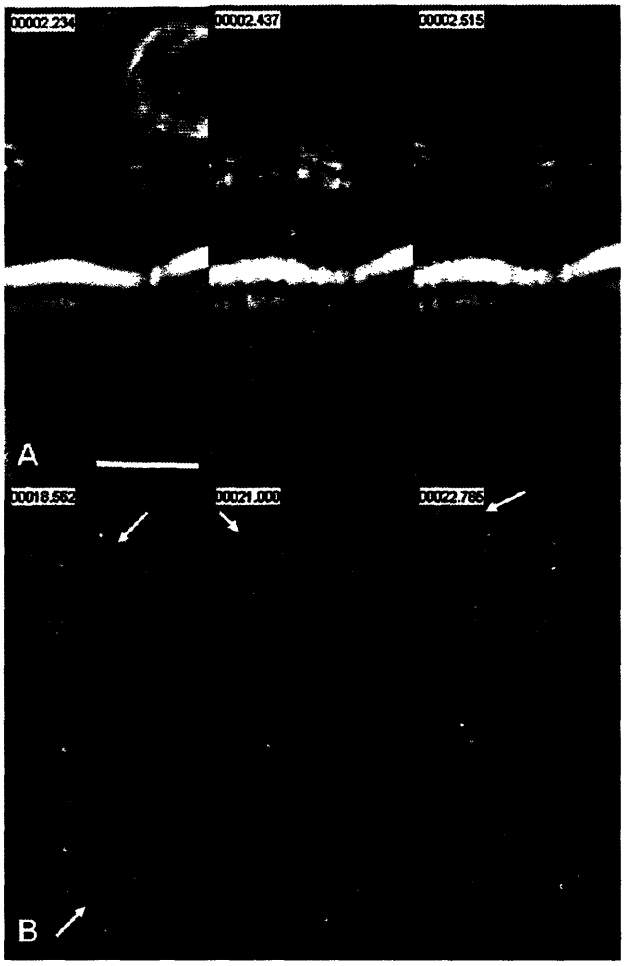

Figure 3.6: Images from neutrophil deformation assay.
(A) A round, passive, untreated neutrophil enters a 7 μm-wide channel while being subjected to a 30mm H_2O pressure differential. (B) Once the cell has entered the channel, the pressure differential is dropped to zero and the cell remains stationary. The arrows in the figure on the left indicate granules that are typically chosen for particle tracking analyses. In the other two images, the arrows point to a pseudopod that is being projected from the cell. Scale bar: 5 μm.

Previous work [46] showed that once inside a microchannel, the time it took for a neutrophil to extend a pseudopod was dependent on how quickly it entered the channel. As such, the entrance times (t_e) for each set of cells deforming into the 7 μm × 2 μm channel at a driving pressure of ΔP = 30mm H_2O was measured, and these values are presented in Figure 3.7.

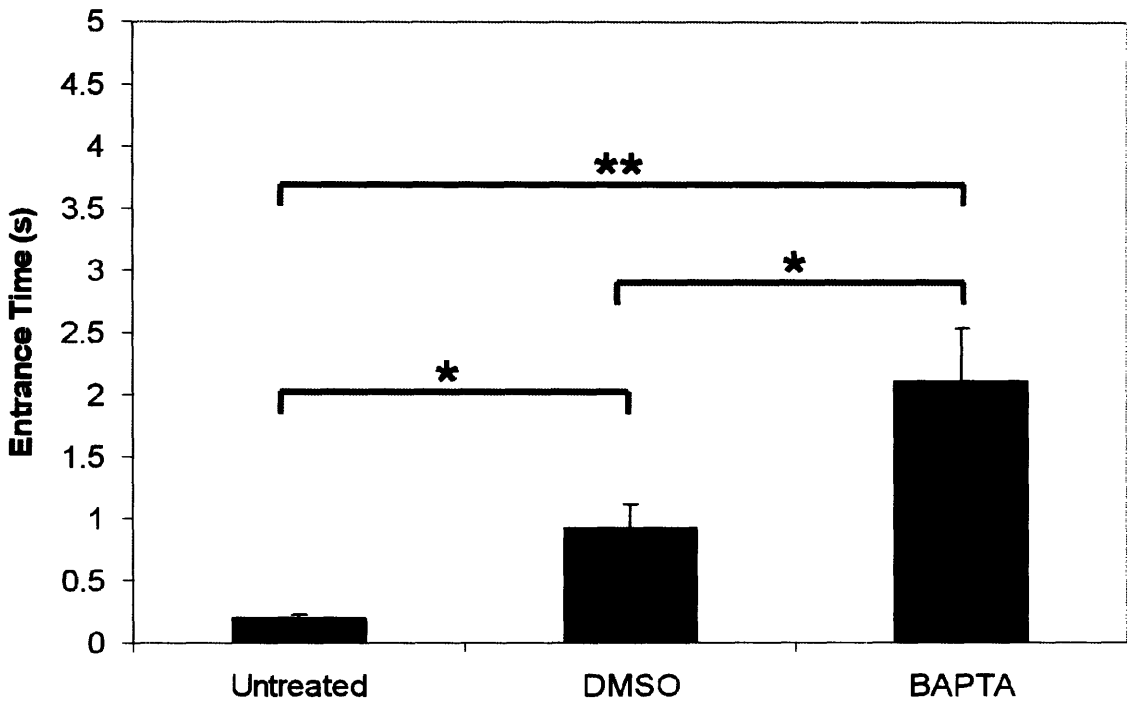

Figure 3.7: Entrance time comparisons.
The entrance time of a cell was defined as the difference between the time its leading edge entered the channel and the time its entire body was present inside the channel. For these measurements, the channel dimensions were 7 μm × 2 μm, and ΔP=30mm H_2O. DMSO concentration was 0.035%, and BAPTA concentration was 3.5 μM. Untreated, n=11; DMSO, n=13; BAPTA, n=11. * $p<0.01$; ** $p<0.001$.

Neutrophils containing the Ca^{2+}-chelator BAPTA exhibited significantly longer entrance times compared to the untreated and DMSO-treated controls. This longer t_e suggests that these cells are less deformable than untreated cells, as all cells were exposed to the same channel sizes and the same pressure drop. In addition, it was observed that after traveling a short distance into the microchannel, these Ca^{2+}-chelated cells would steadily slow down to a complete stop, even with a sustained pressure drop of 30mm H_2O. Nevertheless, Bathe et al. reported that slight differences in capillary entrance geometries can have significant effects on neutrophil entrance times. [81] While the cells were deformed through PDMS microchannels produced from the same silicon wafer, small differences of the channel entrance geometries may have affected the measured entrance times. The channels

used in these experiments were produced from the same master wafer, however, so any differences in these geometries and their effects on channel entrance times were likely slight.

Although these entrance time comparisons alone may not be definitive evidence of the decreased deformability of BAPTA-treated cells, other experiments conducted during this work further support this observation. Prior to switching to a 7 μm-wide channel, a 6μm-wide channel with the same height was used, with D_{eff} = 3.9 μm (within the range of diameters used by Yap and Kamm [46]). Yet while untreated cells deformed readily into this smaller channel at ΔP = 10mm H_2O, BAPTA-treated cells rarely were able to fully enter the channel, even at ΔP values as high as ~50cm H_2O.

In addition to entrance times, the time it took for the deformed neutrophils to form pseudopods was measured. These values are plotted against deformation rate (1/entrance time) in Figure 3.8.

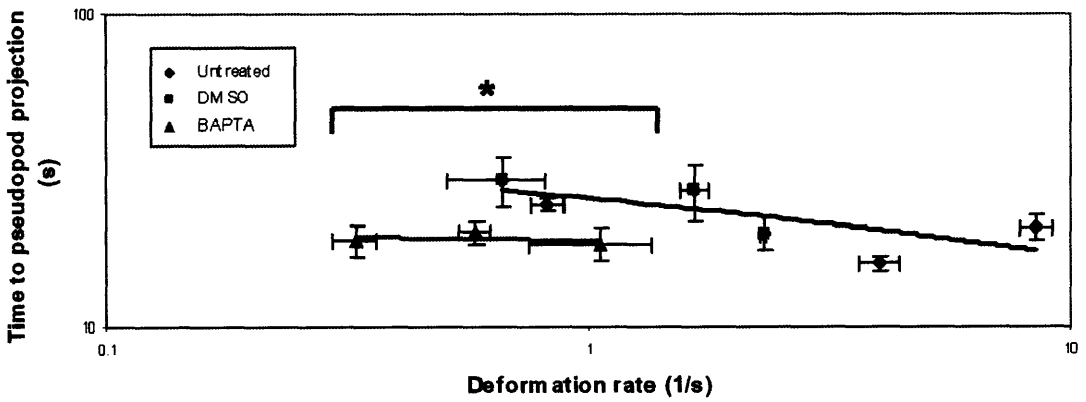

Figure 3.8: Effect of deformation rate on pseudopod projection time.
Cells from each group were deformed into a 7 μm × 2 μm channel at 37°C. Time to pseudopod projection was measured from the time the cell began entering the channel. DMSO controls were exposed to 0.035% DMSO, while BAPTA was loaded at a concentration of 3.5 μM. Untreated, n = 17; DMSO, n = 13; BAPTA, n = 11. Black and blue curves displayed in graph are logarithmic fits to the control cells and the BAPTA-treated cells, respectively. * $p<0.05$, comparing projection times between BAPTA and control populations for the same range of deformation rates.

The downward slopes in pseudopod projection times for the control populations are consistent with the trend seen by Yap and Kamm, [46] although the values are somewhat different. The discrepancy is likely due to the difference in experimental conditions of the current work, including a larger channel and different driving pressure. Experiments performed on untreated cells with a 6 μm-wide channel (D_{eff} = 3.9 μm) at ΔP = 10mm H_2O produced values more similar to their results (see Appendix 5 for graph).

Unlike the control cells, the BAPTA-treated cells do not appear to exhibit a downward trend. While low deformation rates would result in longer times to pseudopod projection in normal cells, the Ca^{2+}-chelated cells project pseudopods at short times, even at low deformation rates. There seems to be a positive relationship between pseudopod projection time and deformation rate in these BAPTA-treated cells, but the upward slope is only slight. These data suggest that intracellular Ca^{2+}-chelation results in a faster activation of deformed neutrophils that may potentially be independent of deformation rate.

Lastly, multiple particle-tracking analyses were performed on deformed cells from each experimental set to determine values for the shear storage and shear loss moduli, G' and G". Graphs that depict the temporal changes in these mechanical properties can be found in Figure 3.9 below.

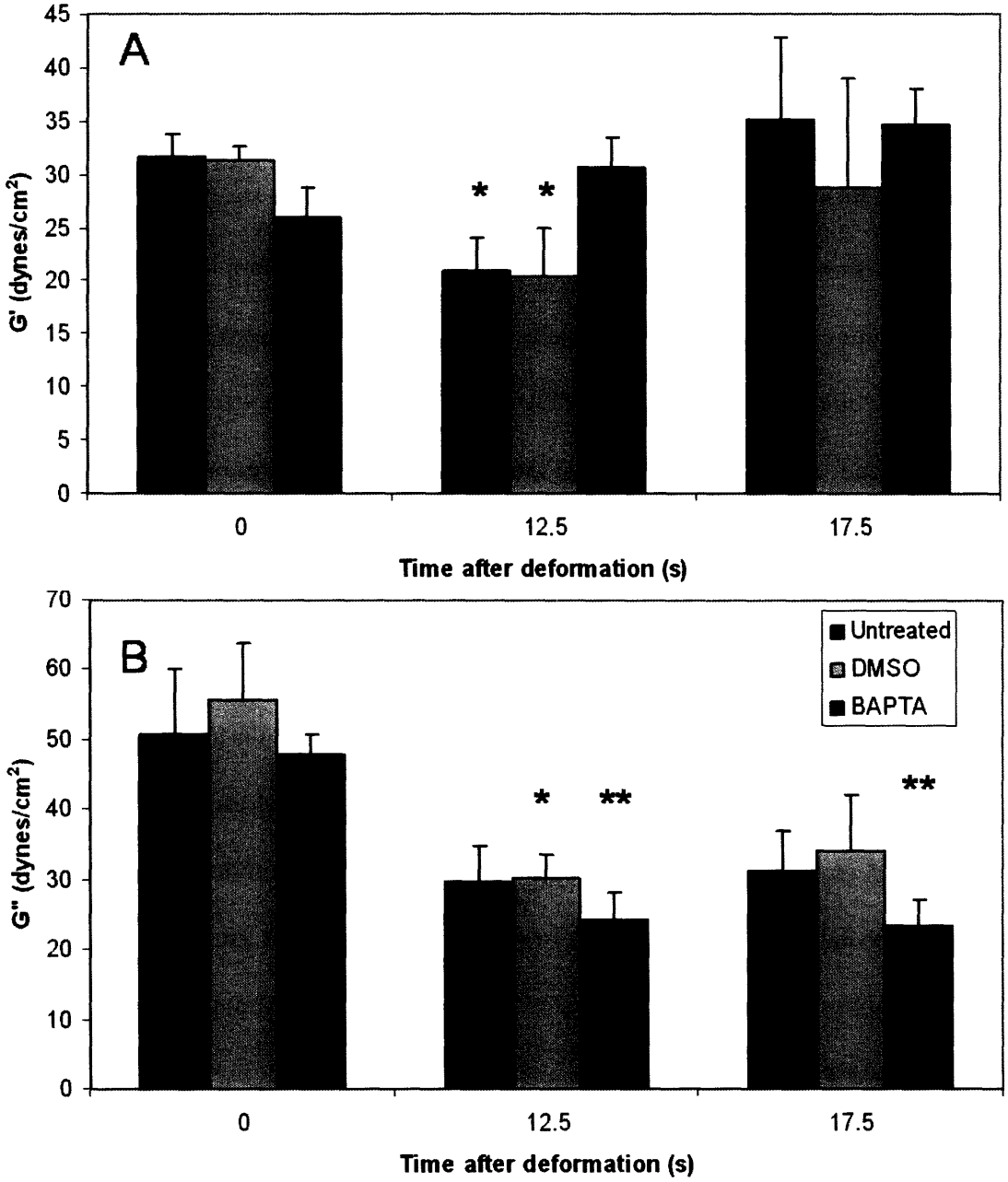

Figure 3.9: Temporal changes in G' and G" following neutrophil deformation.
(A) Shear storage moduli, G', and (B) shear loss moduli, G", for cells before and after deformation. Some cells projected pseudopods before a measurement could be made at 17.5s, but their moduli values at 12.5s were still included. At 12.5s, Untreated: n=8, N=75; DMSO: n=4, N=29; BAPTA: n=11, N=57. At 17.5s, Untreated: n=6, N=44; DMSO: n=2, N=8; BAPTA: n=5, N=20. * $p<0.05$, ** $p<0.001$ compared to pre-deformation values.

Cells from the control populations (untreated and DMSO) behave similarly and exhibit deformation responses comparable to those observed by Yap and Kamm [46]; following deformation, there is a drop in both G' and G". The drop in G' (~35%) was not quite as dramatic as the decreases previously observed, a difference that might be explained by differences in channel dimensions and driving pressures. The change in G" (~42%), however, was comparable to the published work. Furthermore, a recovery in G' was observed in these control cells, and there even seemed to be a stiffening of the cells beyond their original G'. The error bars at this later time are rather large, however, so it is uncertain whether this excess stiffening is actually occurring. G" values, on the other hand, did not appear to recover with time, which is consistent with the observations of Yap and Kamm for their larger channel experiments.

The BAPTA-treated cells exhibited a G' response that was markedly different from that of the control populations. There was no significant drop in G' in these Ca^{2+}-chelated neutrophils after deformation; rather, there appeared to be a slight stiffening of the cells beyond their resting values. This increase was not statistically significant, however, and the cells may have just retained their passive G' values. Contrarily, the G" response was similar to that of the control cells, falling a statistically significant 60% after 12.5 seconds and recovering slightly with time.

Particle-tracking analyses could only be performed on the cell before it extended a pseudopod; measurements afterwards would not be representative of a passive cell. During the experiments, pseudopods would most often form only on one end of the cell, and the neutrophil would then proceed to migrate in that direction that the pseudopod projected. This observation is consistent with what was observed by Yap and Kamm. [46, 54, 70] However, occasionally cells would project pseudopods from both ends, although not

simultaneously. These cells would either begin migrating in one direction, or the opposite ends would appear to migrate away from each other. The central portions of the latter cells would subsequently begin to decrease in width as it was subjected to apparent forces in opposite directions. One explanation for why this occurred in these experiments but not in the previous work may be the significantly larger channel width used here (7 μm, as opposed to 5 μm used by Yap and Kamm), but a precise explanation is unclear.

4.0 DISCUSSION

While traveling through the pulmonary microcirculation, neutrophils are driven through capillaries that often have diameters much smaller than the neutrophil's. [12, 67] The resulting deformation stimulates significant changes in the cell, including an increase in $[Ca^{2+}]_i$ and sharp decreases in both the shear storage (G') and shear loss (G") moduli. [46, 52, 62, 70] The aim of this project was to determine whether a correlation existed between these two events.

Neutrophils were loaded with BAPTA-AM, an intracellular Ca^{2+}-chelating agent, and individual cells were deformed into a microchannel by a physiological driving pressure. Once the cell was stationary inside the channel, its mechanical properties (G' and G") were measured by multiple particle-tracking analysis, in which the neutrophil's endogenous granules were tracked by a computer program.

4.1 Neutrophil Deformability

A major difference between the BAPTA-treated neutrophils and the control cells was their respective entrance times: BAPTA-treated cells took significantly longer to deform into the 7 μm-wide channel at the same pressure drop (ΔP = 30mm H_2O). Additionally, earlier experiments conducted with 6 μm-wide channels further demonstrated the decreased deformability of these neutrophils. While untreated cells entered this smaller channel rather quickly (t_e ~ 0.1-0.5 sec, ΔP = 10mm H_2O), most of the Ca^{2+}-chelated neutrophils were unable to fully enter the channel at a significantly higher pressure drop (ΔP ~ 50cm H_2O). As shown in Figure 4.1, these cells only partially entered the channel, while a portion of the cell body remained stuck at the channel entrance.

Figure 4.1: BAPTA-treated neutrophil stuck at 6 μm-wide channel entrance. The neutrophil was subjected to a high pressure drop of $\Delta P \sim 50$cm H_2O. Channel height: 2 μm. Scale bar: 5 μm.

Previous computational work elucidated the significant effect that channel entrance geometry had on cell entrance times into capillaries. [81] This might explain the observed disparity in entrance times, particularly between the untreated and DMSO-treated cells, as the difference is statistically significant but not dramatic. It seems more likely, however, that the BAPTA-treated cells are in fact less deformable than normal cells. Downey et al. found that lowering $[Ca^{2+}]_i$ in neutrophils induced spontaneous actin polymerization, [71] and Zaffran et al. obtained similar results. [82] Actin polymerization induced by FMLP resulted in the stiffening of neutrophils and their subsequent retention in pulmonary capillaries. [50] Thus, the BAPTA-induced increase in actin polymerization may stiffen the treated neutrophils and might account for their decreased deformability into capillary-sized microchannels.

However, a comparison of the G' values for passive BAPTA-treated cells and their respective controls reveals seemingly contradictory findings. With increased actin

polymerization, the Ca^{2+}-chelated cells might be expected to be stiffer than the controls. Yet, the mean G' for the control cells was measured to be ~31 dynes/cm^2, while the G' for BAPTA-treated cells was found to be lower, at ~26 dynes/cm^2. This unexpected difference might be explained by the relatively small sample size of the BAPTA-treated neutrophils (n=4), as there was no statistically significant difference between the DMSO control and the BAPTA-treated cells. Another explanation may be the method by which the passive cells were analyzed. Since modulus calculations involved tracking the motion of endogenous granules, passive cells were only chosen if they were stationary. These cells probably adhered slightly to the cover-slip surface, but refrained from spreading. This slight adherence may have caused a local polymerization of actin to stabilize the cell, as is observed in fibroblasts [83] and endothelial cells [84] when microbeads bound to the cell membrane are subjected to force. In the fibroblast experiments, chelation of Ca^{2+} ions inhibits this force-induced localized polymerization. While such forces are not imposed on these passive neutrophils, the focal adhesion might still promote a small amount of polymerization, which would be abrogated in the Ca^{2+}-chelated cells. As a result, the measured stiffness value for the minimally adherent untreated cells would be greater than that of the BAPTA-treated cells. This explanation is hypothetical, however, and a localized polymerization might not account for the measured ~6 dynes/cm^2 difference. One other potential explanation is a disparity in the locations of tracked particles, although efforts were made to exclude particles near the center of the cell to avoid wall effects of the nucleus. Nevertheless, it remains unclear why this particular discrepancy in stiffness values was observed.

4.2 G' Response After Deformation

Another remarkable observation of this work was the behavior of Ca^{2+}-chelated neutrophils inside the microchannel. Unlike the control cells, the BAPTA-treated neutrophils were not found to experience a significant drop in G'. Rather, they appeared to retain their initial stiffness, and possibly even stiffened further beyond their original G' once inside the channel. Thus, these results suggest that a deformation-induced increase in $[Ca^{2+}]_i$ (as demonstrated in [62] and [52]) plays a role in the stiffness reduction seen in normal neutrophils as they squeeze into microvessels.

4.2.1 Potential Mechanisms for the Observed Response

The mechanisms for the elevated $[Ca^{2+}]_i$'s effect on the deformed neutrophil's stiffness may lie in the actions of Ca^{2+}-sensitive cytoskeletal proteins. As proposed by Janmey in an excellent review of the effects of intracellular Ca^{2+} on the cytoskeleton, the overall effect of Ca^{2+} increases appears to be solation of the cortical filament layer, rendering the cell more amenable to deformation. [72] Proteins potentially involved in this general response include gelsolin, α-actinin, spectrin, caldesmon, and MARCKS.

Gelsolin is an actin-regulating-protein that, at micromolar concentrations of Ca^{2+}, can cleave and cap F-actin, and also inhibit microfilament assembly. [85-87] Additionally, gelsolin can bind to actin monomers, and these complexes appear to serve as nucleation points that promote actin filament assembly. [51] Such actions have led many to believe that gelsolin serves an important role in allowing for the cytoskeletal remodeling needed during neutrophil motility. Other proteins (fragmin, severin, villin) carry out similar functions, and are also Ca^{2+}-dependent.

Another protein that is directly affected by Ca^{2+} is an F-actin cross-linking protein known as α-actinin. High levels of Ca^{2+} have been shown to inhibit several isoforms of this protein, including macrophage, brain, and *Dictyostelium discoideum* α-actinin. [88-90] This latter isoform, which is a typical non-muscle type of α-actinin, displays exquisite sensitivity at the physiological $[Ca^{2+}]_i$ range in neutrophils; in an *in vitro* experiment, Witke et al. showed that its cross-linking activity decreased by ~80% when $[Ca^{2+}]$ was increased from ~60nM to ~600nM. [90] (Resting neutrophil $[Ca^{2+}]_i$ is roughly 100nM.)

Calcium can also have indirect effects on actin-binding proteins. When Ca^{2+} is bound to calmodulin, the calcium/calmodulin complex can dissociate myristoylated C-kinase substrate (MARCKS) from F-actin, inhibiting its ability to bundle actin filaments. [91] Similarly, calcium/calmodulin induces the dissociation of caldesmon from the sides of actin filaments. [92] When bound to F-actin, caldesmon prevents gelsolin's binding to and cleaving of the filament. The calcium/calmodulin inhibition of caldesmon thereby promotes actin depolymerization.

Also, calcium/calmodulin has been shown to affect the activity of spectrin, particularly the spectrin/4.1 complex. This complex is found in the cortical networks of erythrocytes, which have to undergo the same deformations that neutrophils experience in the microcirculation. In this cortical layer, it serves to cross-link actin filaments both to each other and to the cellular membrane, strengthening the cytoskeleton and supporting the membrane's integrity. [57] These activities are disrupted by calcium/calmodulin, however, and it is possible that increased calcium/calmodulin activity thereby promotes the loss of these cross-links and increases the deformability of the cell. A spectrin homologue, fodrin, has been identified in neutrophils, and its proteolysis by Ca^{2+}-dependent proteases has been

implicated in the degranulation activity of the cell. [93] Calcium chelation in neutrophils inhibits this exocytosis. [94]

It should be noted that these proposed mechanisms for Ca^{2+} action have their limitations. First, the diffusion of Ca^{2+} is considerably small: in experiments performed in cytoplasmic extracts of *Xenopus* oocytes, the effective range of free Ca^{2+} diffusion was calculated to be approximately 100 nm. [95] Moreover, the concentration of Ca^{2+} needed to activate some of the proteins mentioned above *in vitro* is rather high. While the *in vivo* resting $[Ca^{2+}]_i$ is ~100nM, levels needed to activate gelsolin, for instance, are in the micromolar range. [96] In light of the results of Kitagawa et al., in which the deformation-induced increase in $[Ca^{2+}]_i$ stimulated a Ca^{2+} dye fluorescence that was only twice the resting value , it is questionable whether deformation activates actin depolymerization events. Nonetheless, Downey et al. found that raising $[Ca^{2+}]_i$ from 100nM to 500nM results in a ~60% reduction in the F-actin content of electropermeabilized neutrophils, which occurs at the same timescale as the drop in shear modulus (< 30 sec). [71] Calcium concentrations between 100nM and 500nM were not tested, but if a linear fit existed between these two measurements, a doubling of the resting $[Ca^{2+}]_i$ to 200nM could reduce F-actin content by ~30%. Thus, despite the ion's limited diffusivity in the cytoplasm and the high concentrations needed to activate certain depolymerizing proteins, relatively small increases in $[Ca^{2+}]_i$ can still affect the actin network. Heterogeneity of the Ca^{2+} release and the ion's spatiotemporal distribution within the cell may resolve these seemingly contradictory observations. [97]

In summary, the chelation of Ca^{2+} in this work may have attenuated the solation of the neutrophil cytoskeleton by inhibiting Ca^{2+} from acting through one or several of the mechanisms discussed above. The multiple pathways by which Ca^{2+} can depolymerize and

dissociate the cytoskeletal network emphasize the importance of remodeling the cytoskeleton in a cell like the neutrophil. As an immune cell that must travel relatively quickly to sites of infection, neutrophils are highly motile, and such robust involvement of Ca^{2+} in the remodeling process is likely crucial for them to meet their migratory needs. Also, as they are continuously forced to squeeze through numerous small vessels during their transit through the pulmonary circulation, neutrophils repeatedly experience significant physical strain. It would be reasonable to believe that the cells possess an active mechanism to ease this harsh process; such action could operate in concert with force-induced rupture of cross-links and/or actin filaments, as might be inferred from the work of Tseng et al. [98] These needs to migrate rapidly and deform readily possibly led to the evolution of the chemoattractant- and deformation-induced increases in $[Ca^{2+}]_i$, and the subsequent dependency of the cytoskeletal softening and remodeling processes on this calcium rise.

4.3 G" Response After Deformation

Although the shear storage modulus in Ca^{2+}-chelated neutrophils behaved differently from the control group, the G" response was roughly the same. Following deformation, the G" value dropped by ~40% for the control cells and by ~50% for the BAPTA-treated cells. This latter group exhibited a slight recovery at measurements made 5 seconds later, while the control group values approximately remained the same.

Considering the results for the G' response of BAPTA-treated neutrophils, it seems unusual that the G" value would significantly decrease, while G' is hardly affected. If the Ca^{2+}-dependent mechanisms discussed in the previous sections are actively involved in the deformation response, it is intuitive to think that Ca^{2+}-chelation would also abrogate the drop in G". For instance, in normal cells, actin depolymerization induced by gelsolin activity

would potentially reduce the number of actin filaments in the cell, thereby reducing cytoplasmic viscosity. Chelating calcium would inhibit this depolymerization, and as G" is considered an indication of viscosity, G" would remain largely unchanged.

However, a precise description of the factors that contribute to G" has not been developed. The concentration of cytoskeletal filaments may be part of this viscous component, but it is not the sole determinant of viscosity. Influx of fluid into the cell, for example, may produce changes in intracellular viscosity. Thus, Ca^{2+}-independent mechanisms may be at work in the observed reduction of G" in both normal and Ca^{2+}-chelated neutrophils.

4.4 Deformation-induced Activation

Sustained mechanical deformation of neutrophils in capillary-sized microchannels, above a threshold stimulus, activates the cells to extend pseudopods and migrate. [46, 70, 99] The time it takes for neutrophils to become activated is inversely proportional to their deformation rates into a microchannel, as is seen in previous work and in the current results. This dependency and the existence of a threshold stimulus suggest that normal neutrophils can sense the rate and magnitude of their deformation.

Ca^{2+}-chelated neutrophils, on the other hand, demonstrate different behavior. At low deformation rates ($0.1 - 1\ s^{-1}$), these treated neutrophils become activated ~30% more quickly than normal cells. A general trend over a wide range of deformation rates was difficult to determine, however, as BAPTA-treated cells exhibited relatively long entrance times even at high pressure drops. Nevertheless, it appears that these Ca^{2+}-chelated cells are more prone to become activated compared to the control cells. The observation that Ca^{2+}-chelated cells retain the ability to extend pseudopods and migrate is not surprising, as others

have found that actin polymerization, cell locomotion, and shape change can occur independently of $[Ca^{2+}]_i$ increases. [61, 82, 94, 100] Yet an explanation for their relatively shorter activation times remains left to speculation.

Cellular mechanisms for the triggering of pseudopod extensions have yet to be fully determined. Others have studied the effects of fluid shear stress on pseudopod activity in neutrophils; they found that such stresses stimulate pseudopod projection in passive neutrophils, while inducing pseudopod retraction in activated cells. [101-103] In these results, it appears that the initial state of the cell determines how mechanical stress affects its pseudopod behavior. Furthermore, passive neutrophils were demonstrated to require an intact actin network for pseudopod projection to occur. [102]

Given these previous findings and the observations of this work, one possible explanation for the relatively shorter activation times of Ca^{2+}-chelated neutrophils is a dependency of pseudopod projection on the mechanical status of the actin network. Assuming that a deformation-induced increase in $[Ca^{2+}]_i$ depolymerizes and/or dissociates elements of the actin network, normal neutrophils experience a certain level of "softening" of their cytoskeleton. This is followed by cell stiffening, as evidenced by the recovery of both G' and F-actin levels to near initial values, and subsequent pseudopod projection. [46, 70] Meanwhile, BAPTA-treated neutrophils maintain their original stiffness and proceed to stiffen via actin polymerization, which is independent of increased $[Ca^{2+}]_i$ and is potentially initiated by cell deformation. [61, 82] The time at which a pseudopod is projected may be influenced by the stiffness state of the actin cytoskeleton, in a mechanism that involves the actin network achieving a certain level of stiffness for pseudopod projection to occur. Since Ca^{2+}-chelated cells begin their response with a greater G', they may be able to reach this threshold more quickly.

Experimental observations motivated the development of this hypothesis. In the seconds prior to pseudopod projection, granules near the projection site would exhibit less motion and occasionally appear to become stationary. After the extension of the pseudopod, granules would soon move into the newly formed space and again begin to demonstrate reduced movement. Pseudopod projection would then follow, and the cycle would repeat as the cell began to migrate towards one end of the channel. This is consistent with the observations of Yap, [54] and with the finding that pseudopod projection occurs as the deformed neutrophil stiffens inside the channel . [46, 70]

This explanation remains subject to debate, however. Pseudopod projections observed in this work were found to occur at a range of G' values, weakening the support for the existence of a threshold stiffness for projection. Yet, G' measurements were made by tracking particles throughout the cell, while pseudopod projection may be strongly influenced by local stiffness values.

Nevertheless, it is clear that more work is needed to determine the exact mechanisms of deformation-induced neutrophil activation and calcium's actions within them.

4.5 Summary and Recommendations for Future Development

The aim of this study was to investigate calcium's role in the neutrophil response to mechanical deformation, and the results suggest that rapid and transient increases in $[Ca^{2+}]_i$ may help to facilitate neutrophil transit by effectively "softening" the cytoskeleton as the cell squeezes through a narrow capillary. Ca^{2+}-chelated cells exhibited decreased deformability into a microchannel, did not experience the drop in G' seen in normal cells, and became activated more quickly. This work thereby provides further insight into the signaling mechanisms involved in the presumably active response of neutrophils to deformation.

Continued experiments are needed to further elucidate calcium's role in this mechanotransduction response, and to determine the signaling events that occur both upstream and downstream of Ca^{2+} action. One particular experiment that would strongly support the results of this thesis, as well as further the work of Kitagawa et al. [52], is the quantification of the increase in $[Ca^{2+}]_i$ during the deformation process. As mentioned earlier, rather high concentrations are needed to activate actin depolymerizing proteins like gelsolin. Kitagawa et al. demonstrated that a small, transient rise in the fluorescence of a Ca^{2+} indicator occurred after deformation, but were unable to capture and quantify Ca^{2+} dynamics during the deformation process, which is more relevant to this work. Laffafian and Hallett found that poking a neutrophil membrane with a micropipette immediately increased intracellular Ca^{2+} levels, but they did not quantify this response in terms of $[Ca^{2+}]_i$. [62] Additionally, free Ca^{2+} has been shown to have very limited diffusivity in cytoskeletal extracts, signifying the importance of locating where Ca^{2+} increases are occurring within the cell. [95] Thus a quantitative and spatial analysis of the deformation-induced increase in $[Ca^{2+}]_i$ would be of tremendous value in determining how Ca^{2+} is involved in neutrophil mechanotransduction.

Once a method to visualize and quantify Ca^{2+} dynamics during deformation is developed, a worthy pursuit would be identifying whether the source of Ca^{2+} is intracellular stores, the extracellular medium, or both. In response to stretching, the F-actin content of fibroblasts exhibits behavior that is remarkably similar to the neutrophil's mechanical response to deformation, and extracellular Ca^{2+} has a significant role in this fibroblast response. [55] These results point to a role for stretch-activated Ca^{2+} channels, which may mediate an influx of Ca^{2+} ions upon stretching of the fibroblast membrane. It is very likely that neutrophils employ a similar mechanism, as their membranes are considerably deformed

when the cells squeeze through small capillaries. To determine whether this is indeed the case, a rather straightforward experiment would include the observation of Ca^{2+} dynamics during the neutrophil's deformation into a microchannel, both in the presence and absence of extracellular Ca^{2+}.

Such experiments would also reveal whether or not mobilization of Ca^{2+} from intracellular stores occurs during the deformation process. If this is the case, then it would be useful to perform experiments that illuminate the signaling events responsible for the observed release of intracellular Ca^{2+}. With deformation of the cell as the stimulus in these experiments, it is likely that any intracellular signaling would be initiated by the engagement/activation of membrane proteins. Several membrane proteins have been shown to elicit an increase in $[Ca^{2+}]_i$ upon activation in neutrophils. The $P2Y_2$ receptor, for instance, causes elevated intracellular Ca^{2+} levels upon extracellular activation by either ATP or UTP. [104] Interestingly, the same receptor is also implicated in the generation of cAMP via adenylyl cyclase stimulation. [105] Previous work has found that intracellular increases of cAMP serve to modulate neutrophil stiffening responses to stimuli, and in conjunction with prostaglandins released from endothelial cells, it can assist with cell body deformation and facilitate transmigration. [106] Furthermore, the receptor possesses an RGD sequence in its extracellular domain that can interact with $\alpha_v\beta_3$ integrins on the surface of endothelial cells, [107] hinting at a potential physical engagement of the receptor during the neutrophil's transit through endothelial cell-lined capillaries. Experiments to test for the involvement of the $P2Y_2$ receptor would include ATP/UTP depletion and pertussis toxin treatment ($P2Y_2$-stimulated Ca^{2+} signaling operates through a pertussis-toxin sensitive phospholipase C pathway).

Other possible avenues of investigation include the CD11b/CD18 integrin and two Fc receptors, $Fc_\gamma RIIA$ (CD32) and $Fc_\gamma RIIIB$ (CD16B). CD11b/CD18 is the most abundant β_2-integrin in neutrophils, and deformation upregulates its expression on the neutrophil surface. [52] β_2-integrins have been shown to be capable of transiently increasing $[Ca^{2+}]_i$ in neutrophils through both the release of Ca^{2+} from intracellular stores and the influx of Ca^{2+} from the surrounding medium. [108, 109] The signaling mechanisms that are responsible for this increase occur through a phospholipase C pathway that is sensitive to phorbol myristate acetate (PMA) and U73122. [110, 111]

The Fc receptors are more commonly associated with the phagocytic and degranulation activities of neutrophils. Although the other membrane proteins mentioned above seem to be more likely targets, the capability of the Fc receptors to induce similar transient Ca^{2+} responses is worth investigating. Their signaling pathways have been shown to be sensitive to the PI3K inhibitor, wortmannin.

Lastly, it would be interesting to conduct further studies that might relate the work conducted in this thesis more intricately with pathological conditions. Leukostasis, for example, has been associated with acute myeloid leukemia (AML), [112-114] and while the sheer magnitude of the number of leukocytes present in AML patients contributes to leukostasis, there could very well be a role for leukocyte stiffness and deformation response as well. Additionally, neutrophils exhibit altered behavior in patients afflicted with trauma, septic shock, acute respiratory distress syndrome (ARDS), and acute ischemic stroke. Passive neutrophils in septic shock and ARDS patients demonstrate decreased deformability, [115] similar to the passive neutrophils examined in this thesis. Tissue damage of the brain in acute ischemic stroke may be the result of the reduced deformability of leukocytes, combined with their increased adhesiveness to vessel walls. [116] Others have shown that

trauma conditions can impair normal neutrophil function, reducing their chemotactic capabilities and rendering them more likely to damage bystander tissue. [117] Dysregulation of Ca^{2+} signaling may be involved in these pathological mechanisms, and continued studies of neutrophil mechanotransduction may lend tremendous insight into these debilitating conditions.

REFERENCES

1. Goldsby RA, K.T., Osborne BA, and Kuby J., *Immunology*. 5 ed. 2003: WH Freeman.
2. Pryzwansky, K.B. and J. Breton-Gorius, *Identification of a subpopulation of primary granules in human neutrophils based upon maturation and distribution. Study by transmission electron microscopy cytochemistry and high voltage electron microscopy of whole cell preparations.* Lab Invest, 1985. **53**(6): p. 664-71.
3. Pryzwansky, K.B., *Human leukocytes as viewed by stereo high-voltage electronmicroscopy.* Blood Cells, 1987. **12**(3): p. 505-30.
4. *http://medocs.ucdavis.edu/cha/402/xpix/1724/1724054.jpg*. 2006.
5. Schmid-Schonbein, G.W., Y.Y. Shih, and S. Chien, *Morphometry of human leukocytes.* Blood, 1980. **56**(5): p. 866-75.
6. Schmidtke, D.W. and S.L. Diamond, *Direct observation of membrane tethers formed during neutrophil attachment to platelets or P-selectin under physiological flow.* J Cell Biol, 2000. **149**(3): p. 719-30.
7. Zhao Y, C.S., Weinbaum S., *Dynamic contact forces on leukocyte microvilli and their penetration of the endothelial glycocalyx.* Biophys J, 2000. **80**: p. 1124-40.
8. *http://www1.imperial.ac.uk/medicine/about/divisions/nhli/respiration/leukocyte/molecular/default.html*. 2006.
9. Southwick, F.S., et al., *Polymorphonuclear leukocyte adherence induces actin polymerization by a transduction pathway which differs from that used by chemoattractants.* J Cell Biol, 1989. **109**(4 Pt 1): p. 1561-9.
10. Anderson, D.C., et al., *Cytoplasmic microtubules in polymorphonuclear leukocytes: effects of chemotactic stimulation and colchicine.* Cell, 1982. **31**(3 Pt 2): p. 719-29.
11. Fechheimer, M. and S.H. Zigmond, *Changes in cytoskeletal proteins of polymorphonuclear leukocytes induced by chemotactic peptides.* Cell Motil, 1983. **3**(4): p. 349-61.
12. Doerschuk, C.M., et al., *Comparison of neutrophil and capillary diameters and their relation to neutrophil sequestration in the lung.* J Appl Physiol, 1993. **74**(6): p. 3040-5.
13. Howard, T.H. and W.H. Meyer, *Chemotactic peptide modulation of actin assembly and locomotion in neutrophils.* J Cell Biol, 1984. **98**(4): p. 1265-71.
14. Howard, T.H. and C.O. Oresajo, *The kinetics of chemotactic peptide-induced change in F-actin content, F-actin distribution, and the shape of neutrophils.* J Cell Biol, 1985. **101**(3): p. 1078-85.
15. Bevilacqua, M.P., et al., *Endothelial leukocyte adhesion molecule 1: an inducible receptor for neutrophils related to complement regulatory proteins and lectins.* Science, 1989. **243**(4895): p. 1160-5.
16. Anderson, D.C., et al., *The severe and moderate phenotypes of heritable Mac-1, LFA-1 deficiency: their quantitative definition and relation to leukocyte dysfunction and clinical features.* J Infect Dis, 1985. **152**(4): p. 668-89.

17. Von Andrian, U.H., et al., *L-selectin function is required for beta 2-integrin-mediated neutrophil adhesion at physiological shear rates in vivo.* Am J Physiol, 1992. **263**(4 Pt 2): p. H1034-44.
18. Albelda, S.M., C.W. Smith, and P.A. Ward, *Adhesion molecules and inflammatory injury.* Faseb J, 1994. **8**(8): p. 504-12.
19. Zimmerman, G.A., S.M. Prescott, and T.M. McIntyre, *Endothelial cell interactions with granulocytes: tethering and signaling molecules.* Immunol Today, 1992. **13**(3): p. 93-100.
20. Rot, A., *Endothelial cell binding of NAP-1/IL-8: role in neutrophil emigration.* Immunol Today, 1992. **13**(8): p. 291-4.
21. Shamri, R., et al., *Lymphocyte arrest requires instantaneous induction of an extended LFA-1 conformation mediated by endothelium-bound chemokines.* Nat Immunol, 2005. **6**(5): p. 497-506.
22. Kitayama, J., et al., *Shear stress affects migration behavior of polymorphonuclear cells arrested on endothelium.* Cell Immunol, 2000. **203**(1): p. 39-46.
23. Rosengren, S., et al., *Leukotriene B4-induced neutrophil-mediated endothelial leakage in vitro and in vivo.* J Appl Physiol, 1991. **71**(4): p. 1322-30.
24. Liu, Y., et al., *Regulation of leukocyte transmigration: cell surface interactions and signaling events.* J Immunol, 2004. **172**(1): p. 7-13.
25. Schenkel, A.R., et al., *CD99 plays a major role in the migration of monocytes through endothelial junctions.* Nat Immunol, 2002. **3**(2): p. 143-50.
26. Mamdouh, Z., et al., *Targeted recycling of PECAM from endothelial surface-connected compartments during diapedesis.* Nature, 2003. **421**(6924): p. 748-53.
27. Ostermann, G., et al., *JAM-1 is a ligand of the beta(2) integrin LFA-1 involved in transendothelial migration of leukocytes.* Nat Immunol, 2002. **3**(2): p. 151-8.
28. Ma, S., S. K. Shaw, L. Yang, T. Jones, Y. Liu, A. Nusrat, C. A. Parkos, and F. W. Luscinskas, *Dynamics of junctional adhesion molecule 1 (JAM1) during leukocyte transendothelial migration under flow in vitro.* FASEB J, 2003. **17**: p. A1189.
29. Shaw, S.K., et al., *Real-time imaging of vascular endothelial-cadherin during leukocyte transmigration across endothelium.* J Immunol, 2001. **167**(4): p. 2323-30.
30. Feng, D., et al., *Neutrophils emigrate from venules by a transendothelial cell pathway in response to FMLP.* J Exp Med, 1998. **187**(6): p. 903-15.
31. Yang, L., et al., *ICAM-1 regulates neutrophil adhesion and transcellular migration of TNF-alpha-activated vascular endothelium under flow.* Blood, 2005. **106**(2): p. 584-92.
32. Huang, A.J., et al., *Endothelial cell cytosolic free calcium regulates neutrophil migration across monolayers of endothelial cells.* J Cell Biol, 1993. **120**(6): p. 1371-80.
33. van Buul, J.D. and P.L. Hordijk, *Signaling in leukocyte transendothelial migration.* Arterioscler Thromb Vasc Biol, 2004. **24**(5): p. 824-33.
34. Hordijk, P., *Endothelial signaling in leukocyte transmigration.* Cell Biochem Biophys, 2003. **38**(3): p. 305-22.
35. Wang, Q. and C.M. Doerschuk, *The signaling pathways induced by neutrophil-endothelial cell adhesion.* Antioxid Redox Signal, 2002. **4**(1): p. 39-47.

36. Evans, E. and A. Yeung, *Apparent viscosity and cortical tension of blood granulocytes determined by micropipet aspiration.* Biophys J, 1989. **56**(1): p. 151-60.
37. Schmid-Schonbein, G.W., et al., *Passive mechanical properties of human leukocytes.* Biophys J, 1981. **36**(1): p. 243-56.
38. Sung, K.L., et al., *Leukocyte relaxation properties.* Biophys J, 1988. **54**(2): p. 331-6.
39. Kan, H.C.U., H.S.; Shyy, W.; and Tran-Son-Tay, R., *Hydrodynamics of a compound drop with application to leukocyte modeling.* Physics of Fluids, 1998. **10**: p. 760-774.
40. Dong, C., et al., *Passive deformation analysis of human leukocytes.* J Biomech Eng, 1988. **110**(1): p. 27-36.
41. Tsai, M.A., R.S. Frank, and R.E. Waugh, *Passive mechanical behavior of human neutrophils: power-law fluid.* Biophys J, 1993. **65**(5): p. 2078-88.
42. Dao, M.L., CT; Suresh S., *Mechanics of the human red blood cell deformed by optical tweezers.* Journal of the Mechanics and Physics of Solids., 2003. **51**: p. 2259-2280.
43. Li, J., et al., *Spectrin-level modeling of the cytoskeleton and optical tweezers stretching of the erythrocyte.* Biophys J, 2005. **88**(5): p. 3707-19.
44. Yanai, M., et al., *Intracellular elasticity and viscosity in the body, leading, and trailing regions of locomoting neutrophils.* Am J Physiol, 1999. **277**(3 Pt 1): p. C432-40.
45. Yanai, M., et al., *Regional rheological differences in locomoting neutrophils.* Am J Physiol Cell Physiol, 2004. **287**(3): p. C603-11.
46. Yap, B. and R.D. Kamm, *Mechanical deformation of neutrophils into narrow channels induces pseudopod projection and changes in biomechanical properties.* J Appl Physiol, 2005. **98**(5): p. 1930-9.
47. Mason, T.G., K; van Zanten, JH; Wirtz, D; Kuo, SC., *Particle tracking microrheology of complex fluids.* Phys Rev Lett, 1997. **79**(17): p. 3282-3285.
48. Mason, T., *Estimating the viscoelastic moduli of complex fluids using the generalized Stokes-Einstein equation.* Rheol Acta, 2000. **39**: p. 371-378.
49. Saito, H., et al., *Mechanical properties of rat bone marrow and circulating neutrophils and their responses to inflammatory mediators.* Blood, 2002. **99**(6): p. 2207-13.
50. Worthen, G.S., et al., *Mechanics of stimulated neutrophils: cell stiffening induces retention in capillaries.* Science, 1989. **245**(4914): p. 183-6.
51. Howard, T., et al., *Gelsolin-actin interaction and actin polymerization in human neutrophils.* J Cell Biol, 1990. **110**(6): p. 1983-91.
52. Kitagawa, Y., et al., *Effect of mechanical deformation on structure and function of polymorphonuclear leukocytes.* J Appl Physiol, 1997. **82**(5): p. 1397-405.
53. Anderson, G.J., et al., *Effect of mechanical deformation of neutrophils on their CD18/ICAM-1-dependent adhesion.* J Appl Physiol, 2001. **91**(3): p. 1084-90.
54. Yap, B., *Mechanical Deformation of Neutrophil into Pulmonary Capillaries Induces Cytoskeletal Remodeling, Pseudopod Projection and Changes in Biomechanical Properties*. 2005, Massachusetts Institute of Technology.

55. Pender, N. and C.A. McCulloch, *Quantitation of actin polymerization in two human fibroblast sub-types responding to mechanical stretching.* J Cell Sci, 1991. **100 (Pt 1)**: p. 187-93.
56. Elson, E.L., *Cellular mechanics as an indicator of cytoskeletal structure and function.* Annu Rev Biophys Biophys Chem, 1988. **17**: p. 397-430.
57. Lodish, H.B., A; Matsudaira, P; Kaiser, CA; Krieger, M; Scott, MP; Zipursky, SL; and Darnell, J., *Molecular Cell Biology*. 5th ed. 2004: W.H. Freeman and Company.
58. Hoyer, J., et al., *Ca2+ influx through stretch-activated cation channels activates maxi K+ channels in porcine endocardial endothelium.* Proc Natl Acad Sci U S A, 1994. **91**(6): p. 2367-71.
59. Pozzan, T., et al., *Is cytosolic ionized calcium regulating neutrophil activation?* Science, 1983. **221**(4618): p. 1413-5.
60. Marks, P.W. and F.R. Maxfield, *Transient increases in cytosolic free calcium appear to be required for the migration of adherent human neutrophils.* J Cell Biol, 1990. **110**(1): p. 43-52.
61. al-Mohanna, F.A. and M.B. Hallett, *Actin polymerization in neutrophils is triggered without a requirement for a rise in cytoplasmic Ca2+.* Biochem J, 1990. **266**(3): p. 669-74.
62. Laffafian, I. and M.B. Hallett, *Does cytosolic free Ca2+ signal neutrophil chemotaxis in response to formylated chemotactic peptide?* J Cell Sci, 1995. **108 (Pt 10)**: p. 3199-205.
63. Voldman, J., M.L. Gray, and M.A. Schmidt, *Microfabrication in biology and medicine.* Annu Rev Biomed Eng, 1999. **1**: p. 401-25.
64. Whitesides, G.M., et al., *Soft lithography in biology and biochemistry.* Annu Rev Biomed Eng, 2001. **3**: p. 335-73.
65. Tan, J.L., et al., *Cells lying on a bed of microneedles: an approach to isolate mechanical force.* Proc Natl Acad Sci U S A, 2003. **100**(4): p. 1484-9.
66. Sia, S.K. and G.M. Whitesides, *Microfluidic devices fabricated in poly(dimethylsiloxane) for biological studies.* Electrophoresis, 2003. **24**(21): p. 3563-76.
67. Hogg, J.C., et al., *Erythrocyte and polymorphonuclear cell transit time and concentration in human pulmonary capillaries.* J Appl Physiol, 1994. **77**(4): p. 1795-800.
68. Hogg, J.C. and C.M. Doerschuk, *Leukocyte traffic in the lung.* Annu Rev Physiol, 1995. **57**: p. 97-114.
69. Lichtman, M., *Rheology of leukocytes, leukocyte suspensions, and blood in leukemia.* J Clin Invest, 1973. **52**: p. 350-358.
70. Yap, B. and R.D. Kamm, *Cytoskeletal remodeling and cellular activation during deformation of neutrophils into narrow channels.* J Appl Physiol, 2005. **99**(6): p. 2323-30.
71. Downey, G.P., et al., *Actin assembly in electropermeabilized neutrophils: role of intracellular calcium.* J Cell Biol, 1990. **110**(6): p. 1975-82.
72. Janmey, P.A., *Phosphoinositides and calcium as regulators of cellular actin assembly and disassembly.* Annu Rev Physiol, 1994. **56**: p. 169-91.

73. Lipp, P. and E. Niggli, *Ratiometric confocal Ca(2+)-measurements with visible wavelength indicators in isolated cardiac myocytes.* Cell Calcium, 1993. **14**(5): p. 359-72.
74. Floto, R.A., et al., *IgG-induced Ca2+ oscillations in differentiated U937 cells; a study using laser scanning confocal microscopy and co-loaded fluo-3 and fura-red fluorescent probes.* Cell Calcium, 1995. **18**(5): p. 377-89.
75. Novak, E.J. and P.S. Rabinovitch, *Improved sensitivity in flow cytometric intracellular ionized calcium measurement using fluo-3/Fura Red fluorescence ratios.* Cytometry, 1994. **17**(2): p. 135-41.
76. Alteraifi, A.M. and D.V. Zhelev, *Transient increase of free cytosolic calcium during neutrophil motility responses.* J Cell Sci, 1997. **110 (Pt 16)**: p. 1967-77.
77. Anderson, J.R., et al., *Fabrication of topologically complex three-dimensional microfluidic systems in PDMS by rapid prototyping.* Anal Chem, 2000. **72**(14): p. 3158-64.
78. Juncker, D.S., H; Bernard, A; Caelen, I; Michel, B; de Rooij, N; and Delamarche, E., *Soft and rigid two-level microfluidic networks for patterning surfaces.* Journal of Micromechanics and Microengineering, 2001. **11**: p. 532-541.
79. Crocker, J., and Grier, DG., *Methods of digital video microscopy for colloidal studies.* Journal of Colloid and Interface Science, 1996. **179**: p. 298-310.
80. Huang, Y., C.M. Doerschuk, and R.D. Kamm, *Computational modeling of RBC and neutrophil transit through the pulmonary capillaries.* J Appl Physiol, 2001. **90**(2): p. 545-64.
81. Bathe, M., et al., *Neutrophil transit times through pulmonary capillaries: the effects of capillary geometry and fMLP-stimulation.* Biophys J, 2002. **83**(4): p. 1917-33.
82. Zaffran, Y., et al., *F-actin content and spatial distribution in resting and chemoattractant-stimulated human polymorphonuclear leucocytes. Which role for intracellular free calcium?* J Cell Sci, 1993. **105 (Pt 3)**: p. 675-84.
83. Glogauer, M., et al., *Calcium ions and tyrosine phosphorylation interact coordinately with actin to regulate cytoprotective responses to stretching.* J Cell Sci, 1997. **110 (Pt 1)**: p. 11-21.
84. Matthews, B.D., et al., *Cellular adaptation to mechanical stress: role of integrins, Rho, cytoskeletal tension and mechanosensitive ion channels.* J Cell Sci, 2006. **119**(Pt 3): p. 508-18.
85. Yin, H.L. and T.P. Stossel, *Purification and structural properties of gelsolin, a Ca2+-activated regulatory protein of macrophages.* J Biol Chem, 1980. **255**(19): p. 9490-3.
86. Yin, H.L., K.S. Zaner, and T.P. Stossel, *Ca2+ control of actin gelation. Interaction of gelsolin with actin filaments and regulation of actin gelation.* J Biol Chem, 1980. **255**(19): p. 9494-500.
87. Janmey, P.A., et al., *Interactions of gelsolin and gelsolin-actin complexes with actin. Effects of calcium on actin nucleation, filament severing, and end blocking.* Biochemistry, 1985. **24**(14): p. 3714-23.
88. Bennett, J.P., K.S. Zaner, and T.P. Stossel, *Isolation and some properties of macrophage alpha-actinin: evidence that it is not an actin gelling protein.* Biochemistry, 1984. **23**(21): p. 5081-6.

89. Duhaiman, A.S. and J.R. Bamburg, *Isolation of brain alpha-actinin. Its characterization and a comparison of its properties with those of muscle alpha-actinins.* Biochemistry, 1984. **23**(8): p. 1600-8.
90. Witke, W., et al., *The Ca(2+)-binding domains in non-muscle type alpha-actinin: biochemical and genetic analysis.* J Cell Biol, 1993. **121**(3): p. 599-606.
91. Hartwig, J.H., et al., *MARCKS is an actin filament crosslinking protein regulated by protein kinase C and calcium-calmodulin.* Nature, 1992. **356**(6370): p. 618-22.
92. Matsumura, F. and S. Yamashiro, *Caldesmon.* Curr Opin Cell Biol, 1993. **5**(1): p. 70-6.
93. Harris, A.S. and J.S. Morrow, *Calmodulin and calcium-dependent protease I coordinately regulate the interaction of fodrin with actin.* Proc Natl Acad Sci U S A, 1990. **87**(8): p. 3009-13.
94. Baggiolini, M.a.K., P., *Neutrophil Activation: Control of Shape Change, Exocytosis, and Respiratory Burst.* NIPS, 1992. **7**: p. 215-219.
95. Allbritton, N.L., T. Meyer, and L. Stryer, *Range of messenger action of calcium ion and inositol 1,4,5-trisphosphate.* Science, 1992. **258**(5089): p. 1812-5.
96. Lamb, J.A., et al., *Modulation of gelsolin function. Activation at low pH overrides Ca2+ requirement.* J Biol Chem, 1993. **268**(12): p. 8999-9004.
97. Brundage, R.A., et al., *Calcium gradients underlying polarization and chemotaxis of eosinophils.* Science, 1991. **254**(5032): p. 703-6.
98. Tseng, Y., et al., *The bimodal role of filamin in controlling the architecture and mechanics of F-actin networks.* J Biol Chem, 2004. **279**(3): p. 1819-26.
99. Evans, E. and B. Kukan, *Passive material behavior of granulocytes based on large deformation and recovery after deformation tests.* Blood, 1984. **64**(5): p. 1028-35.
100. Bengtsson, T., O. Stendahl, and T. Andersson, *The role of the cytosolic free Ca2+ transient for fMet-Leu-Phe induced actin polymerization in human neutrophils.* Eur J Cell Biol, 1986. **42**(2): p. 338-43.
101. Moazzam, F., et al., *The leukocyte response to fluid stress.* Proc Natl Acad Sci U S A, 1997. **94**(10): p. 5338-43.
102. Coughlin, M.F. and G.W. Schmid-Schonbein, *Pseudopod projection and cell spreading of passive leukocytes in response to fluid shear stress.* Biophys J, 2004. **87**(3): p. 2035-42.
103. Makino, A., et al., *Control of neutrophil pseudopods by fluid shear: role of Rho family GTPases.* Am J Physiol Cell Physiol, 2005. **288**(4): p. C863-71.
104. Meshki, J., et al., *Molecular mechanism of nucleotide-induced primary granule release in human neutrophils: role for the P2Y2 receptor.* Am J Physiol Cell Physiol, 2004. **286**(2): p. C264-71.
105. Huang, N.N., et al., *Multiple signal transduction pathways lead to extracellular ATP-stimulated mitogenesis in mammalian cells: II. A pathway involving arachidonic acid release, prostaglandin synthesis, and cyclic AMP accumulation.* J Cell Physiol, 1991. **146**(3): p. 483-94.
106. Downey, G.P., et al., *Biophysical properties and microfilament assembly in neutrophils: modulation by cyclic AMP.* J Cell Biol, 1991. **114**(6): p. 1179-90.

107. Erb, L., et al., *An RGD sequence in the P2Y(2) receptor interacts with alpha(V)beta(3) integrins and is required for G(o)-mediated signal transduction.* J Cell Biol, 2001. **153**(3): p. 491-501.
108. Ng-Sikorski, J., et al., *Calcium signaling capacity of the CD11b/CD18 integrin on human neutrophils.* Exp Cell Res, 1991. **195**(2): p. 504-8.
109. Petersen, M., J.D. Williams, and M.B. Hallett, *Cross-linking of CD11b or CD18 signals release of localized Ca2+ from intracellular stores in neutrophils.* Immunology, 1993. **80**(1): p. 157-9.
110. Hellberg, C., et al., *The Ca2+ signaling capacity of the beta 2-integrin on HL60-granulocytic cells is abrogated following phosphorylation of its CD18-chain: relation to impaired protein tyrosine phosphorylation.* Exp Cell Res, 1995. **217**(1): p. 140-8.
111. Hellberg, C., et al., *Ca2+ signalling mechanisms of the beta 2 integrin on neutrophils: involvement of phospholipase C gamma 2 and Ins(1,4,5)P3.* Biochem J, 1996. **317 (Pt 2)**: p. 403-9.
112. McKee, L.C., Jr. and R.D. Collins, *Intravascular leukocyte thrombi and aggregates as a cause of morbidity and mortality in leukemia.* Medicine (Baltimore), 1974. **53**(6): p. 463-78.
113. Lichtman, M.A. and J.M. Rowe, *Hyperleukocytic leukemias: rheological, clinical, and therapeutic considerations.* Blood, 1982. **60**(2): p. 279-83.
114. Stucki, A., et al., *Endothelial cell activation by myeloblasts: molecular mechanisms of leukostasis and leukemic cell dissemination.* Blood, 2001. **97**(7): p. 2121-9.
115. Skoutelis, A.T., et al., *Neutrophil deformability in patients with sepsis, septic shock, and adult respiratory distress syndrome.* Crit Care Med, 2000. **28**(7): p. 2355-9.
116. Grau, A.J., et al., *Granulocyte adhesion, deformability, and superoxide formation in acute stroke.* Stroke, 1992. **23**(1): p. 33-9.
117. Tarlowe, M.H., et al., *Prospective study of neutrophil chemokine responses in trauma patients at risk for pneumonia.* Am J Respir Crit Care Med, 2005. **171**(7): p. 753-9.

APPENDIX

A.1 IDL Commands for First Frame

The following is taken from the Appendix of [54], with permission.

The commands used in the tracking of particles is shown below together with a brief description of the utility of each command (in blue). Part of the command lines are highlighted in red; which indicates the parameters that could be varied for each command.

Particle Identification

```
window,0,xsize=740,ysize=252
```
Creates an image window number 0, with horizontal pixel size of 740 and vertical pixel size of 252.

```
wset,0
```
Sets image window 0 as the current active window.

```
a=read_nih('c:\RSI\IDL60\reslice1\frame0000.tif')
```
Reads in a single NIH image from file named 'frame0000.tif' in the c:\RSI\IDL60\reslice1 directory.

```
tvscl,a
```
Displays the image file that has been read in the active window.

```
temp=255b-a
```
Inverts the image color (i.e. white becomes black and vice-versa).

```
b=bpass(temp,1,9)
```
bpass is the spatial bandpass filter which smooths the image and substracts the background off. The two numbers are the spatial wavelength cutoffs in pixels. The first one is almost always '1'. The second number is set to be approximately the size of the granules in pixels.

```
f=feature(b,9)
```
Finds the coordinates of the particles. The parameter (9) is again the diameter of the granules in pixels, similar to that used in the bpass upper cutoff above.

```
fo=fover2d(a,f)
```
Plots dots where each particle was found.

```
plot,f(2,*),f(3,*),psym=6
```
Plots the graph of radius of gyration (vertical axis) vs. brightness (horizontal axis). The brightness helps to distinguish the dots that represent the granules, which are brighter, from the dimmer dots that are due to random noise in the starting image.

```
f=feature(b,9,masscut=5000)
```
Isolates the coordinates of granules by setting the 'masscut', which is the minimum brightness value above which the dots are regarded as granules. The parameter (9) is again the diameter of the granules in pixels.

```
plot_hist,f(0,*) mod 1
```
Plots histogram to test for pixel-biasing. The histogram obtained should look flat if the length scale in **feature** (diameter of granules in pixels) is large enough. If the histogram has a deep dip in the middle, the length scale in **feature** should be increased.

More details on the tracking macros can be found on the website, http://www.physics.emory.edu/~weeks/idl/tracking.html.

A.2 IDL Commands for All Frames

The following is taken from the Appendix of [54], with permission. A slight modification has been made.

The commands used in the tracking of particles is shown below together with a brief description of the utility of each command (in blue). Part of the command lines are highlighted in red; which indicates the parameters that could be varied for each command.

Particle Tracking

```
jpretrackmod,'c:\RSI\IDL60\reslice1\',[1,9,9,5000],297,100,
invert=1
```
Applies the various parameters from the previous particle identification step to all images in the stack. The argument has a 4-component vector: the first two components are the two bpass parameters, the third is the feature size parameter, and the fourth is the masscut parameter. The goal of this command is to create one file of coordinates 'xys.result'.

```
pt=read_gdf('xys.result')
```
Reads in the xys.result file that contains the pre-tracked data.

```
pta=eclip(pt,[0,0,297],[1,0,100])
```
Crops any section of the image of interest for particle tracking. The first bracket crops the x-pixels while the second bracket crops the y-pixels (in this case, the section of the image cropped is between 0 and 297 for x-pixels and between 0 and 100 for y-pixels).

```
plot_hist,pta(0,*) mod 1
```
Plots histogram to test for pixel-biasing again.

```
t=track(pta,5,goodenough=30)
```
Connects the particles identified in the stack of images to form trajectories of particles. The first number represents displacement, i.e. the maximum distance in pixels that the particle is

expected to move between frames. "Goodenough" specifies the minimum duration for the particle trajectory (in no. of frames) for it to be accepted as a valid trajectory.

```
write_gdf,t,'track.result'
```
Creates a file of coordinates 'track.result' that contains the individual trajectories.

```
write_textmod,t,'result.txt'
```
Writes the 'track.result' file in text format so that it can be opened in Excel.

```
plottr,t,goodenough=30
```
Plots all the trajectories that are tracked for at the least the duration specified in "goodenough".

```
window,1
```
Opens a new window. Prevents particle-tracking video from being placed over the particle trajectory plot.

```
info=monitor_mod(t)
```
Rearranges and extracts information out from the track.results file for part_find_mod1 command below.

```
write_gdf,info,'info.result'
```
Creates a file of coordinates 'info.result' from the monitor_mod command above.

```
write_textmod,info,'info.txt'
```
Writes the 'info.result' file in text format so that it can be opened in Excel.

```
part_find_mod1,info,30,797,297,100
```
Animates each granule trajectory separately. Each granule is given a unique particle identification (ID) number. Observation of the individual trajectory animation ensures that the granules do not exhibit directed motion and that the trajectory of each granule is not mistaken for that of neighboring granules that might cross its path. The first number represents the "goodenough" value; The second number specifies the number of frames in the stack of images tracked; while the third and fourth number denotes the number of x-pixels and y-pixels in the images respectively.

```
particle_IDs=part_input(62)
```
After verifying and selecting the granules that satisfies all requirements for tracking, the ID nos of these granules are noted down and input back into the program with this command. The number (in this case 62) represents the total number of granule IDs that has been chosen. After execution of the command, the program returns a commad asking the user to input the ID nos of this particles one after another until all (62 in this case) IDs nos have been keyed in.

```
write_gdf,particle_IDs,'particle_IDs.result'
```
Creates a file of coordinates 'particle_IDs.result' which contain the particle ID nos that was input in the step above.

```
region_time_blocks_front,t,info,particle_Ids,30,0,297,0,100,
1,797,150
```

This command generates the MSD for each granule selected in the steps above. The first number represents the "goodenough" value, the second and third numbers specify the cropped x-pixel values, the fourth and fifth numbers denote the cropped y-pixel values, the fifth and sixth numbers specify the start and end frames for the MSD calculation, and the last number indicates the interval (in no of frames) for each MSD blocks. After execution, the command will return the MSD values at each time interval specified (in this case, 150 frames, i.e. 5 s)

A.3 IDL Codes

The following section is taken directly from [54], with permission.

The following section lists the codes used in the various IDL commands in section A.1 and A.2. Most of the codes were either newly written or modified from their original form to suit the particle tracking requirements for the present study.

A.3.1 bpass

```
; ********** start of bpass.pro
;
; see http://www.physics.emory.edu/~weeks/idl
; for further documentation
;
;+
; NAME:
; bpass
; PURPOSE:
; Implements a real-space bandpass filter which suppress
; pixel noise and slow-scale image variations while
; retaining information of a characteristic size.
;
; CATEGORY:
; Image Processing
; CALLING SEQUENCE:
; res = dgfilter( image, lnoise, lobject )
; INPUTS:
; image: The two-dimensional array to be filtered.
; lnoise: Characteristic lengthscale of noise in pixels.
; Additive noise averaged over this length should
; vanish. MAy assume any positive floating value.
; lobject: A length in pixels somewhat larger than a typical
; object. Must be an odd valued integer.
; OUTPUTS:
; res: filtered image.
; PROCEDURE:
; simple 'wavelet' convolution yields spatial bandpass filtering.
; NOTES:
; MODIFICATION HISTORY:
; Written by David G. Grier, The University of Chicago, 2/93.
```

```
; Greatly revised version DGG 5/95.
; Added /field keyword JCC 12/95.
; Revised & added 'stack','voxel' capability JCC 5/97.
;
; This code 'bpass.pro' is copyright 1997, John C. Crocker and
; David G. Grier. It should be considered 'freeware'- and may be
; distributed freely in its original form when properly attributed.
;-
function bpass, image, lnoise, lobject, field = field, noclip=noclip

nf = n_elements(image(0,0,*))

;on_error, 2                    ; go to caller on error

b = float( lnoise )
w = round( lobject > (2. * b) )
N = 2*w + 1

r = (findgen( N ) - w)/(2. * b)
xpt = exp( -r^2 )
xpt = xpt / total(xpt)
factor = ( total(xpt^2) - 1/N )

gx = xpt
gy = transpose(gx)

bx = fltarr(N) - 1./N
by = transpose(bx)

if keyword_set( field ) then begin
        if N mod 4 eq 1 then indx = 2*indgen(w+1)$
                else indx = 1+ (2*indgen(w))
        gy = gy(indx)
        gy = gy/total(gy)

        nn = n_elements(indx)
        by = fltarr(nn) - 1./nn
endif

res = float(image)
; do x and y convolutions
for i = 0,nf-1 do begin
        g = convol( float(image(*,*,i)), gx )
        g = convol( g, gy )

        b = convol( float(image(*,*,i)), bx )
        b = convol( b, by )

        res(*,*,i) = g-b
endfor
if keyword_set( noclip ) then $
        return,res/factor $
else $
        return,res/factor > 0
end
;********** end of bpass.pro
```

A.3.2 eclip

```
; eclip Eric Weeks, 9-22-98
; see http://glinda.lrsm.upenn.edu/~weeks/idl/

function eclip,data,f1,f2,f3,f4,f5,f6,invert=invert
; data in form (*,*)
;
; datanew=eclip(data,[A,B,C])
; w=where(data(A,*) ge B and data(A,*) le C)
; datanew=data(*,w)
;

if (keyword_set(invert)) then flag=lindgen(n_elements(data(0,*)))

s=size(f1)
if (s(1) gt 1) then begin
        w=where((data(f1(0),*) ge f1(1)) and (data(f1(0),*)) le f1(2),nw)
        if (nw gt 0) then begin
                result=data(*,w)
                if keyword_set(invert) then flag=flag(w)
        endif
endif
s=size(f2)
if (s(1) gt 1) then begin
        w=where((result(f2(0),*) ge f2(1)) and (result(f2(0),*)) le f2(2),nw)
        if (nw gt 0) then begin
        result=result(*,w)
        if keyword_set(invert) then flag=flag(w)
        endif
endif
s=size(f3)
if (s(1) gt 1) then begin
        w=where((result(f3(0),*) ge f3(1)) and (result(f3(0),*)) le f3(2),nw)
        result=result(*,w)
        if keyword_set(invert) then flag=flag(w)
        s=size(f4)
        if (s(1) gt 1) then begin
                w=where((result(f4(0),*) ge f4(1)) and (result(f4(0),*)) le f4(2),nw)
                if (nw gt 0) then begin
                        result=result(*,w)
                        if keyword_set(invert) then flag=flag(w)
                endif
        endif
        s=size(f5)
        if (s(1) gt 1) then begin
                w=where((result(f5(0),*) ge f5(1)) and (result(f5(0),*)) le f5(2),nw)
                if (nw gt 0) then begin
                        result=result(*,w)
                        if keyword_set(invert) then flag=flag(w)
                endif
        endif
        s=size(f6)
        if (s(1) gt 1) then begin
                w=where((result(f6(0),*) ge f6(1)) and (result(f6(0),*)) le f6(2),nw)
                if (nw gt 0) then begin
```

```
                result=result(*,w)
                if keyword_set(invert) then flag=flag(w)
            endif
        endif
endif

if (keyword_set(invert)) then begin
        flag2=lindgen(n_elements(data(0,*)))
        flag2(flag) = -1
        w=where(flag2 ge 0)
        result=data(*,w)
endif

return,result
end
```

A.3.3 feature

```
;+
;
; see http://www.physics.emory.edu/~weeks/idl
; for more information
;
; NAME:
;           Feature
; PURPOSE:
;           Finds and measures roughly circular 'features' within
;           an image.
; CATEGORY:
;           Image Processing
; CALLING SEQUENCE:
;           f = feature( image, diameter [, separation, masscut = masscut,
;               min = min, iterate = iterate, /field, /quiet ] )
; INPUTS:
;           image: (nx,ny) array which presumably contains some
;               features worth finding
;           diameter: a parameter which should be a little greater than
;               the diameter of the largest features in the image.
;               Diameter MUST BE ODD valued.
;           separation: an optional parameter which specifies the
;               minimum allowable separation between feature
;               centers. The default value is diameter+1.
;           masscut:Setting this parameter saves runtime by reducing the
;               runtime wasted on low mass 'noise' features.
;           min: Set this optional parameter to the minimum allowed
;               value for the peak brightness of a feature. Useful
;               for limiting the number of spurious features in
;               noisy images.
;           field: Set this keyword if image is actually just one field
;               of an interlaced (e.g. video) image. All the masks
;               will then be constructed with a 2:1 aspect ratio.
;           quiet: Supress printing of informational messages.
;           iterate: if the refined centroid position is too far from
;               the initial estimate, iteratively recalc. the centroid
```

```
;                       using the last cetroid to position the mask. This
;                       can be useful for really noisy data, or data with
;                       flat (e.g. saturated) peaks. Use with caution- it
;                       may 'climb' hills and give you multiple hits.
; OUTPUTS:
;               f(0,*): this contains the x centroid positions, in pixels.
;               f(1,*): this contains the y centroid positions, in pixels.
;               f(2,*): this contains the integrated brightness of the
;                       features.
;               f(3,*): this contains the square of the radius of gyration
;                       of the features.
;               f(4,*): this contains the eccentricity, which should be
;                       zero for circularly symmetric features and order
;                       one for very elongated images.
; SIDE EFFECTS:
;               Displays the number of features found on the screen.
; RESTRICTIONS:
;               To work properly, the image must consist of bright,
;               circularly symmetric regions on a roughly zero-valued
;               background. To find dark features, the image should be
;               inverted and the background subtracted. If the image
;               contains a large amount of high spatial frequency noise,
;               performance will be improved by first filtering the image.
;               BPASS will remove high spatial frequency noise, and
;               subtract the image background and thus provides a good
;               complement to using this program. Individual features
;               should NOT overlap.
; PROCEDURE:
;               First, identify the positions of all the local maxima in
;               the image ( defined in a circular neighborhood with diameter
;               equal to 'diameter' ). Around each of these maxima, place a
;               circular mask, of diameter 'diameter', and calculate the x & y
;               centroids, the total of all the pixel values, and the radius
;               of gyration and the 'eccentricity' of the pixel values within
;               that mask. If the initial local maximum is found to be more
;               than 0.5 pixels from the centroid and iterate is set, the mask
;               is moved and the data are re-calculated. This is useful for
;               noisy data. If the restrictions above are adhered to, and the
;               features are more than about 5 pixels across, the resulting x
;               and y values will have errors of order 0.1 pixels for
;               reasonably noise free images.
;
; ********* READ THE FOLLOWING IMPORTANT CAVEAT! **********
;               'feature' is capable of finding image features with sub-pixel
;               accuracy, but only if used correctly- that is, if the
;               background is subtracted off properly and the centroid mask
;               is larger than the feature, so that clipping does not occur.
;               It is an EXCELLENT idea when working with new data to plot
;               a histogram of the x-positions mod 1, that is, of the
;               fractional part of x in pixels. If the resulting histogram
;               is flat, then you're ok, if its strongly peaked, then you're
;               doing something wrong- but probably still getting 'nearest
;               pixel' accuracy.
;
;               For a more quantitative treatment of sub-pixel position
;               resolution see:
```

```
;                   J.C. Crocker and D.G. Grier, J. Colloid Interface Sci.
;                   *179*, 298 (1996).
;
; MODIFICATION HISTORY:
;                   This code is inspired by feature_stats2 written by
;                           David G. Grier, U of Chicago, 1992.
;                   Written by John C. Crocker, U of Chicago, optimizing
;                           runtime and measurement error, 10/93.
;                   Added field keyword, 4/94.
;                   Added eccentricity parameter, 5/95.
;                   Added quiet keyword 12/95.
;                   Added iteration, fixed up the radius/diameter fiasco and
;                   did some debugging which improves non-centroid data. 4/96.
;
;          This code 'feature.pro' is copyright 1997, John C. Crocker and
;          David G. Grier. It should be considered 'freeware'- and may be
;          distributed freely in its original form when properly attributed.
;-
;          produce a parabolic mask
;
function rsqd,w,h

if n_params() eq 1 then h = w
r2 = fltarr(w,h,/nozero)
xc = float(w-1) / 2.
yc = float(h-1) / 2.
x = (findgen(w) - xc)
x = x^2
y = (findgen(h)- yc)
y = y^2

for j = 0, h-1 do begin
          r2(*,j) = x + y(j)
endfor

return,r2
end
;
;          produce a 'theta' mask
;
function thetarr,w

theta = fltarr(w,w,/nozero)
xc = float(w-1) / 2.
yc = float(w-1) / 2.

x = (findgen(w) - xc)
x(xc) = 1e-5
y = (findgen(w) - yc)
for j = 0, w-1 do begin
          theta(*,j) = atan( y(j),x )
endfor

return,theta
end
;
```

```
;       This routine returns the even or odd field of an image
;
function fieldof,array,odd=odd,even=even

sz = size(array)
if sz(0) ne 2 then message,"Argument must be a two-dimensional array!"
if keyword_set(odd) then f=1 else f=0

ny2 = fix( (sz(2)+(1-f))/2 )
rows = indgen(ny2)*2 + f
return,array(*,rows)

end
;
;       barrel "shifts" a floating point arr by a fractional pixel amount,
;       by using a 'lego' interpolation technique.
;
function fracshift,im,shiftx,shifty

ipx = fix( shiftx )
ipy = fix( shifty )
fpx = shiftx - ipx
fpy = shifty - ipy
if fpx lt 0 then begin
        fpx=fpx+1 & ipx=ipx-1
endif
if fpy lt 0 then begin
        fpy=fpy+1 & ipy=ipy-1
endif

image = im

imagex = shift( image,ipx+1,ipy )
imagey = shift( image,ipx ,ipy+1 )
imagexy = shift( image,ipx+1,ipy+1 )
image = shift( image,ipx ,ipy )

res = ( (1. - fpx) * (1. - fpy) * image ) + $
        ( ( fpx) * (1. - fpy) * imagex ) + $
        ( (1. - fpx) * ( fpy) * imagey ) + $
        ( ( fpx) * ( fpy) * imagexy )

return,res
end
;
;       John's version of local_max2, which supports the field keyword
;       and is otherwise identical.
;
function lmx, image, sep, min = min, field = field

range = fix(sep/2)
a = bytscl(image)
w = round( 2 * range + 1 )          ; width of sample region
s = rsqd( w )                       ; sample region is circular
good = where( s le range^2 )
mask = bytarr( w, w )
```

```
mask(good) = 1b
yrange = range
if keyword_set( field ) then begin
        mask = fieldof( mask, /even )
        yrange = fix(range/2.) +1
endif

b = dilate( a, mask, /gray )        ; find local maxima in given range
                                    ; but don't include pixels from the
                            ; background which will be too dim
if not keyword_set( min ) then begin
        h = histogram( a )
        for i = 1, n_elements(h) - 1 do $
                h(i) = h(i) + h(i-1)
        h = float( h ) / max( h )
        min = 0
        while h(min) lt 0.64 do $
        min = min + 1
        min = min + 1
        endif

r = where( a eq b and a ge min )

                                    ; Discard maxima within range of the edge
sz = size( a )
nx = sz(1) & ny = sz(2)
x = r mod nx & y = r / nx
x0 = x - range & x1 = x + range
y0 = y - yrange & y1 = y + yrange
good = where( x0 ge 0 and x1 lt nx and y0 ge 0 and y1 lt ny,ngood )
if ngood lt 1 then $
        return,[-1]
r = r(good)
x = x(good) & y = y(good)
x0 = x0(good) & x1 = x1(good)
y0 = y0(good) & y1 = y1(good)
                                    ; There may be some features which get
                                    ; found twice or which have flat peaks
                                    ; and thus produce multiple hits. Find
                                    ; and clear such spurious points.
c = 0b * a
c(r) = a(r)
center = w * yrange + range
for i = 0D, n_elements(r) - 1D do begin
        b = c(x0(i):x1(i),y0(i):y1(i))
        b = b * mask                ; look only in circular region
        m = max( b, location )
        if location ne center then $
                c(x(i),y(i)) = 0b
        endfor
                                    ; Ideally, the above routine would shrink
                                    ; clusters of points down to their center.
                                    ; As written, this will leave the lower
                                    ; right (?) pixel of a cluster.

r = where( c ne 0 )                 ; What's left are valid maxima.
```

```
return,r                    ; return their locations

end
;
;       John's version of DGG's feature_stats2.
;       which: a) avoids some unnecessary computation (convolutions)
;              b) uses fractional shift techniques to reduce pixel bias in m and Rg
;              c) has the field keyword
;
function feature, image, extent, sep, min=min, masscut = masscut, field = field,$
       quiet = quiet,iterate = iterate

extent = fix(extent)
if (extent mod 2) eq 0 then begin
       message,'Requires an odd extent. Adding 1...',/inf
       extent = extent + 1
       endif

sz = size( image )
nx = sz(1)
ny = sz(2)
if n_params() eq 2 then sep = extent+1

;      Put a border around the image to prevent mask out-of-bounds
a = fltarr( nx + extent, ny + extent )
a(extent/2:(extent/2)+nx-1,extent/2:(extent/2)+ny-1) = float( image )
nx = nx + extent

;      Finding local maxima
if keyword_set( field ) then $
       if not keyword_set( min ) then loc = lmx(a,sep,/field) else $
              loc=lmx(a,sep,min=min,/field) $
else $
       if not keyword_set( min ) then loc = lmx(a,sep) else $
              loc=lmx(a,sep,min=min)

if loc(0) eq -1 then return,-1
x = float( loc mod nx )
y = float( loc / nx )

nmax=n_elements(loc)
xl = x - fix(extent/2)
xh = xl + extent -1
m = fltarr(nmax)

;      Set up some masks
rsq = rsqd( extent )
t = thetarr( extent )
mask = rsq le (float(extent)/2.)^2
mask2 = make_array( extent , extent , /float, /index ) mod (extent ) + 1.
mask2 = mask2 * mask
mask3= (rsq * mask) + (1./6.)
cen = float(extent-1)/2.
cmask = cos(2*t) * mask
smask = sin(2*t) * mask
```

```
cmask(cen,cen) = 0.
smask(cen,cen) = 0.

;       Extract fields of the masks, if necessary
if keyword_set( field ) then begin
        suba = fltarr(extent , fix(extent/2) , nmax)
        mask = fieldof(mask,/odd)
        xmask = fieldof(mask2,/odd)
        ymask = fieldof(transpose(mask2),/odd)
        mask3 = fieldof(mask3,/odd)
        cmask = fieldof(cmask,/odd)
        smask = fieldof(smask,/odd)

        halfext = fix( extent /2 )
        yl = y - fix(halfext/2)
        yh = yl + halfext -1
        yscale = 2
        ycen = cen/2

endif else begin
        suba = fltarr(extent, extent, nmax)
        xmask = mask2
        ymask = transpose( mask2 )

        yl = y - fix(extent/2)
        yh = yl + extent -1
        yscale = 1
        ycen = cen
endelse

; Estimate the mass
for i=0,nmax-1 do m(i) = total( a(xl(i):xh(i),yl(i):yh(i)) * mask )

if keyword_set( masscut ) then begin
        w = where( m gt masscut, nmax )
        if nmax eq 0 then begin
                message,'No features found!',/inf
                return,-1
        endif
        xl = xl(w)
        xh = xh(w)
        yl = yl(w)
        yh = yh(w)
        x = x(w)
        y = y(w)
        m = m(w)
endif

if not keyword_set(quiet) then message, strcompress( nmax ) + ' features found.',/inf

;       Setup some result arrays
xc = fltarr(nmax)
yc = fltarr(nmax)
rg = fltarr(nmax)
e = fltarr(nmax)
```

```
;       Calculate feature centers
for i=0,nmax-1 do begin
        xc(i) = total( a(xl(i):xh(i),yl(i):yh(i)) * xmask )
        yc(i) = total( a(xl(i):xh(i),yl(i):yh(i)) * ymask )
endfor

;       Correct for the 'offset' of the centroid masks
xc = xc / m - ((float(extent)+1.)/2.)
yc = (yc / m - ((float(extent)+1.)/2.)) / yscale

;       Iterate any bad initial estimate.
if keyword_set( iterate ) then begin
counter = 0
repeat begin
        counter = counter + 1

        w = where( abs(xc) gt 0.6, nbadx )
        if nbadx gt 0 then begin
                dx = round( xc(w) )
                xl(w) = xl(w) + dx
                xh(w) = xh(w) + dx
                x(w) = x(w) + dx
        endif
        w = where( abs(yc) gt 0.6, nbady )
        if nbady gt 0 then begin
                dy = round( yc(w) )
                yl(w) = yl(w) + dy
                yh(w) = yh(w) + dy
                y(w) = y(w) + dy
        endif

        w = where( (abs(xc) gt 0.6) or (abs(yc) gt 0.6), nbad )
        if nbad gt 0 then begin ; recalculate the centroids for the guys we're iterating

                for i=0,nbad-1 do m(w(i)) = total( a(xl(w(i)):xh(w(i)),$
                        yl(w(i)):yh(w(i))) * mask )
                for i=0,nbad-1 do begin
                        xc(w(i)) = total( a(xl(w(i)):xh(w(i)),yl(w(i)):yh(w(i))) * xmask )
                        yc(w(i)) = total( a(xl(w(i)):xh(w(i)),yl(w(i)):yh(w(i))) * ymask )
                endfor

                xc(w) = xc(w) / m(w) - ((float(extent)+1.)/2.)
                yc(w) = ( yc(w) / m(w) - ((float(extent)+1.)/2.) ) / yscale
        endif
endrep until (nbad eq 0) or (counter eq 10)
endif

;       Update the positions and correct for the width of the 'border'
x = x + xc - extent/2
y = ( y + yc - extent/2 ) * yscale

;       Construct the subarray
for i=0,nmax-1 do suba(*,*,i) = fracshift( a(xl(i):xh(i),yl(i):yh(i)), -xc(i) , -yc(i) )

;       Calculate the 'mass'
for i=0,nmax-1 do m(i) = total( suba(*,*,i) * mask )
```

```
;       Calculate radii of gyration squared
for i=0,nmax-1 do rg(i) = total( suba(*,*,i) * mask3 ) / m(i)

;       Calculate the 'eccentricity'
for i=0,nmax-1 do e(i) = sqrt(( total( suba(*,*,i) * cmask )^2 ) +$
        ( total( suba(*,*,i) * smask )^2 )) / (m(i)-suba(cen,ycen,i)+1e-6)

params = [transpose(x),transpose(y),transpose(m),transpose(rg),transpose(e)]
return,params
end
```

A.3.4 fover2d

```
;function fover2d,image,points,radius=radius,big=big,nodot=nodot,circle=circle
;
; see http://www.physics.emory.edu/~weeks/idl
; for more information and software updates
;+
; NAME:
;               fover2d
; PURPOSE:
;               Overlay points onto a 2d image.
; CALLING SEQUENCE:
;               newimage=foverlay,image,points
; INPUTS:
;               image: 2D data set onto which the points should be overlaid
;               points: (2,npoints) array of overlay points
; OUTPUTS:
;               returns an image ready for 'tv'. The color palette
;               is adjusted to be the foverlay palette. Redraws screen.
; KEYWORDS:
;               radius sets size of circles
;       /big doubles the picture in size in each direction
;       /nodot turns off the black dot at the center of each circle
;       /circle draws a circle around each point, rather than a disk
; PROCEDURE:
;               Rescale the image to leave some color table indices free.
;               Make the rest of the color table into a grey ramp and
;               turn the 3 highest indices into 3 new colors. Plot a
;               disk at each particle position.
; MODIFICATION HISTORY:
;               Lookup table code taken from David G. Grier's f_overlay
;               routine. Mostly written by Eric Weeks in summer '98.
;               Ability to handle movies added 2-20-99.
;-
;First a utility function....
; circarray.pro, started 6-22-98 by ERW
; shortened into fo_circ 2-20-99 by ERW
;
function fo_circ,array,radius=radius,center=center,circle=circle
; returns an array, size equal to "array" variable, with value 1
; everywhere within a circle of diameter of the array size. Circle
; is at center of array.
;
; 'radius' sets a radius different from the default radius (half the array size)
```

```
; 'center' overrides the default center of the circle

s=size(array)
result=array*0

sx=s(1) & sy=s(2)
minsize = (sx < sy)
cx=(sx-1)*0.5 & cy=(sy-1)*0.5
if keyword_set(center) then begin
        cx=center(0)
        cy=center(1)
endif
if keyword_set(radius) then begin
        irad=radius
endif else begin
        irad=minsize/2
endelse
jrad=(irad-1.2)*(irad-1.2)
irad = irad*irad
if (keyword_set(circle)) then begin
        for j=0,sy-1 do begin
                rad2 = (cy-j)*(cy-j)
                for k=0,sx-1 do begin
                        rad3 = rad2 + (cx-k)*(cx-k)
                        result(k,j) = ((rad3 le irad) and (rad3 ge jrad))
                endfor
        endfor
endif else begin
        for j=0,sy-1 do begin
                rad2 = (cy-j)*(cy-j)
                for k=0,sx-1 do begin
                        rad3 = rad2 + (cx-k)*(cx-k)
                        result(k,j) = (rad3 le irad)
                endfor
        endfor
endelse

return,result
end

function fover2d,image,points,radius=radius,big=big,nodot=nodot,circle=circle
if not keyword_set(radius) then radius=5
if (not keyword_set(nodot)) then nodot=0
if not keyword_set(circle) then begin
        circle=0
endif else begin
        nodot=1
endelse

nc = !d.table_size
if nc eq 0 then message,'Device has static color tables: cannot adjust'
red = byte(indgen(nc))
green = red
blue = red
green(nc-1) = 0b
;blue(nc-1)=128b
```

```
tvlct,red,green,blue

output = byte ( ((image*0.98) mod (nc-5)) + floor(image / (nc-5))*256 )
x=reform(points(0,*))
y=reform(points(1,*))
s = size(output)
if (s(0) eq 3) then begin
        ; 3-D array
        nel=n_elements(points(*,0))
        t = reform(points(nel-1,*))
        tmax=max(t,min=tmin)
endif
if (keyword_set(big)) then begin
        if (s(0) eq 2) then begin
                output=rebin(output,s(1)*2,s(2)*2); 2-D array
        endif else begin
                output=rebin(output,s(1)*2,s(2)*2,s(3)); 3-D array
        endelse
        x = x * 2 & y = y * 2
endif
x2=n_elements(output(*,0,0))    ; 3rd array index just for safety
y2=n_elements(output(0,*,0))
w=where((x ge 0) and (x lt x2))
x=x(w) & y=y(w)
w=where((y ge 0) and (y lt y2))
x=x(w) & y=y(w)

for i = 0,n_elements(x)-1 do begin
        minx = long((x(i)-radius) > 0)
        miny = long((y(i)-radius) > 0)
        maxx = long((x(i)+radius) < (x2-1))
        maxy = long((y(i)+radius) < (y2-1))
        foo=[x(i)-minx,y(i)-miny]
        blob=fo_circ(output[minx:maxx,miny:maxy], $
                        center=foo,radius=radius,circle=circle)
        blob = (blob < 1) * (nc - 1b)
        if (s(0) eq 2) then begin
                ; 2-D image
                output(minx:maxx,miny:maxy) = $
                        output(minx:maxx,miny:maxy) > blob
                if (nodot eq 0) then begin
                        if (x(i) gt 1) and (x(i) lt (x2-1)) then $
                                output(x(i)-1:x(i)+1,y(i))=0b
                        if (y(i) gt 1) and (y(i) lt (y2-1)) then $
                                output(x(i),y(i)-1:y(i)+1)=0b
                endif
        endif else begin
                ; 3-D image
                tnow=t(i)-tmin
                output(minx:maxx,miny:maxy,tnow) = $
                        output(minx:maxx,miny:maxy,tnow) > blob
                if (nodot eq 0) then begin
                        if (x(i) gt 1) and (x(i) lt (x2-1)) then $
                                output(x(i)-1:x(i)+1,y(i),tnow)=0b
                        if (y(i) gt 1) and (y(i) lt (y2-1)) then $
                                output(x(i),y(i)-1:y(i)+1,tnow)=0b
```

```
                endif
        endelse
endfor

tv,output
return, output
end
```

A.3.5 jpretrackmod

```
;
;
; see http://www.physics.emory.edu/~weeks/idl
; for more information
;
; dead simple routine to analyse 2+1d 'stacks' into trackable files
; whammy = [lnoise,extent1,extent2,masscut]
;
; ppretrack -- Peter's version (begun 7/8/97)
; jpretrack -- John's version (begun 7/8/98)
;
pro jpretrackmod,name,whammy,horpix,verpix,invert=invert,field=field,first=first,fskip=fskip,$
        gdf=gdf

if n_elements(whammy) ne 4 then $
        message,'usage: pretrack,fname,[lnoise,extent1,extent2,masscut],invert=invert,field=field'

lnoise = whammy(0)
extent1 = whammy(1)
extent2 = whammy(2)
masscut = whammy(3)

filetotal = findfile(name +'*.tif')
if filetotal(0) eq '' then message,"No file '"+name+"' found"
ns = n_elements(filetotal)

filen=strarr(ns)

if (ns gt 1000) then begin
        for k=1000,ns-1 do begin
                l=string(k)
                m=strcompress(l,/remove_all)
                filen(k)=findfile(name +'frame'+ m + '.tif')
        endfor
        for k=100,999 do begin
                l=string(k)
                m=strcompress(l,/remove_all)
                filen(k)=findfile(name +'frame0'+ m + '.tif')
        endfor
        for k=10,99 do begin
                l=string(k)
                m=strcompress(l,/remove_all)
                filen(k)=findfile(name +'frame00'+ m + '.tif')
        endfor
```

```
        for k=0,9 do begin
                l=string(k)
                m=strcompress(l,/remove_all)
                filen(k)=findfile(name +'frame000'+ m + '.tif')
        endfor
endif else begin
        if (ns gt 100) then begin
                for k=100,ns-1 do begin
                        l=string(k)
                        m=strcompress(l,/remove_all)
                        filen(k)=findfile(name +'frame0'+ m + '.tif')
                endfor
                for k=10,99 do begin
                        l=string(k)
                        m=strcompress(l,/remove_all)
                        filen(k)=findfile(name +'frame00'+ m + '.tif')
                endfor
                for k=0,9 do begin
                        l=string(k)
                        m=strcompress(l,/remove_all)
                        filen(k)=findfile(name +'frame000'+ m + '.tif')
                endfor
        endif else begin
                for k=10,ns-1 do begin
                        l=string(k)
                        m=strcompress(l,/remove_all)
                        filen(k)=findfile(name +'frame00'+ m + '.tif')
                endfor
                for k=0,9 do begin
                        l=string(k)
                        m=strcompress(l,/remove_all)
                        filen(k)=findfile(name +'frame000'+ m + '.tif')
                endfor
        endelse
endelse

; fskip is the frame/field # increment during time lapse video
if not keyword_set(fskip) then fskip=1

stk=bytarr(horpix,verpix,ns)

for j=0,ns-1 do begin

        print,'reading image stack: '+filen(j)
        if keyword_set(gdf) then stk = read_gdf(filen(j)) else $
                frame = read_nih(filen(j))
        if keyword_set(invert) then frame = 255b-frame
        stk(*,*,j)=frame
        ns = n_elements(stk(0,0,*))
endfor
        ss=size(stk(*,*,0))
        sx = ss(1)

        if keyword_set(first) then ns = 1 ;handy for a quick looksee...

        res = fltarr(6)
```

```
        if keyword_set(field) then begin
                for i = 0,ns-1 do begin
                print,'processing fields of frame'+strcompress(i)+' out of'+$
                        strcompress(ns)+'....'
                im = bpass(fieldof(stk(*,*,i)),lnoise,extent1,/field)
                f = feature(im(2*extent1:sx-2*extent1,*),extent2,masscut = masscut,/field)
                if f(0) ne -1 then begin
                        f(0,*,*) = f(0,*,*)+2*extent1
                        nf = n_elements(f(0,*))
                        res = [[res],[f,fltarr(1,nf)+2*i*fskip]]
                endif
                im = bpass(fieldof(stk(*,*,i)),lnoise,extent1,/field)
                f = feature(im(2*extent1:sx-2*extent1,*),extent2,masscut = masscut,/field)
                if f(0) ne -1 then begin
                        f(0,*,*) = f(0,*,*)+2*extent1
                        f(1,*) = f(1,*)+1
                        nf = n_elements(f(0,*))
                        res = [[res],[f,fltarr(1,nf)+2*i*fskip+1]]
                endif
                endfor
        endif else begin
                for i = 0,ns-1 do begin
                print,'processing frame'+strcompress(i)+' out of'+$
                        strcompress(ns)+'....'
                im = bpass(stk(*,*,i),lnoise,extent1)
                f = feature(im,extent2,masscut = masscut)
                nf = n_elements(f(0,*))
                if (f(0) ne -1) then res = [[res],[f,fltarr(1,nf)+i*fskip]]
                endfor
        endelse

        wname = 'xys.result'
        print,'writing output file to:' + wname
        write_gdf,res(*,1:*),wname
end
```

A.3.6 monitor_mod

```
function monitor_mod,t
sz=size(t)
n_rows=sz(2,0)
extract=extrac(t,6,0,1,n_rows)
max_track=max(extract)
max_track_int=uint(max_track)
info=fltarr(7,max_track_int+1)
for i=0,max_track_int do begin
        w=where(t(6,*) eq i)
        nf=n_elements(w)
        first_frame=w(0)
        info(0,i)=t(0,first_frame)
        info(1,i)=t(1,first_frame)
        info(2,i)=t(4,first_frame)
        info(3,i)=nf
        info(4,i)=t(5,first_frame)+1
```

```
        info(5,i)=info(4,i)+nf-1
        info(6,i)=t(6,first_frame)
endfor
return,info
end
```

A.3.7 part_find_mod1

```
pro part_find_mod1,info,goodenough,total_frames,xpixel,ypixel

for i=1,total_frames-goodenough+1 do begin
        p=string(i)
        w=where (info(4,*) eq i)
        sz=size(w)
        type=sz(0,0)

        if type ne 0 then begin
        n=n_elements(w)
        for j=0,n-1 do begin
                print,'start frame = '+p
                particle_no=w(j)
                s=info(4,particle_no)-1
                frame_no=long(s)

                if (frame_no lt 10) then begin
                        l=string(frame_no)
                        m=strcompress(l,/remove_all)
                        no='000'+m
                        a=read_nih('c:\RSI\IDL60\reslice1\frame'+no+'.tif')
                        tvscl,a
                endif

                if (frame_no ge 10) and (frame_no lt 100) then begin
                        l=string(frame_no)
                        m=strcompress(l,/remove_all)
                        no='00'+m
                        a=read_nih('c:\RSI\IDL60\reslice1\frame'+no+'.tif')
                        tvscl,a
                endif

                if (frame_no ge 100) and (frame_no lt 1000) then begin
                        l=string(frame_no)
                        m=strcompress(l,/remove_all)
                        no='0'+m
                        a=read_nih('c:\RSI\IDL60\reslice1\frame'+no+'.tif')
                        tvscl,a
                endif

                if (frame_no ge 1000) then begin
                        l=string(frame_no)
                        m=strcompress(l,/remove_all)
                        no=m
                        a=read_nih('c:\RSI\IDL60\reslice1\frame'+no+'.tif')
                        tvscl,a
```

```
endif

fo=fover2d(a,info(*,particle_no),/circle,rad=7)
d=long(info(5,particle_no))
end_frame=string(d)
particle_info=string(particle_no)
print,'end frame= '+end_frame
print,'particle no= '+particle_info
no_frames=info(3,particle_no)

if no_frames ge 230 then no_frames=230

base = WIDGET_BASE(TITLE = 'Animation Widget')
animate = CW_ANIMATE(base, xpixel, ypixel, no_frames,/track)
WIDGET_CONTROL, /REALIZE, base
for k=0,no_frames-1 do begin
if (frame_no lt 10) then begin
        l=string(frame_no)
        m=strcompress(l,/remove_all)
        no='000'+m
        a=read_nih('c:\RSI\IDL60\reslice1\frame'+no+'.tif')
        CW_ANIMATE_LOAD, animate, FRAME=k, IMAGE=a
endif

if (frame_no ge 10) and (frame_no lt 100) then begin
        l=string(frame_no)
        m=strcompress(l,/remove_all)
        no='00'+m
        a=read_nih('c:\RSI\IDL60\reslice1\frame'+no+'.tif')
        CW_ANIMATE_LOAD, animate, FRAME=k, IMAGE=a
endif

if (frame_no ge 100) and (frame_no lt 1000) then begin
        l=string(frame_no)
        m=strcompress(l,/remove_all)
        no='0'+m
        a=read_nih('c:\RSI\IDL60\reslice1\frame'+no+'.tif')
        CW_ANIMATE_LOAD, animate, FRAME=k, IMAGE=a
endif

if (frame_no ge 1000) then begin
        l=string(frame_no)
        m=strcompress(l,/remove_all)
        no=m
        a=read_nih('c:\RSI\IDL60\reslice1\frame'+no+'.tif')
        CW_ANIMATE_LOAD, animate, FRAME=k, IMAGE=a
endif

frame_no=frame_no+1

        endfor

CW_ANIMATE_RUN, animate,40
XMANAGER, 'CW_ANIMATE Demo', base, EVENT_HANDLER = 'EHANDLER'

prom=''
```

```
        read, prom

        endfor
        endif
endfor
end
```

A.3.8 part_input

```
function part_input,no_particle

particles=intarr(no_particle)
for i=1,no_particle do begin
        read,a
        particles(i-1)=a
endfor

return,particles

end
```

A.3.9 plot_hist

```
; plot_hist
;
; see http://www.physics.emory.edu/~weeks/idl
; for more information and software updates
;
; A user-friendly way to plot roughly normal distributed histograms
; easily with optional gaussian fits.
; The relevant data can be returned with the optional parameter 'data'
; and coff. set number of terms in fit (must be 3 or more) using nterms
;
; original version by John C. Crocker
; slightly revised, Feb '99, Eric R. Weeks; /log added 2-23-99
;
pro plot_hist,d,data,coff,nterms=nterms,fit=fit,xrange=xrange,binsize=binsize,$
        noplot=noplot,oplot=oplot,jitter = jitter,center=center,log=log

if keyword_set(fit) then center=1; ERW 2-22-99
if not keyword_set(jitter) then jitter = 0
if keyword_set(nterms) then begin
        if (nterms lt 3 or nterms gt 6) then begin
                print,'Resetting nterms to 6. nterms must be 3, 4, 5, or 6! See gaussfit.'
                nterms = 6
        endif
endif
if not keyword_set(nterms) then nterms = 3

; don't know why, just gotta do it
data = float(d)

; get a little info about the distribution
n=n_elements(data)
```

```
logn=alog10(n)
min = min(data,max=max)
stdev = stdev(data,mean)
min = min([min,mean-(6*stdev)])
max = max([max,mean+(4*stdev)])
if keyword_set(xrange) then begin
        min = xrange(0)
        max = xrange(1)
        w=where(data ge min and data le max,ndata)
        logn = alog10(ndata)
        stdev=stdev(data(w))
endif

; calculate a nice binsize if the user doesn't give us one
if not keyword_set(binsize) then begin
        binsize=stdev/logn
        ; reduce the binsize slightly so that its either 1,2 or 5 times a power of ten
        logbin=alog10(binsize)
        fp = (logbin-fix(logbin))
        ip = fix(logbin)
        if (fp lt 0) then begin
                fp = fp+1 & ip = ip-1
        endif
        coeff = 10^(fp)
        if (coeff lt 2) then fp = 0
        if (coeff ge 2) AND (coeff lt 5) then fp = alog10(2)
        if (coeff ge 5) then fp = alog10(5)
        binsize = 10^(float(ip + fp))
endif

; adjust the min value down so that 0 is at the center of a partition
minbin = long(min/binsize)
if minbin lt 0 then minbin = minbin-1
min = minbin * binsize
if (keyword_set(center) and (not keyword_set(xrange))) then xrange=[min,max]

; oh yeah, calculate the histogram
hist = histogram(data,binsize=binsize,min=min-(binsize*jitter),max=max+binsize*jitter)

; pad out the hist with a zero so the plot doesn't hang in the air!
hist=[hist,[0]]
np = n_elements(hist)

; make an 'x' vector for the plot and the fit
x = (findgen(np)*binsize) + min - (binsize*jitter)

if (not keyword_set(center)) then begin
        w=where(hist gt 0,nw)
        minw=w(0) > 1
        maxw=w(nw-1) < (n_elements(hist)-2)
        hist=hist(minw-1:maxw+1)
        x=x(minw-1:maxw+1)
endif
; plot the histogram
if not keyword_set(noplot) then begin
        if keyword_set(oplot) then begin
```

```
                oplot,x,hist,psym=10
        endif else begin
                w=where(hist gt 0)
                if (keyword_set(xrange)) then begin
                        if (keyword_set(log)) then begin
                                plot,x(w),hist(w),xrange=xrange,psym=4,/ylog
                        endif else begin
                                plot,x,hist,xrange=xrange,psym=10
                        endelse
                endif else begin
                        if (keyword_set(log)) then begin
                                plot,x(w),hist(w),psym=4,/ylog
                        endif else begin
                                plot,x,hist,psym=10
                        endelse
                endelse
        endelse
endif
data = [transpose(x),transpose(hist)]

; do the fit, if desired
if keyword_set(fit) then begin
        ft = gaussfit(x,hist,coff,nterms=nterms)
        data = [transpose(x),transpose(hist),transpose(ft)]
        if not keyword_set(noplot) then begin
                oplot,x,ft,linestyle=3
                dy = !y.crange(1)-!y.crange(0)
                dx = !x.crange(1)-!x.crange(0)
                yy = !y.crange(0)
                xx = !x.crange(0)
                if (keyword_set(log)) then begin
                        xyouts, xx + (dx*0.15), 10^(yy + (dy*.90)), "Height = "+$
                                strcompress(string(coff(0),format='(g9.4)')) ,alignment=0.5
                        xyouts, xx + (dx*0.15), 10^(yy + (dy*.85)), "Offset = "+$
                                strcompress(string(coff(1),format='(g9.4)')) ,alignment=0.5
                        xyouts, xx + (dx*0.15), 10^(yy + (dy*.80)), "Sigma = "+$
                                strcompress(string(coff(2),format='(g9.4)')) ,alignment=0.5
                endif else begin
                        xyouts, xx + (dx*0.15), yy + (dy*.90), "Height = "+$
                                strcompress(string(coff(0),format='(g9.4)')) ,alignment=0.5
                        xyouts, xx + (dx*0.15), yy + (dy*.85), "Offset = "+$
                                strcompress(string(coff(1),format='(g9.4)')) ,alignment=0.5
                        xyouts, xx + (dx*0.15), yy + (dy*.80), "Sigma = "+$
                                strcompress(string(coff(2),format='(g9.4)')) ,alignment=0.5
                endelse
                if (nterms gt 3) then begin
                        if (keyword_set(log)) then begin
                        xyouts, xx + (dx*0.15), 10^(yy + (dy*.75)), "Polynomial:" ,alignment=0.5
                        xyouts, xx + (dx*0.15), 10^(yy + (dy*.70)), $
                                strcompress(string(coff(3),format='(g10.4)')) ,alignment=0.5
                                endif else begin
                        xyouts, xx + (dx*0.15), yy + (dy*.75), "Polynomial:" ,alignment=0.5
                        xyouts, xx + (dx*0.15), yy + (dy*.70), $
                                strcompress(string(coff(3),format='(g10.4)')) ,alignment=0.5
                                endelse
```

```
                if (nterms gt 4) then begin
                        if (keyword_set(log)) then begin
                xyouts, xx + (dx*0.15), 10^(yy + (dy*.65)), "+ "+$
                        strcompress(string(coff(4),format='(g9.4)'))+" x" ,alignment=0.5
                        endif else begin
                xyouts, xx + (dx*0.15), yy + (dy*.65), "+ "+$
                        strcompress(string(coff(4),format='(g9.4)'))+" x" ,alignment=0.5
                        endelse
                if (nterms gt 5) then begin
                        if (keyword_set(log)) then begin
                xyouts, xx + (dx*0.15), 10^(yy + (dy*.60)), "+ "+$
                        strcompress(string(coff(5),format='(g10.4)'))+" x^2" ,alignment=0.5
                        endif else begin
                xyouts, xx + (dx*0.15), yy + (dy*.60), "+ "+$
                        strcompress(string(coff(5),format='(g10.4)'))+" x^2" ,alignment=0.5
                        endelse
                endif ; five
                endif ; four
                endif ; three
        endif
endif

end
```

A.3.10 plot_tr

```
;pro plottr,tarray,result,goodenough=goodenough,tv=tv,noconnect=noconnect, $
; x=x,y=y,_extra=eee
;
; see http://www.physics.emory.edu/~weeks/idl
; for more information and software updates
;
; plottr.pro (formerly ericplot2.pro)
;
; started 6-15-98 Eric R. Weeks
; /tv added 8-13-98
; /noconnect added 8-13-98
; uberized 9-21-98
;
; duplicates somewhat "plot_tracks"
;
; lentrk Eric Weeks 9-22-98
;
; modified from JCC's len_trk.pro

function pt_lentrk,t
; works for either uber or normal tracked data
;
; returns (2,*) array: (0,*) is the length, (1,*) is particle #

s=size(t)
if (s(0) eq 2) then begin
        ; UBER TRACKER
        ; get the indices of the unique id's
```

```
        ndat=n_elements(t(*,0))
        u = uniq(t(ndat-1,*))
        ntracks = n_elements(u)
        u = [-1,u]

        res = fltarr(2,ntracks)
        for i = 1L,ntracks do begin
                res(0,i-1) = t(ndat-2,u(i))-t(ndat-2,u(i-1)+1)
                res(1,i-1) = t(ndat-1,u(i))
        endfor
endif else begin
        ; OLD TRACKER
        ntracks=n_elements(t(0,*,0))
        res=fltarr(2,ntracks)
        for i=0,ntracks-1 do begin
                w=where(t(0,i,*) ge 0)
                res(0,i)=w(n_elements(w)-1)-w(0)+1
                res(1,i)=i
        endfor
endelse

return,res
end
; first a utility function:
; eline.pro started 8-13-98 by Eric Weeks
;
; linearray=eline(pt1,pt2)
; pt1, pt2 are n-dimensional pofloors (integers)
; result is an array of pofloors connecting them
;
; vectorized 11-2-98
; turned into pt_eline 2-25-99

function pt_eline,pt1,pt2

ndim=n_elements(pt1)
ndim2=n_elements(pt1)
if (ndim ne ndim2) then message,"error! pts must be same dimension"
result=floor(pt1)

delta=pt2-pt1
max=max(abs(delta))
epsilon=float(delta)/float(max)
if (max le 0) then begin
        message,"warning! begin and end pts are identical",/inf
endif else begin
        pt0=float(pt1)
        temp=epsilon # findgen(max+1)
        n=n_elements(pt1)
        result=intarr(n,max+1)
        for i=0,n-1 do begin
                result(i,*)=floor(pt0(i)+temp(i,*))
        endfor
endelse

return,result
```

```
end

pro plottr,tarray,result,goodenough=goodenough,tv=tv,noconnect=noconnect, $
x=x,y=y,_extra=eee
; tarray is an array of tracked data (2D for the moment)
; goodenough works like plot_tracks -- only tracks at least 'goodenough'
; in duration will be plotted
; /tv uses tv mode to plot, rather than axes; use x and y to adjust size
; result gets picture from /tv
;
; WARNING: tracked data must be "uberize'd" before using! (if ubertracker)

s = size(tarray)
if (s(0) eq 2) then uber=1

if (not keyword_set(x)) then x=512
if (not keyword_set(y)) then y=480
if (not keyword_set(noconnect)) then connect=1

if (not keyword_set(uber)) then begin
        ; REGULAR TRACKER
        if not keyword_set(goodenough) then goodenough=s(3)
        ; default is number of frames
        ww=where( total(tarray(0,*,*) ge 0,3) ge goodenough )
        ; ww locates all valid data pts (not equal to -1)
        if (keyword_set(tv)) then begin
                ; added 8-13-98
                picture=bytarr(x,y)
                if (keyword_set(connect)) then begin
                        for i=0,s(2)-1 do begin
                                ; loop over each particle
                                w1=where(tarray(0,i,*) gt 0)
                                pt0=tarray(0:1,i,w1(0))
                                for j=1,n_elements(w1)-1 do begin
                                        ; loop over each valid frame
                                        pt1=tarray(0:1,i,w1(j))
                                        lineline=pt_eline(pt0,pt1)
                                        picture(lineline(0,*),lineline(1,*)) = 255
                                        pt0=pt1
                                endfor
                        endfor
                endif else begin
                        for i=0,s(3)-1 do begin
                                ; loop over each frame
                                if (ww(0) ge 0) then begin
                                        w = where(tarray(0,ww,i) gt 0)
                                        ptrs=ww(w)
                                        picture(tarray(0,ptrs,i),tarray(1,ptrs,i)) = 255
                                endif
                        endfor
                endelse
                tv,picture
                result=picture
        endif else begin
                ; original pre-August 1998 routine
                if (ww(0) ge 0) then begin
```

```
                        w = where(tarray(0,ww,0) gt 0)
                        ptrs=ww(w)
                        plot,tarray(0,ptrs,0),tarray(1,ptrs,0),/nodata, $
                                _extra=eee,/ynozero,/ysty,/xsty,/isotropic
                        ; loop over each frame
                        if (keyword_set(connect)) then begin
                                for i=0,s(3)-1 do begin
                                        w = where(tarray(0,ww,i) gt 0)
                                        ptrs=ww(w)
                                        oplot,tarray(0,ptrs,i),tarray(1,ptrs,i),psym=3
                                endfor
                        endif else begin
                                for i=0,s(3)-1 do begin
                                        w = where(tarray(0,ww,i) gt 0)
                                        ptrs=ww(w)
                                        oplot,tarray(0,ptrs,i),tarray(1,ptrs,i),psym=3
                                endfor
                        endelse
                endif
        endelse
endif else begin
        ; UBER-TRACKER
        ndat=n_elements(tarray(*,0))
        ntime=max(tarray(ndat-2,*))
        if not keyword_set(goodenough) then goodenough=ntime
        length=pt_lentrk(tarray)
        w=where(length(0,*) ge goodenough,nw)
        if (keyword_set(tv)) then begin
                picture=bytarr(x,y)
                u=uniq(tarray(ndat-1,*))
                ntracks=n_elements(u)
                u=[-1,u]
                if (keyword_set(connect)) then begin
                        for i=0L,nw-1L do begin
                                j=length(1,w(i))
                                traj=tarray(*,u(j)+1:u(j+1))
                                k=n_elements(traj(0,*))
                                pt0=traj(0:1,0)
                                for kk=1L,k-1L do begin
                                        pt1=traj(0:1,kk)
                                        lineline=pt_eline(pt0,pt1)
                                        picture(lineline(0,*),lineline(1,*)) = 255
                                        pt0=pt1
                                endfor
                        endfor
                endif else begin
                        for i=0L,nw-1L do begin
                                j=length(1,w(i))
                                traj=tarray(*,u(j)+1:u(j+1))
                                picture(traj(0,*),traj(1,*)) = 255b
                        endfor
                endelse
                tv,picture
                result=picture
        endif else begin
                plot,tarray(0,*),tarray(1,*),/nodata,/ynozero,_extra=eee, $
```

```
                    /ysty,/xsty,/isotropic
                u=uniq(tarray(ndat-1,*))
                ntracks=n_elements(u)
                u=[-1,u]
                if (keyword_set(connect)) then begin
                    for i=0L,nw-1L do begin
                        j=length(1,w(i))
                        traj=tarray(*,u(j)+1:u(j+1))
                        oplot,traj(0,*),traj(1,*)
                    endfor
                endif else begin
                    for i=0L,nw-1L do begin
                        j=length(1,w(i))
                        traj=tarray(*,u(j)+1:u(j+1))
                        oplot,traj(0,*),traj(1,*),psym=3
                    endfor
                endelse
        endelse
endelse

end
; this ends the procedure
```

A.3.11 read_gdf

```
function read_gdf,filespec
;
; see http://www.physics.emory.edu/~weeks/idl
; for more information
;
;+
; NAME:
; read_gdf
; PURPOSE:
; Read in data files created by WRITE_GDF.
; CATEGORY:
; General Purpose Utility
; CALLING SEQUENCE:
; data = read_gdf(file)
; INPUTS:
; file: Complete pathname of the file to be read.
; OUTPUTS:
; data: Data structure. For example, if the original
; data was stored as an array of bytes, then
; DATA will be returned as an array of bytes also.
; RESTRICTIONS:
; Current implementation does not support structures or
; arrays of structures.
; PROCEDURE:
; Reasonably straightforward.
; Determines if the file is ASCII or binary, reads the size
; and dimension info from the header, and reads in the data
; MODIFICATION HISTORY:
```

```
; Written by David G. Grier, AT&T Bell Laboratories, 9/91
; 12/95 Figures out how to deal with data from different-endian
; machines DGG.
;-
on_error,2 ; return to caller on error

MAGIC = 082991L
HEADER = 'GDF v. 1.0'
debug = keyword_set(debug)

file = findfile(filespec, count=nfiles)

if nfiles eq 0 then message,'No files matched specification '+filespec

d = -1
ascii = 0

openr,lun,file(0),/get_lun

mgc = 0L
readu,lun,mgc
doswap = swap_endian(mgc) eq MAGIC ; Check for binary GDF file written on
                                   ; different-endian machine
                                   ; Check for ASCII GDF file

if (mgc ne MAGIC) and (not doswap) then begin
        point_lun,lun,0
        str = ''
        fmt = '(A'+strtrim(strlen(HEADER),2)+')'
        readf,lun,format=fmt,str
        if str eq HEADER then $
                ascii = 1 $
        else begin
                message,filespec+' is not a GDF file',/inf
                goto,done
                endelse
        endif
ndim = 0L

; Get number of data dimensions
if ascii then readf,lun,ndim else readu,lun,ndim
if doswap then ndim = swap_endian(ndim)
sz = lonarr(ndim+2,/nozero)

; Get data type description
if ascii then readf,lun,sz else readu,lun,sz
if doswap then sz = swap_endian(sz)
sz = [ndim,sz]

d = make_array(size=sz,/nozero)
if ascii then readf,lun,d else readu,lun,d
if doswap then d(*) = swap_endian(d(*))

done:
close,lun
free_lun,lun
```

```
return,d
end
```

A.3.12 read_nih

```
function read_nih,fname,first=first,last=last
;
; see http://www.physics.emory.edu/~weeks/idl
; for more information
;
;
; reads 2 and 3 dimensional 8-bit TIFF files as produced by
; NIH Image. It tries to detect and fix 'endian' problems.
; Also allows user to read a subset of frames, which is useful
; for really big files.
;
f = findfile(fname) ; check to see if the file is actually *there*
if f(0) eq '' then message,'File: "'+fname+'" not found!'

cookie = intarr(1)
head = intarr(383)

; check for endian independent cookie
openr,1,fname
readu,1,cookie
if (cookie(0) ne 19789 and cookie(0) ne 18761) then begin
        close,1
        message,'"'+fname+'" is not a valid NIH Image tiff file!'
endif
readu,1,head

; fix endian
if head(2) eq 2048 then head = swap_endian(head)
; check endian
if head(2) ne 8 then begin
        close,1
        message,'"'+fname+'" is not a valid NIH Image tiff file!'
endif

tmp = FSTAT(1)

x = head(14) + 0L
y = head(20) + 0L
z = head(257) + 0L
if z eq 0 then z = 1L ; fix for 2d nih tiff images

; watch out for EOF errors- is the file big enough?
sz = (x*y*z) + 768L
if sz gt tmp.size then $
        message,'"'+fname+'" is not a valid NIH Image tiff file!'
; do Peter's browsing thing
s = 0
if keyword_set( first ) then begin
        if (first le z-1) and (first ge 0) then s=first $
```

```
                else begin
                        close,1
                        message,'invalid first position!!'
                endelse
endif
if keyword_set( last ) then begin
        if (last ge s) and (last le z-1) then z=last $
                else begin
                        close,1
                        message,'invalid last position!'
                endelse
endif

if (s gt 0) then begin
        z = z - s + 1
        offset = x * y * s + 768L
        point_lun,1,offset
endif

; read in the data
im = bytarr(x,y,z)
readu,1,im
close,1

; fix the data up for IDL conventions
for i = 0,z-1 do im(*,*,i) = 255b-rotate(im(*,*,i),7)

return,im

end
```

A.3.13 region_time_blocks_front

```
pro region_time_blocks_front,t,info,particle_IDs,goodenough,$
        xpixel_min,xpixel_max,$
        ypixel_lowerfrontproj,ypixel_upperfrontproj,$
        start_frame,end_frame,frame_duration

m=n_elements(particle_IDs)

sel_part_orig=fltarr(7,m)

for i=0,m-1 do begin
        sel_part_orig(*,i)=info(*,particle_IDs(i))
endfor

no_block=(end_frame-start_frame)/frame_duration

end_block=start_frame-1

for j=0,no_block-1 do begin
        n=0
        sel_part=sel_part_orig
```

```
        l=string(j+1)
        r=strcompress(l,/remove_all)

        start_block=end_block+1
        end_block=start_block+frame_duration-1

        for k=0,m-1 do begin
                if (sel_part(0,k) ge xpixel_min) and (sel_part(0,k) le xpixel_max) $
                and (sel_part(1,k) ge ypixel_lowerfrontproj) and
                (sel_part(1,k)leypixel_upperfrontproj) $
                then begin
                if sel_part(4,k) lt end_block then begin
                        if sel_part(4,k) lt start_block then begin
                        sel_part(4,k)=start_block
                endif

                if sel_part(5,k) gt start_block then begin
                if sel_part(5,k) gt end_block then begin
                        sel_part(5,k)=end_block
                endif
                endif

                if (sel_part(5,k)-sel_part(4,k)) ge goodenough then begin
                n=n+1
                endif
        endif
   endif
endfor

sel_part=sel_part_orig
pt_info=fltarr(7,n)
n=0

for k=0,m-1 do begin
        if (sel_part(0,k) ge xpixel_min) and (sel_part(0,k) le xpixel_max) $
        and (sel_part(1,k) ge ypixel_lowerfrontproj) and (sel_part(1,k) le ypixel_upperfrontproj) $
        then begin
        if sel_part(4,k) lt end_block then begin
                if sel_part(4,k) lt start_block then begin
                sel_part(4,k)=start_block
                endif

        if sel_part(5,k) gt start_block then begin
          if sel_part(5,k) gt end_block then begin
                sel_part(5,k)=end_block
          endif
        endif

        if (sel_part(5,k)-sel_part(4,k)) ge goodenough then begin
      pt_info(*,n)=sel_part(*,k)
      write_gdf, pt_info, 'pt_info 3 quarter front projection block'+r+'.result'
        write_textmod,pt_info,'pt_info 3 quarter front projection block'+r+'.txt'
        n=n+1
        endif
       endif
```

```
    endif
   endfor

   h=MSD_header_mod1(t,pt_info)
   write_textmod,h,'particle track header 3 quarter front projection block'+r+'.txt'
   p=msd_mod3(t,pt_info)
   write_textmod,p,'particle track 3 quarter front projection block'+r+'.txt'
   average=ave_timelag(p)
   write_textmod,average,'average particle track 3 quarter front projection block'+r+'.txt'
  endfor
end
```

A.3.14 write_gdf

```
pro write_gdf, data, file, ascii=ascii
; see http://www.physics.emory.edu/~weeks/idl
; for more information
;+
; NAME:
; write_gdf
; PURPOSE:
; Writes IDL-style data to disk in a format which can be
; easily read back in.
; CATEGORY:
; General Purpose Utility
; CALLING SEQUENCE:
; write_gdf,data,file
; INPUTS:
; data: Data structure to be written to disk.
; file: Complete pathname of the file to be written.
; KEYWORD:
; ascii: Produce an ASCII file rather than the default
; binary file.
; SIDE EFFECTS:
; Creates a file.
; RESTRICTIONS:
; Current version does not support structures or arrays of
; structures.
; PROCEDURE:
; Writes a header consisting of a long MAGIC number followed
; by the long array produced by SIZE(DATA), followed by the
; data itself.
; If the file is ASCII, the header tag is an identifying
; statement, followed by all of the same information in
; ASCII format.
; MODIFICATION HISTORY:
; Written by David G. Grier, AT&T Bell Laboratories, 9/91
;-
on_error,2 ; return to caller on error
MAGIC = 082991L
HEADER = 'GDF v. 1.0'
openw, lun, file, /get_lun
sz = size(data)
if keyword_set(ascii) then begin
```

```
        printf,lun,HEADER
        printf,lun,sz(0)
        printf,lun,sz(1:*)
        printf,lun,data
        endif $
else begin
        writeu,lun,MAGIC
        writeu,lun,sz
        writeu,lun,data
        endelse
close,lun
free_lun, lun
end
```

A.3.15 write_textmod

```
; Written by John C. Crocker
;
;
; Saves the data in an array as a tab delimited text file
; which can be easily read in by a spread sheet program.
; default delimiter is the tab
;
pro write_textmod,data,filename,comma=comma

sz = size(data)
if sz(0) ne 2 then message,'Array argument must be 2 dimensional'

if keyword_set( comma ) then num_delter = ',' else num_delter = string( 9B ) ; tab is ASCII 9

close,1
openw,1,filename

for i=0.0,sz(2)-1 do begin
        astring = ''
        for j=0.0,sz(1)-2 do begin
                astring = astring + strcompress( string( data(j,i) ), /remove_all ) + num_delter
        endfor
        astring = astring + strcompress( string( data(sz(1)-1,i) ), /remove_all )
        printf,1,astring
endfor

close,1

end
```

A.4 Matlab m-files

The following m-files were used to calculate the shear storage and shear loss moduli, G' and G", using the methods of Mason et al. [47, 48].

A.4.1 Shear modulus calculation at 30 Hz

```
%   Code to obtain one complex modulus value given a single averaged
%   MSD over time
clear all

%   Define values for thermal energy, KT, and radius of particle
(granule)
KT = 4.278e-21;
rad = 300e-9;

%  Insert file name and load file
msd1 = load('MSD06302006_011930block1.txt');

%  Calculate the ln of each time point
lot1 = log(msd1(:,1));

%  Obtain a frequency value at each point
invt1 = 1./msd1(:,1);

%  Define t1 as frequency.  Used for plotting purposes.
t1 = invt1(1:size(invt1)-2);

%  Find the ln of the MSD values, used for the Mason calculation.
Multiply
%  by conversion factor to convert to units of meters.
lomsd1 = log(msd1(:,2)*3.55e-15);

%  Convert the MSD values into meters with a conversion factor.
msdval1 = msd1(:,2)*3.55e-15;

%   Find the value for alpha (see Mason 2000 for definition of alpha) at
%   each time point
for i = 1: size(lot1,1)-1
    slop1(i) = (lomsd1(i+1)-lomsd1(i))/(lot1(i+1)-lot1(i));
end


for i = 1: size(lot1,1)-2
    gamm1(i) = 0.457*(1+slop1(i))^2-1.36*(1+slop1(i))+1.90;
    g1(i) = KT / pi / rad / msdval1(i) / gamm1(i);

    % Calculate values for G' (gp1) and G" (gpp1)
    % The values are multiplied by 10 to convert units from Pa
    % to dynes/cm^2
    gp1(i) = 10*[abs(g1(i)) * cos(pi*slop1(i)/2)];
        gpp1(i) = 10*[abs(g1(i)) * sin(pi*slop1(i)/2)];
end


%  Plot G' vs. frequency
for i = 1: size(lot1,1)-2
```

```
    loglog(invt1(i), gp1(i),'x');
    hold on
    grid off
end
xlabel('Frequency (1/s)')
ylabel('Storage Modulus, G* (dyn/cm^2)')
title('Storage Modulus (G*) versus frequency')

%  Plot G" vs. frequency
figure(2)
for i = 1: size(lot1,1)-2
    loglog(invt1(i),gpp1(i),'o');
    hold on
    grid off
end
xlabel('Frequency (1/s)')
ylabel('Loss Modulus, G** (dyn/cm^2)')
title('Loss Modulus (G**) versus frequency')
% legend('G*','G**','Location','SouthEast')


%  Output the values for G' and G" at 30 Hz
stormod = [gp1(1)]
lossmod = [gpp1(1)]
```

A.5 Pseudopod Projection Times in 6 μm-wide Channel

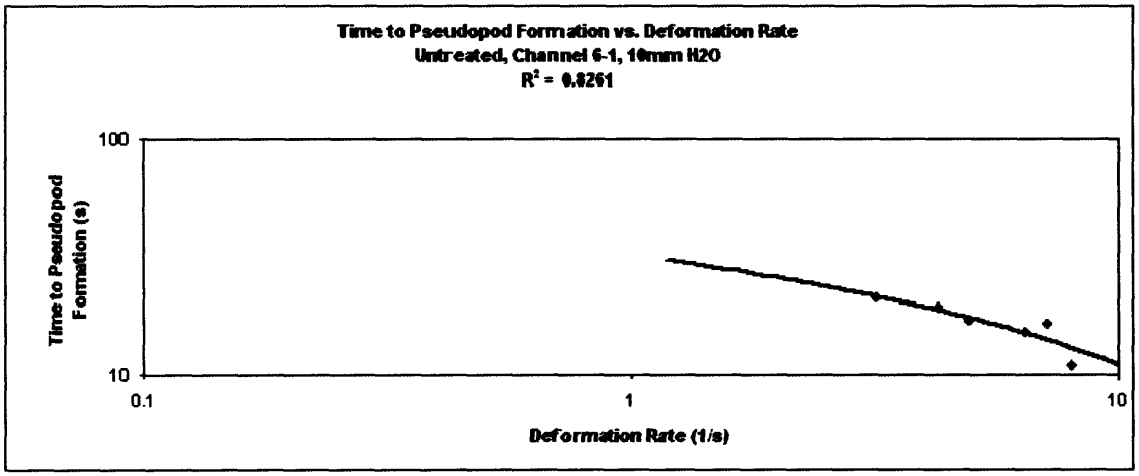

A.6 Individual Cell Data

	Cell ID	Time After Deformation	G' (dyn/cm^2)	G" (dyn/cm^2)	N
Passive Neutrophils Untreated	06132006_000005	0	25.9736	33.0998	4
	06152006_003200	0	24.4042	43.4917	3
	06162006_001230	0	36.3492	71.3678	6
	06152006_013930	0	33.9416	87.4945	3
	06302006_011930	0	33.0174	37.1422	17
	06302006_012830	0	36.202	31.5871	5
Deformed Neutrophils Untreated 30mm H2O pressure drop	07072006_000730	12.5	19.8283	9.3657	16
		17.5	21.219	14.996	7
	07072006_001300	12.5	7.1695	56.7142	4
		17.5	9.024	38.8099	4
	07072006_001500	12.5	31.6763	31.9864	11
		17.5	42.1666	34.526	6
	07072006_002100	12.5	21.3525	41.6506	8
		17.5	27.9409	38.1014	13
	07072006_002430	12.5	19.7681	34.888	8
		17.5	53.9434	12.9164	5
	07072006_003230	12.5	31.0003	23.4166	17
		17.5	56.0959	48.3608	9
	07132006_035400	12.5	9.5242	23.0393	11
	07132006_035600	12.5	27.1009	16.0638	9
Passive Neutrophils 3.5uM BAPTA	06302006_013630	0	22.1272	46.3484	3
	06302006_013730	0	25.3888	49.5551	5
	06302006_014100	0	34.2405	54.4262	7
	06302006_013430	0	21.6805	41.2716	5
Deformed Neutrophils 3.5uM BAPTA 30mm H2O pressure drop	06292006_001300	12.5	31.2049	18.4614	2
		17.5	44.4802	26.8851	2
	06292006_002330	12.5	21.0207	11.8596	4
	06292006_004900	12.5	26.6413	21.0793	4
		17.5	41.9645	37.9808	2
	06292006_010000	12.5	41.0909	31.2539	4
		17.5	40.9148	30.9034	3
	06292006_011930	12.5	28.9599	19.9726	10
		17.5	28.5767	16.9493	11
	06292006_010800	12.5	27.935	12.8886	3
	06292006_012400	12.5	25.2325	27.2291	4

	06292006_003030	12.5	26.8416	9.5872	4
		17.5	20.3929	24.2935	2
	07192006_000130	12.5	54.1401	26.0894	2
		17.5	37.7776	15.2832	4
	07192006_000800	12.5	27.1987	51.0688	14
		17.5	28.1444	11.8148	12
	07192006_001100	12.5	27.0393	37.6413	6
Passive Neutrophils 0.035% DMSO	06302006_010800	0	34.462	73.6865	3
	06302006_011130	0	13.2829	35.8738	3
	06302006_010730	0	29.9275	35.4148	11
	06302006_011130	0	13.2829	35.8738	3
Deformed Neutrophils 0.035% DMSO 30mm H2O pressure drop	07072006_015800	12.5	13.302	34.9676	10
		17.5	18.6557	25.896	2
	07072006_020800	12.5	33.4976	35.8936	5
		17.5	38.9434	42.0646	6
	07072006_023130	12.5	18.7605	21.995	4
	07072006_023130	12.5	16.3881	28.0538	10

A.7 Flow Cytometry Histograms

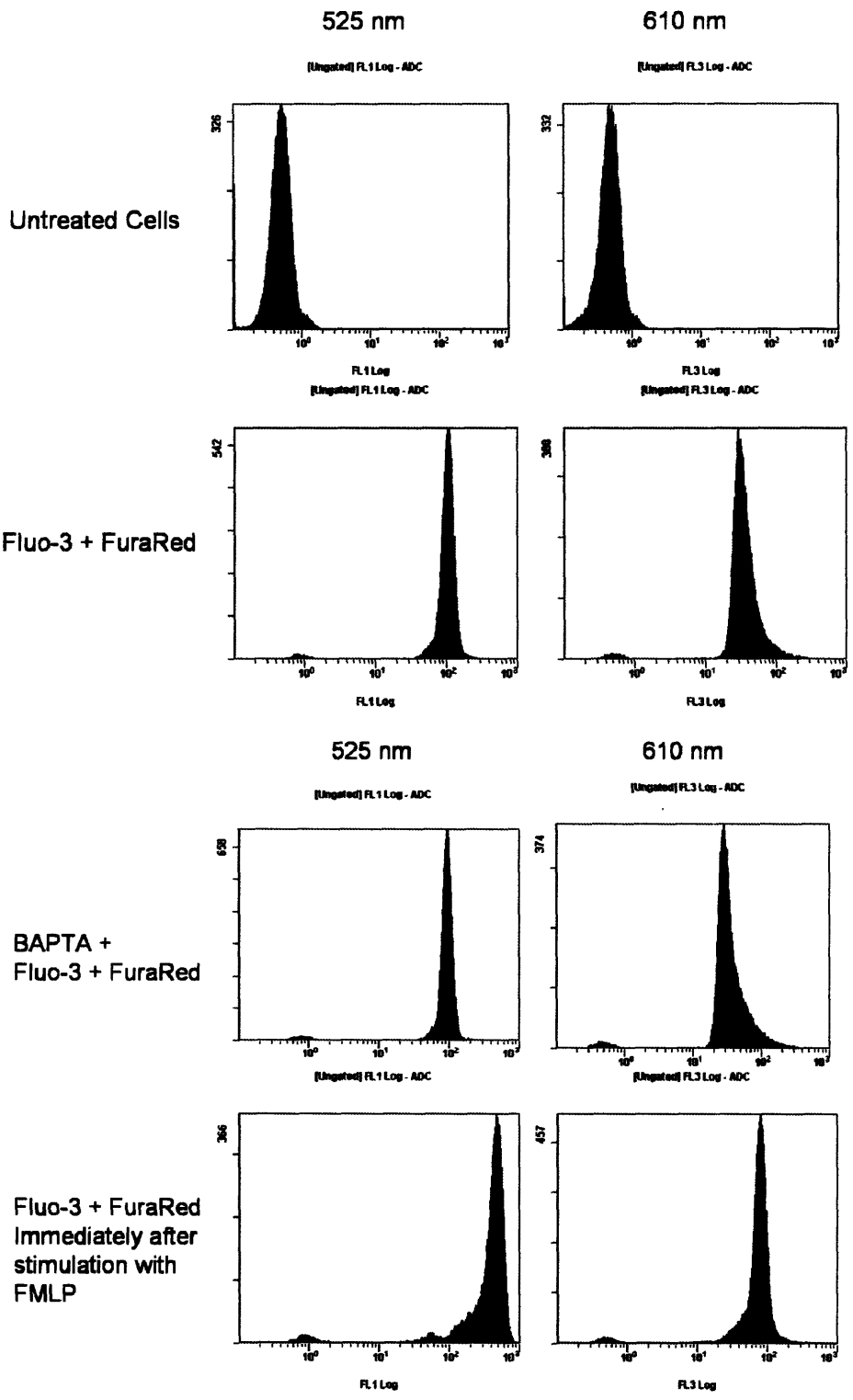

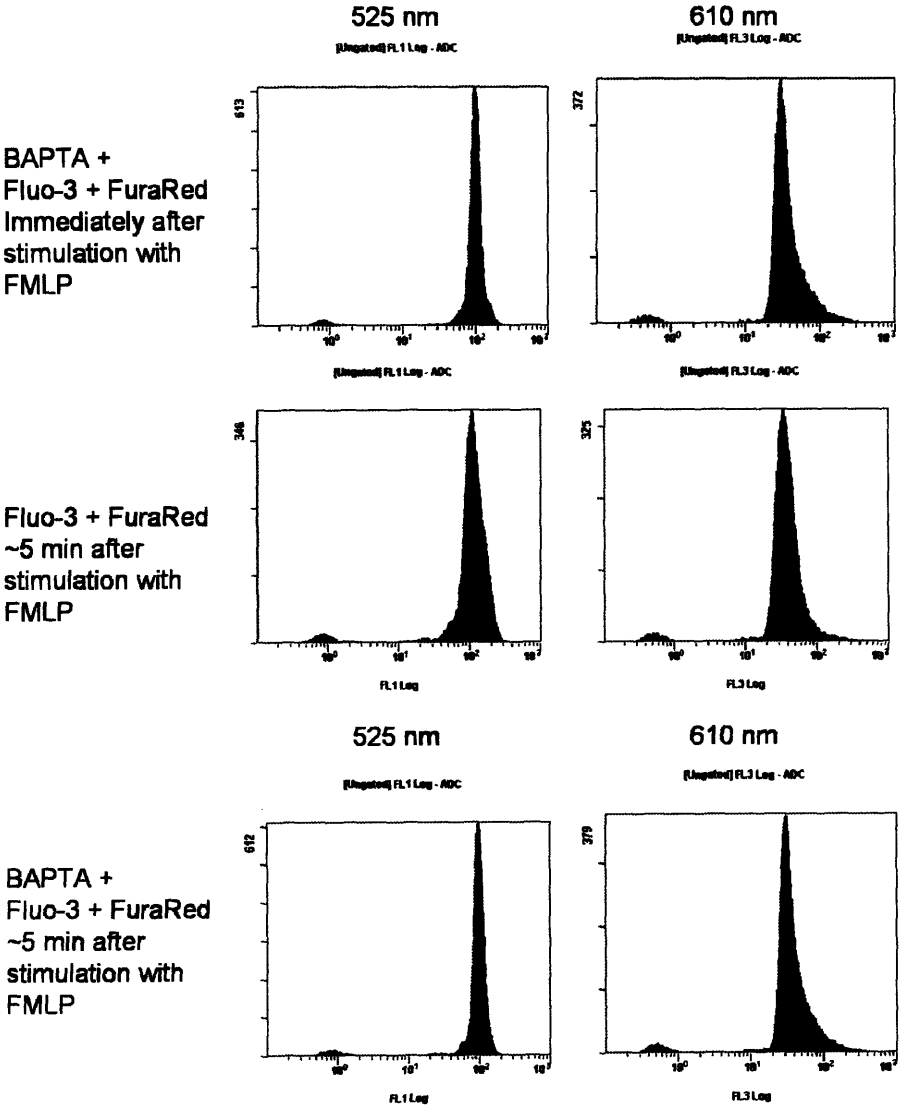
525 nm
610 nm
BAPTA +
Fluo-3 + FuraRed
Immediately after
stimulation with
FMLP
Fluo-3 + FuraRed
~5 min after
stimulation with
FMLP
525 nm
610 nm
BAPTA +
Fluo-3 + FuraRed
~5 min after
stimulation with
FMLP